The Spectroscopic Analysis of Di-copper Helicates as Receptors for Encapsulating Anions

A thesis presented in partial fulfilment of the requirements for the degree of

Master of Science

in

Chemistry

at

Massey University, Palmerston North,

New Zealand.

Quintin Wayne Knapp

2009

Abstract

The application of neutral dicopper helicates to the encapsulation of a number of anions was investigated. Two dicopper salen derived helicates were studied which contained phenolic and either iminophenyl (**1**) or oxime (**2**) donor groups. UV-visible spectroscopy was used to determine the binding stoichiometry and formation constants of the anion complexes. Complex binding was supported by electrospray ionisation mass spectrometry. Receptor **1** possessed a remarkable selectivity for sulfate in isopropanol (IPA) for which a log K value of 5.07 ± 0.24 was obtained. Receptor **2** bound all anions studied more strongly than **1.** Crystal structural data supports the proposition that there is a steric barrier to contraction of **1** from the bulky iminophenyl groups. Receptor **2** was not restricted by the small oxime moieties allowing for optimum copper-anion interactions.

Acknowledgements

I would like to extend my gratitude to my supervisor Dr. Paul Plieger whose advice and encouragement throughout this project I could not have done without. His continued support and patience with my endless questions has been greatly appreciated. I would also like to thank my wife Katie. Without her love and continued support throughout the last two years this thesis would never have come to fruition.

Contents

List of Figures

List of Tables

Abbreviations

$\subset$	Signifies encapsulation of a guest within a host molecule.
1	Anion free complex formed between copper(II) acetate and ligand $\mathbf{L^1}$. It is ambiguously used throughout the text to represent the unprotonated and tetraprotonated form.
1.BF_4	$\left[BF_4 \subset Cu_2\mathbf{L_2^1}\right](BF_4)_3$
1.ClO_4	$\left[ClO_4 \subset Cu_2\mathbf{L_2^1}\right](ClO_4)_3$
1.I	$\left[I \subset Cu_2\mathbf{L_2^1}\right]BF_4I_2$
1.SO_4	$SO_4\left[SO_4 \subset Cu_2\mathbf{L_2^1}\right]SO_4$
1.NO_3	$\left[NO_3 \subset Cu_2\mathbf{L_2^1}\right]NO_3(PF_6)_2$
2	$[Cu_2(\mathbf{L^2}\text{-}2H)_2$
2.BF_4	$\left[BF_4 \subset Cu_2\mathbf{L_2^2}\right](BF_4)_3$
2.SO_4	$\left[SO_4 \subset Cu_2\mathbf{L_2^2}\right]SO_4$
β	Cumulative formation constant.
DBU	1,8-diazabicyclo[5.4.0]undec-7-ene.
DCE	1,2-Dichloroethane.
DCE-IPA	Binary solvent system used in this study consisting of 50% (v/v) of 1,2-dichloroethane and 50% (v/v) isopropanol.
ESI-MS	Electrospray ionisation mass spectrometry.
Free base	General term for **1** or **2**. Refers to the non-protonated form of the complexes.
IPA	Isopropanol.
IR	Infrared spectroscopy

K	Formation constant. The equilibrium constant for the formation of a complex in solution. Also referred to as the binding and stabilisation constant throughout the text.
L^0	3,3-[1,6-hexanediylbis[(methylimino)methylene]]bis[2-hydroxy-5-*tert*butyl-benzaldehyde]
L^1	2,2-[1,6-hexanediylbis[(methylimino)methylene]]bis[4-*tert*butyl-6-(phenylazomethinyl)phenol]
L^2	3,3-[1,6-hexanediylbis[(methylimino)methylene]]bis[2-hydroxy-5-*tert*butyl-benzaldehyde oxime]
Λ_0	Molar conductivity at infinite dilution.
Λ_e	Equivalent conductance.
MeCN	Acetonitrile.
MeOH	Methanol.
NMR	Nuclear magnetic resonance.
PBP	Phosphate binding protein of Escherichia coli.
pK_a	Negative logarithm (with base ten) of the acid dissociation constant.
pK_s	Negative logarithm (with base ten) of the autodissociation constant of an amphiteric solvent.
Salph	Schiff base condensation product of salicylic aldehyde and 1,2-phenylenediamine.
TBACl	Tetrabutylammonium chloride.
$TBAH_2PO_4$	Tetrabutylammonium dihydrogen phosphate.
TBAI	Tetrabutylammonium iodide.

Chapter 1

Introduction

1.1 Anion Binding Systems

1.1.1 Anion Background

Anions are omnipresent in the environment and their importance is widespread. More than two thirds of known enzymes operate on anions or make use of anionic substrates.[1] Examples of anion interaction within systems can be found throughout the literature. Anions have been shown to be involved in systems as templating agents.[2] An example of this is in the folding of macromolecular proteins.[3] Recently, synthetic systems that can selectively transport anions across lipid bilayer membranes have been produced.[4] Anions are used in biological processes,[5, 6] in medicine,[7] and as catalysts.[8] Excessive concentration of anions often presents environmental problems. Pastoral run-off of phosphates and nitrates contributes to the eutrophication of natural waterways.[6] Radioactive iodide and the highly mobile pertechnate anion from the nuclear fuel cycle contribute to nuclear pollution.[9] As such, there is an increasing need for the application of anion-binding systems for detection and binding of anions and for research into the mechanisms of these systems.

Cation binding has received far more attention than anion binding due to the inherent difficulties of binding anions. As a result of the weak co-ordinating ability of anions many anions such as BF_4^-, ClO_4^-, and NO_3^- have been labelled as non-coordinating based on their behaviour in aqueous solutions. Upon removal of water these anions can be found to exhibit co-ordination.[10] The weak binding of anions can be largely attributed to the many inherent difficulties of anion binding compared to cation binding. Anions are larger than their corresponding isoelectronic cations. The

charge density for anions will therefore be lower than the isoelectronic cations and electrostatic effects will have less of an impact. To compensate, charge complimentary receptors must also incorporate additional binding methods to compete with solvent interactions, particularly in protic media. In non-polar solvents ion-pairing can be quite important. The pH dependence must be taken into account when binding anions as electrostatic effects and hydrogen bonding ability will be affected by the protonation state of the anion.[11] Hydrogen bonding exhibits a high amount of regioselectivity.[12] Consequently, hydrogen bonding functional groups in receptors must be constructed so that they match the guest anions geometry. This structure must be redesigned if it is desired to fit one of the many possible geometries of anions. Due to the large range of anion sizes and charges they possess varying degrees of hydrophobicity. Knowledge of this anion property must also be incorporated into the anion receptor. These difficulties may explain why cation binding has received far more attention in the published literature than anion binding.[11]

1.1.2 Anion Receptors

In 1968, Park and Simmons[13-15] reported the encapsulation of halide ions within diazabicyclo[k.l.m]alkanes for which $k = l = m \geq 9$. These papers laid the foundation for the field of supramolecular anion binding.[16-18] Although slow initially, interest in anion receptor chemistry has recently exploded.[11, 19-25] Anion recognition can be achieved in a number of ways. The most common reported methods of binding include hydrogen bonding, electrostatic effects, hydrophobicity effects, and metal ion co-ordination.[23] Recently, anion binding with electron deficient pi orbital systems has been investigated creating more possibilities when designing anion receptor systems.[26] Even well known molecules are not exempt from the excitement of anion recognition. Calix[4]pyrroles were recently shown to strongly interact with several anions including fluoride, chloride and phosphate in polar aprotic media.[27]

Due to the multiple modes of binding anions the receptors can possess many forms. Early examples of anion receptors exhibited simple designs such as the elongated diazabicyclo[k.l.m] alkyls of Park and Simmons,[13-15] and the spherical cryptates of Lehn and Graf[16] based upon polyammonium ion structures. Recently reported anion structures are often more complex. Selectivity can be incorporated by integrating compatible symmetry for the receptor to the target anion(s). An example of

this is Anslyn and coworkers' C_{3v} copper complex (Figure 1).[28] This complex demonstrated binding constants in the order of 2.5 x 10^4 M^{-1} for arsenate and phosphate anions in 98:2 H_2O/MeOH at pH 7 (5 mM HEPES) compared to <900 M^{-1} for acetate or less than 20 M^{-1} for nitrate. Kwon and Jeong produced a receptor containing hydrogen bond donors and acceptors capable of very high selectivity for phosphate with a K_a of 1.1×10^5 M^{-1} in CH_3CN. [29] This was in comparison to that of the tetrahedral sulfate anion which possessed a K_a of 1.6 x 10^3 M^{-1} (Figure 2).[29] In addition to designing systems of greater selectivity, there has been much attention given to incorporating reporting groups into anion receptors in order to allow for the sensing of general or specific anions by macroscopic electrochemical or optical responses.

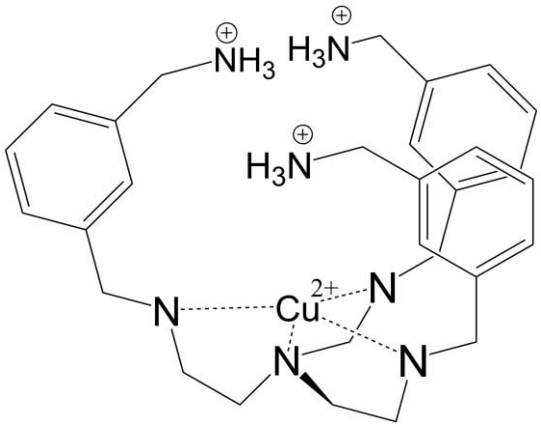

Figure 1. Anslyn and co-workers' copper complex.[28]

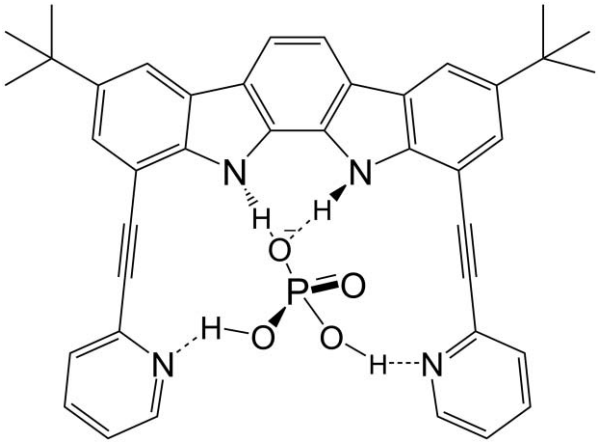

Figure 2. Kwon and Jeongs' phosphate receptor.[29]

When the salph (Schiff base product of salicylic aldehyde and 1,2-phenylenediamine) uranyl complexes **I** and **II** (Figure 3) of Cametti *et al.* were exposed to the presence of hard anions in dimethyl sulfoxide, the absorbance, due to the salph moiety, was altered to an extent that a visible change was observed.[30] Noticing the high selectivity of **I** and the even greater selectivity of **II** due to steric reasons for fluoride, complex **III** (Figure 4) was envisaged and created.[30] This macrocycle incorporates a short ethylenediimine bridge at the metal coordination site and a diphenylmethane unit which inhibited the binding of acetate and phosphate which had bound significantly to complex **I**. The complex bound fluoride to the Lewis acidic uranyl with a binding constant greater than 10^6 M^{-1} with selectivity so great that even the small linear cyanide anion was not bound to a measurable effect.[30]

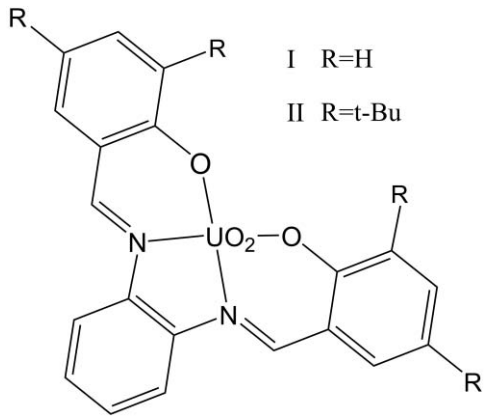

Figure 3. Uranyl complexes **I** and **II** of Cametti *et al.*[30]

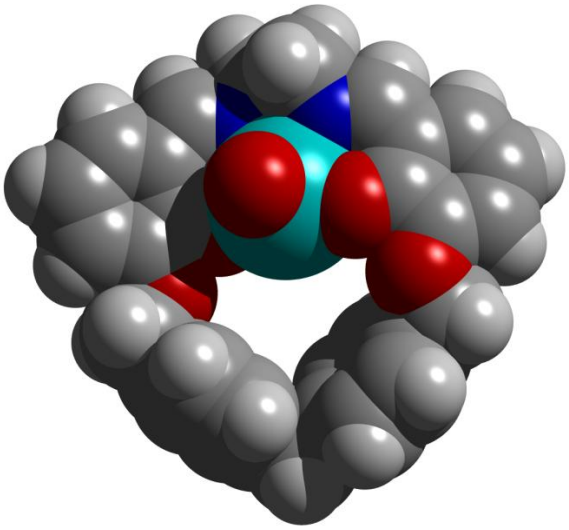

Figure 4. Solid state structure of the uranyl complex **III** of Cametti *et al*. Uranyl bound methanol has been omitted in order to display the binding cavity.[30]

Tasker and his colleagues used a similar ligand to that used for **III** but incorporated tertiary amines in the form of morpholine groups in place of the bridging diphenylmethane unit. This salen system was able to simultaneously bind nickel and its corresponding sulfate anion (Figure 5).[31] Upon co-ordination of Ni^{2+} to the $N_2O_2^{2-}$ salen binding site, the phenol protons were transferred to the morpholine nitrogen atoms to form the zwitterion complex. The protonated nitrogen atoms encourage binding of the sulfate anion via electrostatic and hydrogen bonding effects.[31]

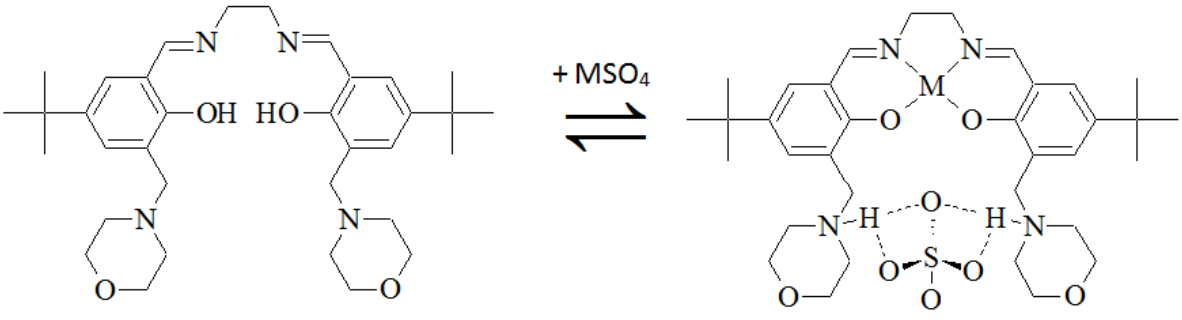

Figure 5. The ligand of Tasker and his colleagues and the ligand binding a cation and anion simultaneously.[31]

A related system was used in 2002 by Plieger *et al.* in which unchained iminophenyl replaced the previously used ethylenediimine linker. In addition, an *N*,*N*'-dimethylhexane-1,6-diamine strap replaced the morpholine groups originally used (Figure 6). When copper salts of sulfate and tetrafluoroborate were introduced into solutions of the ligand, a helicate structure was formed with a metal ligand ratio of 1:1 (Figure 7). The NO^- binding sites of two ligands coordinate to a single copper ion while the second NO^- binding site of each ligand is then bound to a second copper ion in a similar manner. The two metal binding sites are separated by the alkyldiamine straps which form the walls of a cavity between the metal centres. A proton shift from the phenols upon metal binding to the amine nitrogen atoms form the zwitterion complex. The cavity was shown to encapsulate either sulfate or tetrafluoroborate counter anions which were bound covalently to the metals (SO_4^{2-}) or via electrostatic and hydrogen bonding by the internal facing protonated amines (BF_4^-).[32]

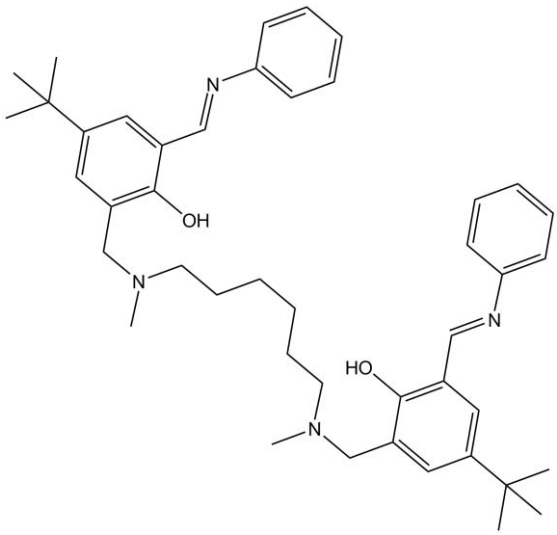

Figure 6. Helicate ligand used by Tasker *et al.*[32]

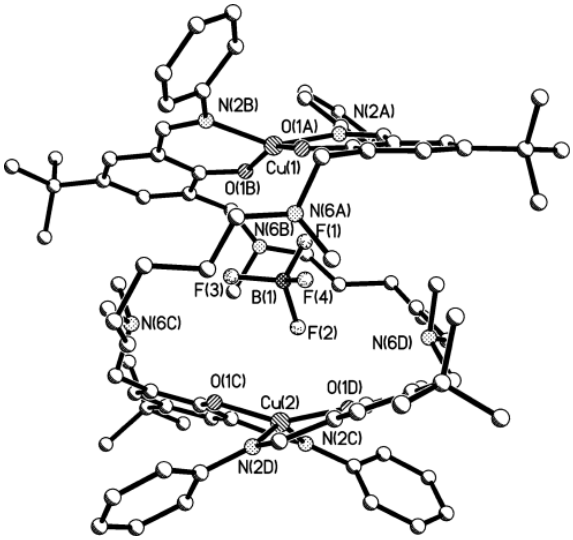

Figure 7. Copper helicate with encapsulated BF_4^-.[32]

Encapsulation of a guest molecule within the interior cavity of a supramolecular host molecule is known as molecular encapsulation and is a sub-branch of supramolecular chemistry. Many examples are present in the literature including hosts for cationic,[33] anionic,[34] and neutral molecules such as endohedral fullerenes.[35] Due to the differing interactions of the host environment, the guest molecule is subject to different chemical characteristics than the free molecule. This creates systems which allow the stabilisation of a guest such as the molecular cage reported by Fiedler *et al.*,

consisting of a gallium tetrahedral cluster (Ga_4L_6).[36] Although the organometallic ruthenium guest is rapidly decomposed in water, the host complex was found to protect its reactive guest from decomposition in water for weeks due to isolation from solvent encounters.[36] By separating a subject anion from solvent interactions, biological molecules such as the Escherichia coli phosphate binding protein (PBP) have been shown to encapsulate anions exceedingly well.[37] PBP possesses 12 hydrogen bonds from both charged and neutral peptide residues deep within the protein. This excludes the phosphate anion from solvent interactions. An aspartate hydrogen bond acceptor repels the similar sulfate anion but binds to protonated phosphates resulting in a very high affinity for phosphate anions. The high selectivity of phosphate over sulfate is a reminder that the molecular encapsulation of anions is subject to the same advantages and restrictions of anion binding.

An interesting feature of Tasker and Pliegers' complexes is that in addition to the anion binding abilities they show they are also themselves copper helicates. Although helicates have been studied extensively,[38, 39] utilisation of helicates as anion encapsulating systems have received little attention. The first example of an anion encapsulated inside a helical structure was the chloride templated circular double helicate reported by Hasenknopf *et al* in 1996.[40] Two years later the first encapsulation of a polyatomic anion was reported by Steel and McMorran.[41] They established the encapsulation of the hexafluorophosphate anion by a quadruply stranded palladium helicate in the solid state (Figure 8) and in dimethyl sulfoxide solution. It was shown by the appearance of two doublets in the ^{19}F NMR that the PF_6^- anion was tumbling within the cavity. In 2006, Kruger and Gotez reported a helicate produced by reaction of iron(II) salts with amide-based bis-bipyridine ligands in a 2:3 ratio.[42] The helicate was found to be templated by the anions introduced via the iron(II) salt. Tetrahedral anions were found to produce a mixture of the *rac*- and *meso*- isomers. Upon addition of tetrabutylammonium chloride (TBACl) the chloride anion was shown to replace the previous anions and convert the helicate so that only the *rac* isomer was present in solution. The two chloride anions were thought to be held within the intrahelical cavity adjacent to the iron(II) centres.[42]

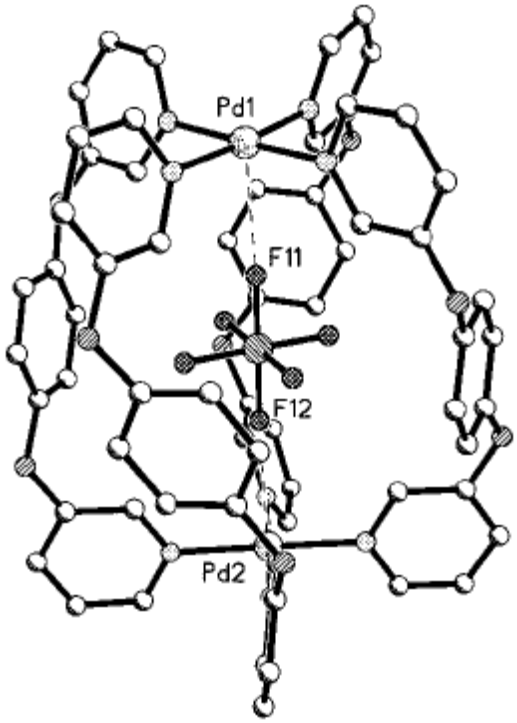

Figure 8. Solid state structure of Steel and McMorrans' helicate with encapsulated hexafluorophosphate ion.[41]

1.2 Analysis and Evaluation of Anion Receptor Systems

Once an anion receptor has been synthesised, it is necessary to evaluate how effectively an anion will bind to it. A number of techniques are valuable in doing this. Electrospray ionization mass spectrometry (ESI-MS) has become a standard technique for the analysis of large non-volatile macromolecules including proteins, and supramolecular complexes.[43] The technique of ESI-MS involves pumping a dilute solution of analyte through a capillary with a large potential (2-5 kV) across the capillary tip. The potential may be positive or negative and results in charge separation at the liquid surface. Droplets with excess charge are expelled from the capillary into the mass spectrometer. These droplets are split until vapour phase ions are obtained. These ions are analysed for mass to charge ratio by the mass spectrometer.[44] It has been shown to be very useful in analysing complexes with multiple counter ions as the weak ionising nature of ESI-MS allows counter ions to be sufficiently removed from the analyte. A number of peaks are then observed which are representative of the parent ion with a mass to charge ratio dependent on the number of ions removed. Bruere's work on a dicopper helicate with perchlorate counterions demonstrates this well.[45]

Conductivity studies are traditionally used to determine the stoichiometry of coordination complexes. They can also determine if an electrolyte is weakly or strongly

dissociated. If an anion bound receptor is found to be a weak electrolyte, then the receptor binds strongly to the bound anion. The conductance of electrolyte solutions is dependent on the concentration of the ions, charges and mobilities, and it differs for strong and weak electrolytes. The conductance increases with the concentration of ions, so by comparing the conductivity with similar complexes of known ion stoichiometry, the number of anions present can be estimated.[46] This method however cannot differentiate between the complex stoichiometries of $[ML_n^{2+}][A^-]_2$ and $[M_2L_{2n}^{4+}][A^-]_4$. This can be achieved by recording the change in equivalent conductance (Λ_e) with the square root of the equivalent concentration (c_e).[47] The change in Λ_e with respect to concentration is giving by the Onsager equation;

$$\Lambda_e = \Lambda_0 - (A + \omega B \Lambda_0)\sqrt{c_e} \quad \textbf{(1-1)}$$

The concentration coefficient ($A+\omega B\Lambda_0$) incorporates the charges of the ions involved and thus allows the determination of the above electrolyte types. Usually Λ_e is plotted as a function of $\sqrt{c}$ to give the equivalent conductivity at infinite dilution (Λ_0). Then by plotting Λ_0 - Λ_e as a function of $\sqrt{c}$, the gradient can be compared to known electrolytes under similar conditions to establish the electrolyte type for the investigated complex. This method enables several complexes to be compared on the same set of ordinates.[47, 48]

It is useful to determine how strongly an anion is bound to a receptor. Generally this is accomplished by the calculation of stability constants for the association of the anion guest. If an anion is titrated into a solution of a molecule which possesses sufficiently strong interactions to bind the said anion, then the equilibrium;

$$rR + aA \rightleftharpoons [R_rA_a] \quad \textbf{(1-2)}$$

is established, where A and R represent the anion and receptor molecule respectively. The values of *a* and *r* can be determined by constructing a mole-ratio plot or via the method of continuous variation.[49, 50] The mole-ratio plot is constructed by monitoring a physical change that occurs when anions interact with the host as a function of the equivalents of added anion. If the binding is significantly strong, a sharp change in this

property should occur at the stoichiometric binding ratio. Weaker binding however causes a less distinct change, resulting in a curve over which the tangents can be extrapolated to determine the predominant species. The method of continuous variations, often referred to as a job plot, involves plotting the changes in the measured property as a function of the mole equivalents of either the anion or receptor so that the total concentration of both components at any point is constant. Once adjusted for the presence of reactants, the plot will show a maximum or minimum at the receptor-anion stoichiometry, corresponding to the product. The most commonly used properties are ^{1}H NMR shifts and UV-visible absorbance.

From equation 1-2 the overall formation constant of anion-receptor binding is given by the equation;[50]

$$\beta_{ra} = \frac{[\mathrm{R}_r\mathrm{A}_a]}{[\mathrm{R}]^r\,[\mathrm{A}]^a}$$

(1-3)

In order to calculate the formation constant, the concentration of one of the species must be known. By titrating a solution of the anion into a solution of the host, the desired concentration for a series of solutions of known reactant concentration is determined. The concentrations in the above equation can then be calculated. The formation constants are derived by best-fitting the experimental data with a chemical model of the equilibrium system. These initial values are then refined using a non-linear least squares analysis. Potentiometric, NMR chemical shifts measurements, and spectrophotometry including absorbance and fluorescence measurements are the most frequently used experimental methods for calculating formation constants.[49]

Potentiometry is the most accurate and widely utilised technique available for the study of ionic equilibria. Selective electrodes have been prepared for many types of ions. The most studied system is the hydrogen ion selective glass electrode. Calibration of the recorded pH of a solution against the hydrogen ion concentration allows the $[H^+]$ to be determined for a solution containing a proton receptor. By monitoring the change in concentration of free protons as a function of change in acidity, the protonation constants of a receptor can be determined in a similar way to the formation constants described above. The use of metal ion and anion selective

electrodes allows for the determination of metal complex formation constants in a similar way.[50]

The calculation of formation constants and stoichiometries by UV-visible spectrophotometry is quite common due to many anion receptors naturally exhibiting absorbance over the wavelengths of 900 to 200 nm. UV-visible absorbing moieties can also be incorporated into an anion receptor system. The advantage of possessing UV-visible absorption is that upon anion interaction with the receptor, the electronic environment of the molecule may be disturbed enough to exhibit a change in the UV-visible spectrum. This change can be monitored as a function of anion addition in order to give information about how strongly the anion is interacting with the receptor or if an anion is interacting at all. It is assumed that the Beer-Lambert law applies, so the reactants are restricted to dilute concentrations. Fluorescence is also applicable provided the emission spectra are sufficiently affected by guest interaction and assuming that the scattered light intensity is directly proportional to the species' concentrations.[49] The formation constant may be calculated at a single wavelength over which the guest species produces an absorbance change. If the species present are spectroscopically similar or they interact with one another, this technique is less reliable. By recording the entire UV/visible spectrum formation constants can be estimated more reliably. Information about the host-guest system is contained over the range of the recorded spectrum and each digitised data point can be considered as a separate variable. Multivariate analysis can be applied to this data to identify the patterns which represent the required information.[51] SPECFIT/32™ is one such multivariate data analysis program which allows modelling and fitting of chemical kinetics equilibrium titration data. This program allows analysis of data sets consisting of simultaneous measurements of absorbance as a function of wavelength and an independent variable such as time, pH, or titrant concentration.

For receptors which possess nuclei with non-zero quantum spin, nuclear magnetic resonance (NMR) spectroscopy can be utilised. Most commonly this will involve analysing the chemical shifts of protons as they are affected by the interaction with binding anions. As chemical exchange is rapid on the NMR time-scale, the individual chemical shifts ($\bar{\delta}$) represent the mole-fraction weighted average of the shifts of the nuclei involved. The change in chemical shift can be analysed by best-fitting the experimental data to the appropriate chemical model. This model will be based on the determined reaction stoichiometry which can be determined via the method of

continuous variation of mole-ratio plots. These involve the change in chemical shift of effected nuclei which is multiplied by the mole-ratio of guest for the job plot.[49] An advantage of NMR shifts is that information regarding individual hydrogen-bond donors is recorded giving information on the method and orientation of binding. This makes NMR a very powerful technique for investigating anion-receptor systems as it indicates where in the receptor molecule binding occurs in solution. Despite the advantages of NMR for the study of binding constants, due to limitations such as higher required solubility and the inability to study paramagnetic compounds, optical spectroscopy surpasses NMR as the most widely applied technique for determining binding constants.[49]

The above techniques all involve studying the receptor guest interaction in solution. If NMR is not possible on the host-guest system under study then crystallography offers an alternative method to determine how anions bind to a host complex. These interactions are assumed to approximate those of the solution interactions. It is of course limited by the ability to grow suitable crystals of an anion-receptor complex. X-ray crystallography enables the determination of the precise spatial arrangement of atoms in a chemical compound in its crystalline state. This spatial data includes information on the connectivity, conformation, bond lengths and bond angles of molecules. Additionally, it implies the stoichiometry, density, symmetry and the three dimensional packing of atoms in the solid state. With such a girth of information available from this technique, it is little wonder why so much effort is put into growing X-ray quality molecular crystals. If successfully produced, the crystals contain a basic pattern of atoms which is repeated in three dimensions. Due to this repeating nature, irradiating the crystal lattice with radiation and recording angles of diffraction allows for the determination of the interatomic distances using the Bragg equation ($2d\sin\vartheta=n\lambda$). [52]

1.3 Project Objectives

This project investigated the dicopper helicates synthesised from the salicylaldimine ligands of Tasker and Plieger. As copper(II) is paramagnetic, NMR could not be utilised. The complexes exhibit excellent chromophore activity due to the salicylaldimine moiety of the helicates. This absorbance undergoes a change upon the addition of anions which allowed investigation via UV-visible spectroscopy. The anion binding ability of a dicopper ‘anion free’ receptor was therefore investigated using UV-

visible titrations. The titrations were performed in collaboration with electrospray ionization mass spectrometry which provided additional support for solution binding of the anions. During the titrations, it was assumed that the amines are protonated independently and at a similar pK_a due to their wide geometric dispersion. To investigate this hypothesis, potentiometric titrations on the 'anion free' iminophenyl system were performed. Crystallisation attempts were made to provide insight into the solid state properties of the complexes. X-ray studies on a similar ligand system to those used in this work suggest that ligands of this general type do not form a helicate upon reaction with copper chloride. This was investigated for the two ligand systems used. Conductivities of the helicates were also accurately measured to establish the utility of this technique for these large complexes.

Chapter 2

Titrations of $[Cu_2(L^1\text{-}2H)_2]$

2.1 Introduction

Plieger *et al.* investigated the structure of helicates formed between $\mathbf{L^1}$ (Figure 9) and copper(II) perchlorate, sulfate tetrafluoroborate[32] and nitrate.[53] Coordination of the sulfate compound to the copper centres was observed in the solid state but was absent from the remaining anion complexes determined. This thesis was aimed at investigating the solution interactions between a selection of anions and the helicate formed between copper(II) and $\mathbf{L^1}$.

By reacting $\mathbf{L^1}$ with copper(II) acetate it was found that a neutral anion free version (**1**≡$[Cu_2(\mathbf{L^1}\text{-}2H)_2]$) was produced (synthesis contained in Chapter 6). The high basicity of acetate prevents the protonation of the amine groups of $\mathbf{L^1}$. This results in a neutral helicate with no encapsulated anion (Figure 10). This is referred to as the free base form of the complex. The large change in UV-visible spectral data upon addition of sulfuric acid to **1** and the ESI-MS spectra of the **1**-H_2SO_4 solutions suggested the encapsulation of the sulfate anion. Thus this technique has been employed to study the ability of anions to bind to the ammonium form of **1**.

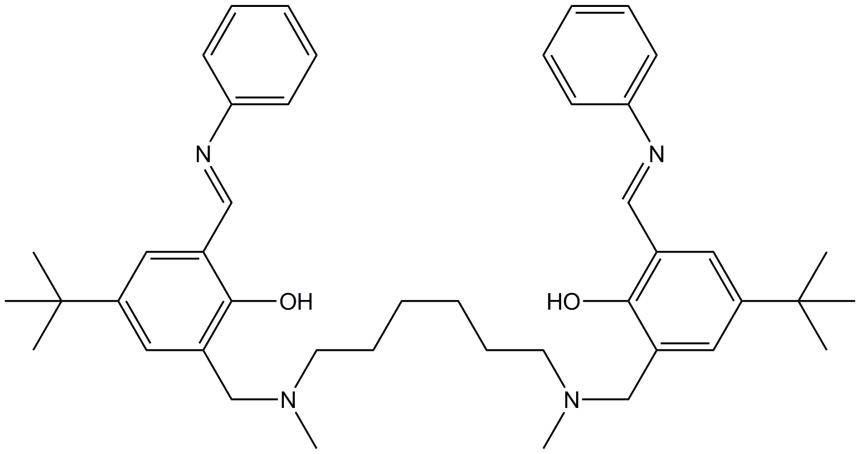

Figure 9. The ligand utilised by Plieger *et al.* and within this study. Referred to as $\mathbf{L^1}$ throughout this text.

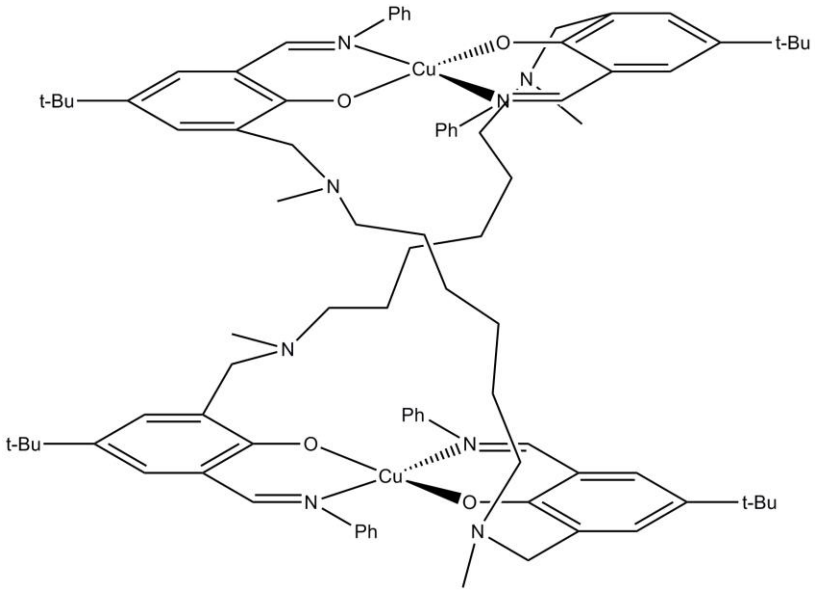

Figure 10. Proposed structure of **1** used in the UV-visible titrations in this chapter.

2.2 Results and Discussion

*2.2.1 Absorption Spectra of **1***

Preliminary titrations of solutions of **1** with methanoic solutions of sulfuric acid indicated that anion binding was far less effective in this solvent. This strongly polar protic solvent may have decreased binding due to hydrogen bonding with the protonated amines or possibly because of solvent co-ordination to the copper centres. As sulfate is

strongly hydrated in aqueous solution by hydrogen bonding[54] it is quite probable that methanol may be strongly solvating the sulfate anion, inhibiting encapsulation by **1.**

The solvent chosen for the titrations was isopropyl alcohol (IPA). IPA solutions of **1** showed a slow reproducible change in UV-visible absorption until a fixed point which could be restored after drying and reproducing the solution. ESI-MS evidence of solvent co-ordination to the similar oxime ligand system suggested that encapsulated IPA could be causing this spectral change. To minimise this potential solvent co-ordination, the complex was dried under vacuum for one hour prior to preparation of the titration solutions and the titrations were performed immediately after. After the titrations were performed, evidence was found for the immediate protonation of **1** upon dissolving in IPA (see Section 2.2.5). This protonation allows for hydrogen bonding toward the phenolate moieties which would result in a change in the UV-visible spectrum. This phenomenon may be the basis of the absorbance change noted above and might not necessarily be due to solvent coordination.

The spectra of the complex exhibited two intense ultraviolet spectral bands with maxima at 233, 288. An intense spectral band was also exhibited in the visible region at 405 nm (Figure 11). The latter band was responsible for the yellow colour of their solutions. The bands showed very high molar extinction coefficients of 9.3, 7.3, and 2.9 x 10^4 M^{-1} cm^{-1} respectively. The three bands have been assigned as ligand based by reference to the literature.[55] Electron transfer from the π to π_2^* orbitals resulted in the 288 nm absorption band. The electron transfer from the π to π_1^* orbitals was responsible for the band at 405 nm. This band is characteristic of the phenolate moiety. As a result, any interaction of anions or solvents with the coordinated metal would be expected to affect this absorption band due to perturbation of the phenolate π system.[55]

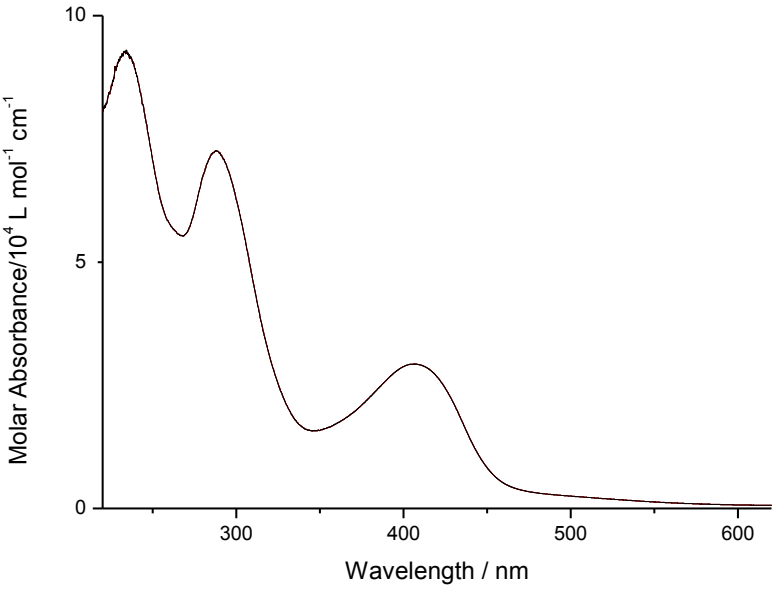

Figure 11. UV-Visible absorbance spectra of **1** in IPA. The band at 405 nm is characteristic of the phenolate $\boldsymbol{\pi}$ to $\boldsymbol{\pi_1^*}$ electron transition.

As the replication of the absorption of the 233 nm band showed some inconsistencies under identical experimental conditions, the spectrum was recorded from 900 to 250 nm for the titration experiments. Acid was titrated into solutions of the complex and the solution stirred. The UV-visible spectra were recorded immediately after each titration in order to investigate the effect of acid addition on the UV-visible absorption of the complex solution. The anions were added as their conjugate acids because protonation of the complex was necessary for the anions to be bound. It was assumed that protonation occurred fast on the UV-visible absorbance timescale. The titration mixtures possess a small amount of water in combination with acid. Although these components are known to catalyse hydrolysis of imine compounds, past research suggests that the presence of metal-imine bonds significantly increases the stability of the imine bond in the presence of water. This effect has been observed to be greatest for copper-imine compounds suggesting **1** was stable under the titration conditions used.[56] The acids titrated were; sulfuric, phosphoric, perchloric, tetrafluoroboric, hydroiodic, hydrobromic, hydrochloric and nitric acids. The tetrabutylammonium dihydrogen phosphate salt was also titrated in order to investigate the more complex spectra resulting from phosphate binding.

*2.2.2 Sulfuric Acid Titration of **1***

Upon addition of sulfate to a solution of the complex the 288 and 405 nm bands were both hypsochromically shifted by 13 nm and 14 nm respectively. Isosbestic points formed up until two equivalents of added acid at 278, 357 and 407 nm (Figure 12). The presence of isosbestic points typically signifies the equilibrium of two coloured species in solution. The coloured product formed was the anion encapsulated species based on comparison with the UV-visible absorbance of the directly synthesised sulfate encapsulated dicopper helicate and ESI-MS data of the titration solution which showed the presence of a dominant $[SO_4 \subset Cu_2\mathbf{L}^1_2]^{2+}$ peak at 666.92 *m/z*. Construction of a mole-ratio plot at 287 nm suggested the formation of one complex until four equivalents of added acid. At this point, the change in absorbance with respect to acid addition began to decrease more rapidly. A job plot was constructed for changing ratios of **1** and sulfuric acid. It showed a peak at 0.5 mole ratio of acid showing that a dominant product possessing one to one stoichiometry was being produced. Multivariate analysis utilising the programme SPECFIT/32™ modelled the data well assuming a one to one stoichiometry. The predicted spectra are displayed in Figure 13. As can be observed by comparison of the predicted and recorded spectra (Figure 12), the model produced by SPECFIT/32™ appears very applicable to the raw data. A calculated log K value of 5.07 shows strong binding of the sulfate containing complex. It is of similar magnitude to the complex by Chantelle *et al.* in dimethyl sulfoxide which possessed a total of eight hydrogen bonds towards the sulfate anion in addition to electrostatic effects of proximity to the palladium centre.[57] Structural evidence supported a strong interaction of sulfate with the copper centres. The Cu-O-SO_3 distance of 2.18 Å was approaching that of the phenolate copper bond of 1.89 Å.[32] The log K values, stoichiometry, and the dominant peak observed in the ESI spectrum for titrations of **1** with the various acids used are summarised in Table 1.

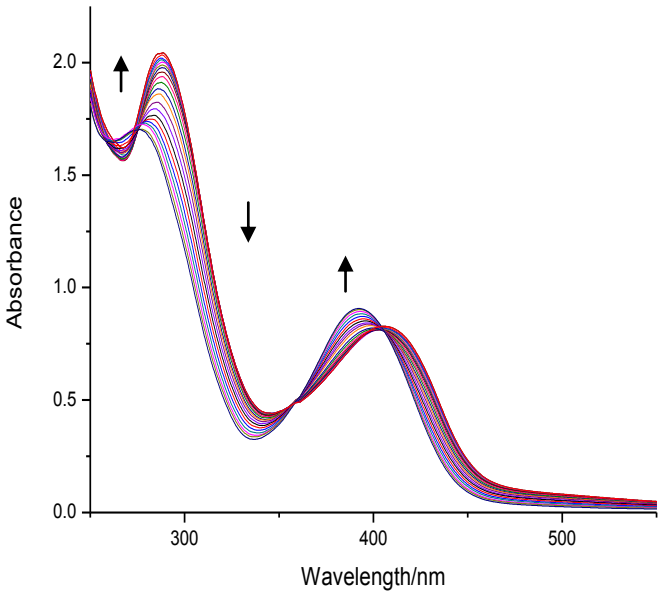

Figure 12. Recorded UV-visible titration spectra of **1** upon titration of up to two equivalents of H_2SO_4. Each spectrum corresponds to the addition of 0.1 equivalences. Arrows indicate relative intensity changes.

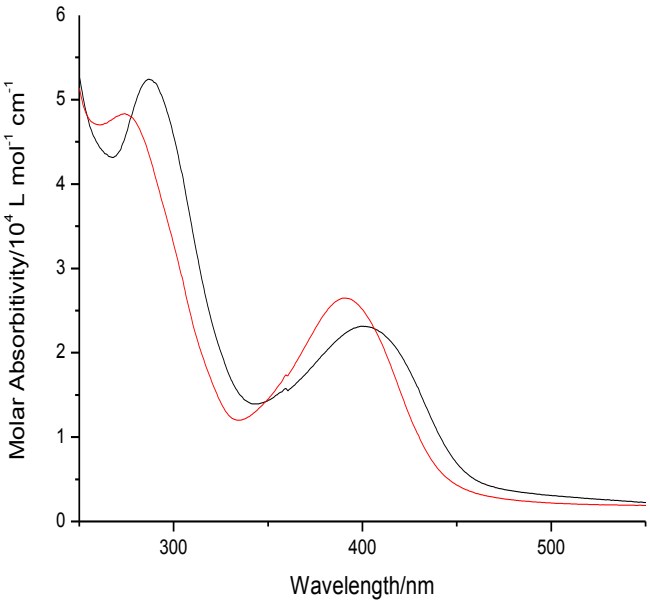

Figure 13. Predicted molar absorptivity spectra of the **1**:sulfate adduct (red) and of **1** (black).

Acid	Log K	Stoichiometry	ESI-MS Peaks
H_3PO_4	4.30 ± 0.02	1:1	$[PO_4\subset\mathbf{1}H_4](H_3PO_4)_x^+$, x=0-2
$H_2PO_4^-$	4.34 ± 0.13	1:1	$[HPO_4\subset\mathbf{1}H_4]^{2+}$
H_2SO_4	5.07 ± 0.24	1:1	$[SO_4\subset\mathbf{1}H_4]^{2+}$
HBF_4	3.03 ± 0.29	1:1	$[BF_4\subset\mathbf{1}H_3]^{2+}$
$HClO_4$	3.38 ± 0.12	1:1	$[ClO_4\subset\mathbf{1}H_3]^{2+}$
HNO_3	2.95 ± 0.04	1:1	ǂ
HI	*	1:1	$[LCuI]^+$
HBr	3.12 ± 0.36	1:1	$[LCuBr]^+$
HCl	*	*	$[LCu_2Cl_x]^+$,x=2,3

*; not determined, ǂ; no evidence of encapsulation/binding via ESI-MS

Table 1. The log K, stoichiometry, isosbestic points and the dominant helicate peaks observed in the ESI-MS spectra for titrations of **1** with the various acids used.

*2.2.3 Acid Titrations of **1***

The acids $HClO_4$, H_3PO_4, HBF_4, HNO_3, HCl and HBr were titrated against solutions of **1** (see Appendix B for spectra). The solid state structures of encapsulated sulfate,[32] tetrafluoroborate,[32] perchlorate,[45] and nitrate[53] of **1** had been previously determined. Additionally, the crystal structure of iodide encapsulated within **1** is contained within this report (Section 2.2.8). These structures demonstrate the encapsulation of the said anions within the helical cavity generated between the copper centres. There are two important underlying assumptions for the titrations performed. The first assumption is that in solution, the titrated anion is capable of entering this cavity. The second underlying assumption is that the spectral change is solely the result of interactions within the cavity. It is assumed that spectral changes arising from interactions with solvent or counter ions exterior to the molecule are minimal. Crystals of the phosphate encapsulated structure were poorly diffracting so the crystal structure could not be refined. The structural similarity of phosphate to sulfate and the crystal structure of phosphate encapsulated within **2**[58] suggests that phosphate will also be bound within the cavity of **1**.

The acid titrations attempted resulted in similar changes to the spectrum of **1** as in the previously described case for H_2SO_4 addition for the majority of anions. Namely, a hypsochromic shift of the $\pi_1^*\leftarrow\pi$ and $\pi_2^*\leftarrow\pi$ electronic bands. Hydroiodic acid

possesses a yellow colour which begins to dominate the absorbance spectra of **1** above four equivalents of added acid (Figure 14). This was included in the multivariate analysis but restricts the use of measurements recorded to 6.0 equivalents of added acid due to high absorption. Binding constants were attempted for iodide binding, however a satisfactory fit was not produced and no value could be obtained. When more concentrated solutions of the iodide titration of **1** were prepared, substantial precipitation was observed immediately. Although this would occur to a lesser extent for the dilute titrations performed for UV-visible analysis, this precipitation may explain why the stability constants for iodide encapsulation could not be determined.

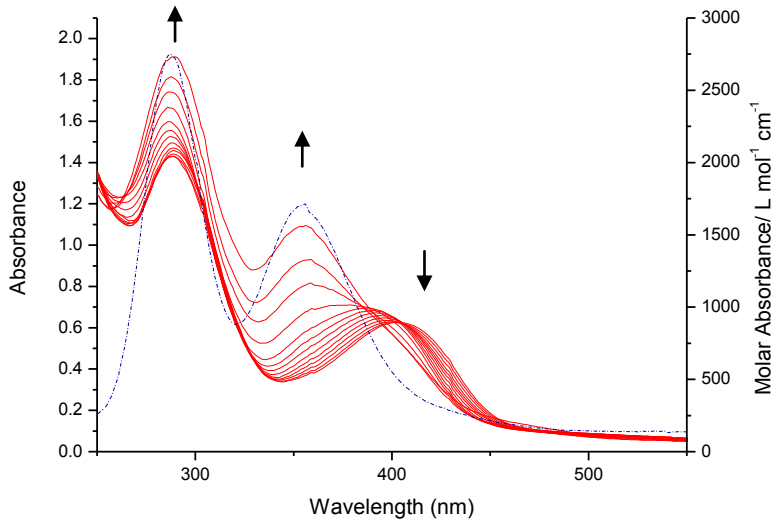

Figure 14. Recorded UV-visible titration spectra of **1** upon titration of up to six equivalents of HI. Each spectrum corresponds to the addition of 0.5 equivalences. Arrows indicate relative intensity changes. The molar absorbance of HI is overlaid in blue (dashed, right axes).

The method of continuous variation for titrations of **1** with the various acids with the exception of hydrochloric acid are shown in Figure 15. These consisted of a single peak situated at 0.5 mole ratio of acid suggesting the presence of one dominant species consisting of a 1:1 stoichiometry of acid and free base complex. When applied to the hydrochloric acid titration there were two separate peaks (~0.6 and 0.8) suggesting that there was not a simple equilibrium between the two coloured species occurring.

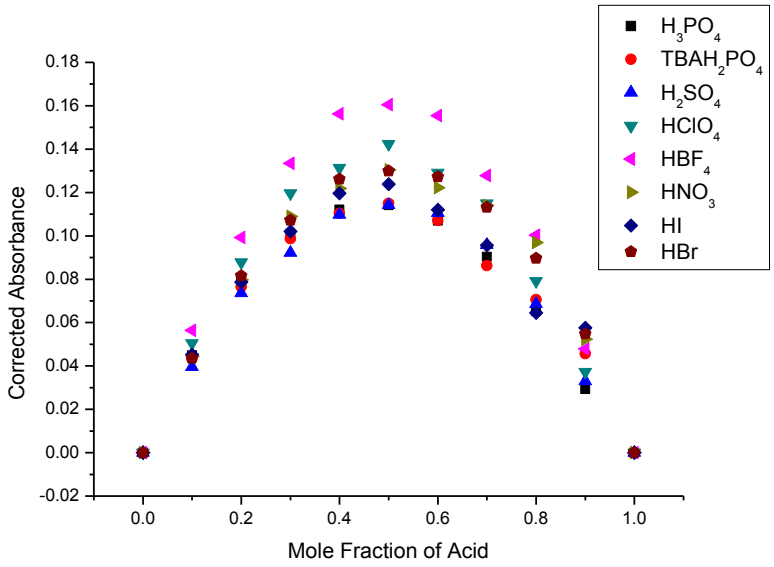

Figure 15. Method of continuous variation applied to the acids titrated against **1.** The absorbance was recorded at the phenolate absorption peak.

In order to investigate what was occurring upon addition of HCl, synthesis of the copper(II) chloride complex of $\mathbf{L^1}$ was attempted. ESI measurements of the reaction mixture showed the presence of a small amount of helicate. In addition, a large proportion of $\mathbf{L^1}Cu_2Cl_x$ species where x is between two and four were present (Figure 16).

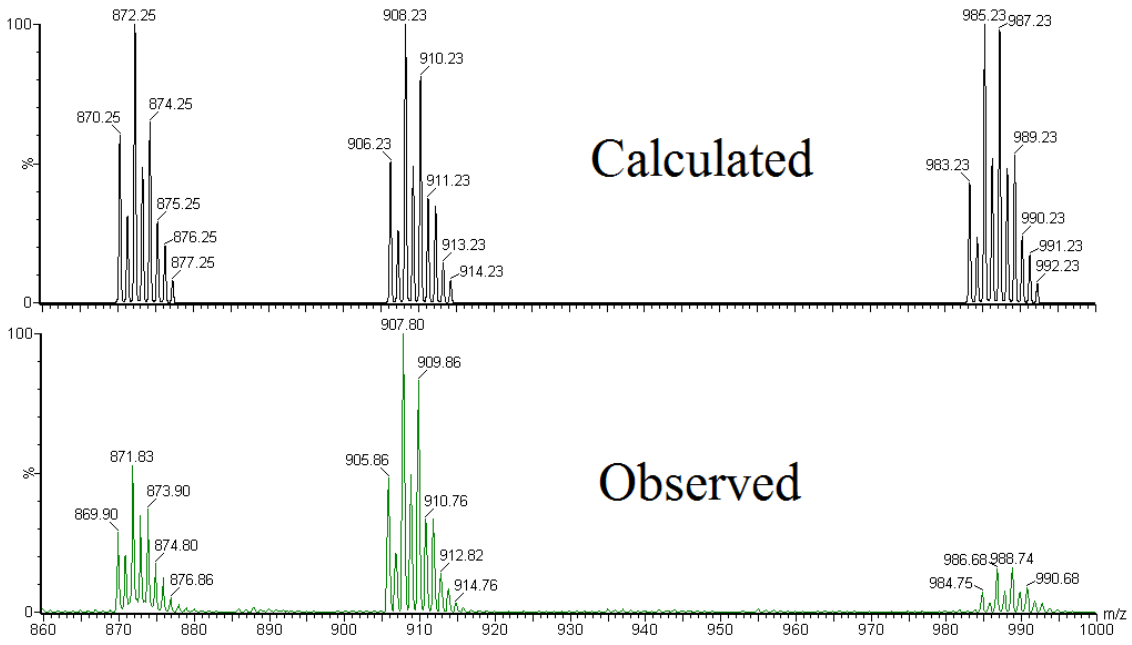

Figure 16. The ESI-MS of attempted $[Cl\subset\mathbf{1}H_4]^{3+}$ synthesis. From left to right, the peaks are representative of $[(\mathbf{L^1}\text{-}H)Cu_2Cl_2]^+$, $[\mathbf{L^1}Cu_2Cl_3]^+$ and $[(\mathbf{L^1}+H)Cu_2Cl_4.MeCN]^+$.

The production of LCu_2Cl_x species had been observed previously with the ligand $\mathbf{L^3}$ (Figure 17). This ligand is similar to $\mathbf{L^1}$ but oxime groups are present in place of iminophenyl groups. Benzyl functionality also replaces the methyl groups on the amines. Additionally the alkyl chain only contains five methylene carbons in comparison to the six present in $\mathbf{L^1}$. When reacted with copper(II) chloride $\mathbf{L^3}$ produced a complex of type LCu_2Cl_4 which immediately precipitated from the reaction solution. The complex contained chloride bound directly to the metal centres as shown by the crystal structure (Figure 18).[58] The ESI spectra of the HCl titration produced similar results. There was a small amount of the helicate present and evidence of small amounts of $\mathbf{L^1}Cu_2Cl_x$ species with x values of two and three. A successful model assuming either a 1:1 or a 1:4 stoichiometry could not be fit using the SPECFIT/32™ software for HCl addition. It was concluded that a complex equilibrium was established in solutions of **1** and HCl creating a mixture of helicate and $\mathbf{L^1}Cu_2Cl_x$ species.

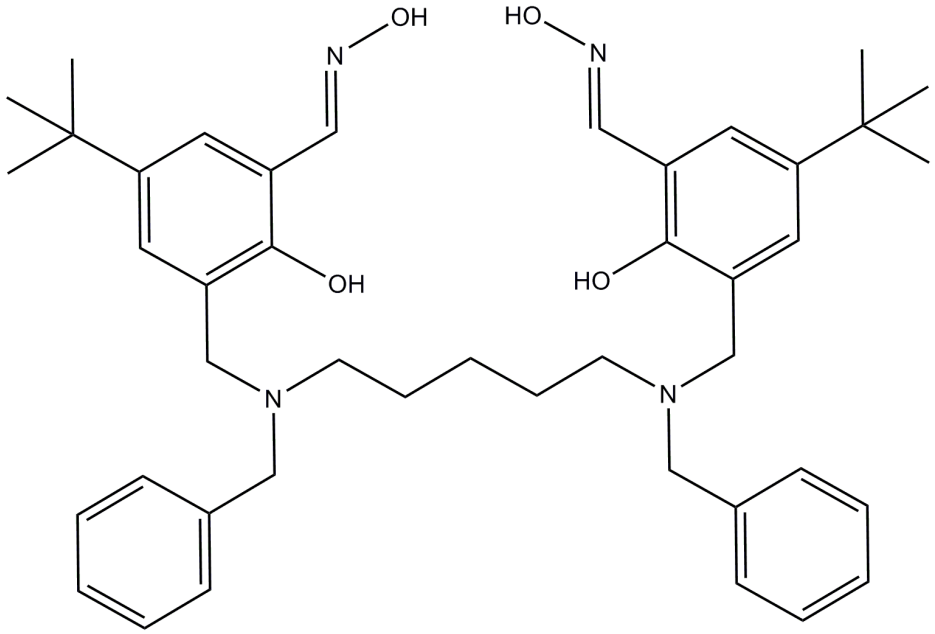

Figure 17. $\mathbf{L^3}$ ligand used by Forgan and Plieger. $\mathbf{L^3}$ is similar to $\mathbf{L^2}$ but with benzyl groups in place of the methyl groups on the amines and only 5 methylene groups in the alkyl linker chain.[58]

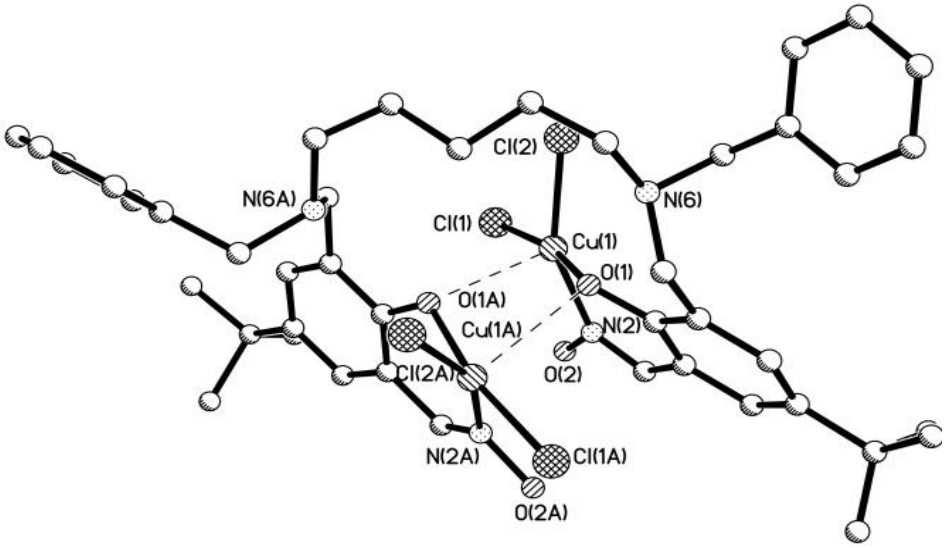

Figure 18. Crystal structure of $L^3Cu_2Cl_4$ produced by Forgan and Plieger. It shows the binding of copper(II) chloride to each salicylaldimine moiety of L^3.[58]

Phosphoric, perchloric, hydrobromic and nitric acid produced satisfactory fits using SPECFIT/32™. Their binding constants are summarised in Table 1. Figure 19 plots $\log_{10}K$ as a function of anion size (as reported by Jenkins *et al.*[59]). Within experimental error there is an increase in binding with increasing anion volume. The strongly co-ordinating anions phosphate and sulfate exhibit far greater stability constants than the remaining anions.

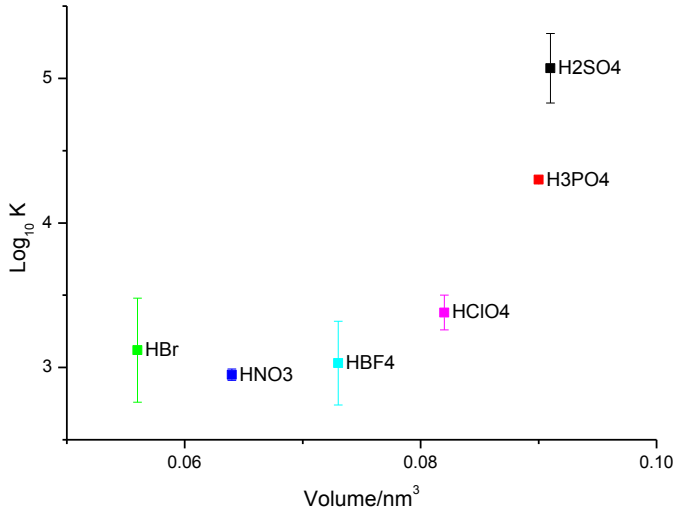

Figure 19. The calculated stability constants for anions binding within the cavity of **1** as a function of anion volume. The anion volumes used are taken from the paper by Jenkins *et al.*[59]

*2.2.4 Phosphate encapsulation within **1***

The titration of phosphoric acid differed from the other acids titrated. Isosbestic points for H_3PO_4 addition lasted until one equivalent of added acid as shown in Figure 20. Upon further acid addition, a new set of isosbestic points formed after two equivalents of phosphoric acid (Figure 21). Further acid addition resulted in no further spectral changes. The formation of a single species until one equivalent of added acid implies the production of a neutral phosphate encapsulated complex. The protonation of phosphate was thought to be causing the formation of the second set of spectra. To test this, titrations of tetrabutylammonium dihydrogen phosphate ($TBAH_2PO_4$) were performed against **1**.

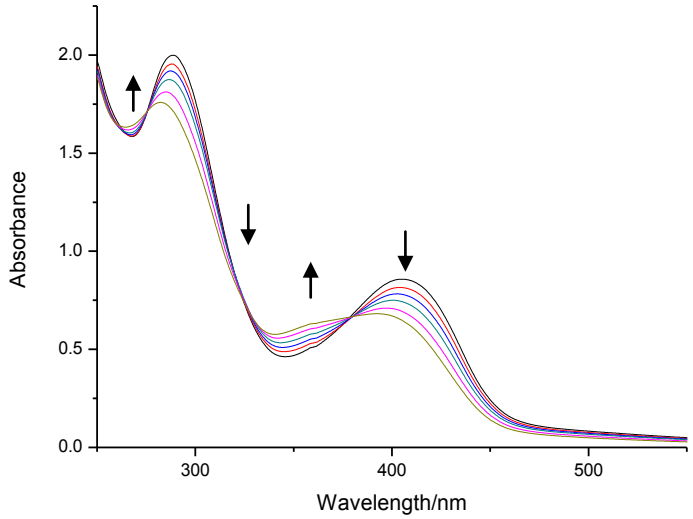

Figure 20. Recorded UV-visible titration spectra of **1** upon titration of up to one equivalence of H_3PO_4. Each spectrum corresponds to the addition of 0.2 equivalences. Arrows indicate relative intensity changes.

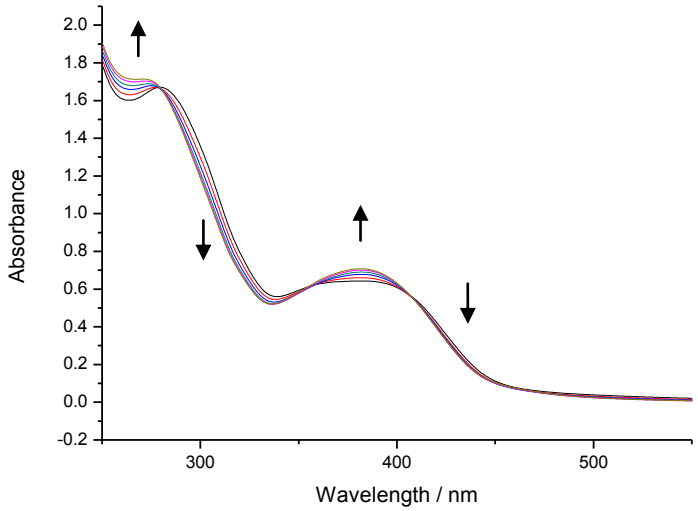

Figure 21. Recorded UV-visible titration spectra of **1** upon titration of two to five equivalences of H_3PO_4. Each spectrum corresponds to the addition of 0.5 equivalences. Arrows indicate relative intensity changes.

The spectra formed from the titration of **1** with up to two equivalents of $TBAH_2PO_4$ (Figure 22) are very similar to those upon addition of one equivalent of phosphoric acid (Figure 20). There is no formation of a second set of spectra and isosbestic points observed for the TBA salt system. As the initial spectra were the same for the two phosphate titrations, it is assumed the initial complex formed is the same for each system. Coordination to the copper metal is expected for this strongly coordinating anion and this is reflected in the large changes in the UV spectra. Similar large changes were observed in the sulfate titrations. The pK_a values for phosphoric acid in aqueous solution are 2.1, 7.4 and 11.9.[60] **1** is expected to be fully protonated upon acid addition (see section 2.2.5). Due to the poor proton donor ability, weaker Lewis base behaviour and lower relative permittivity constant of IPA[61] in comparison to H_2O the phosphoric acid pKa values are expected to increase from the values obtained in water. This results in at least a single deprotonation of phosphoric acid with a proportion of the doubly deprotonated species formed. A one to one ratio of either phosphoric acid or tetrabutylammonium phosphate to helicate will therefore result in monohydrogen phosphate encapsulated within the tetraprotonated helicate.

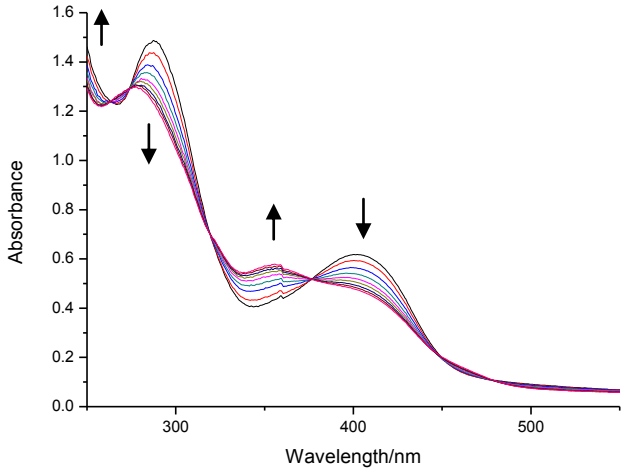

Figure 22. Recorded UV-visible titration spectra of **1** upon titration of up to two equivalents of $TBAH_2PO_4$. Each spectrum corresponds to the addition of a 0.25 equivalence of acid. Arrows indicate relative intensity changes.

The additional proton in the phosphoric acid system and the fact that $H_2PO_4^-$ is a weaker acid than the H_3PO_4 species will result in the acidity of the solution increasing more rapidly for the phosphoric acid addition. This decrease in pH could protonate the encapsulated phosphate molecule forming $[H_2PO_4 \subset \mathbf{1}H_4]$. This will result in a rearrangement of the helicate due to previous hydrogen bonding from the amines to the phosphate becoming unfavourable. The metal-anion co-ordination will still be the dominant binding mechanism. **1** has been shown to be capable of internal hydrogen bonding from the protonated amines to the phenolate oxygen atoms.[53] The structural rearrangement due to the protonation of $H_2PO_4^-$ could result in hydrogen bonding to the phenolate oxygen atoms by the protonated amines. This would result in a change in the phenolate absorption as was observed. A crystal structure of phosphate encapsulated in **1** at a low pH would be excellent support for this but was not obtained. The addition of a large excess of a strong acid (containing a non-interacting spectator anion) into a $TBAH_2PO_4$ titration may cause changes that align with the phosphoric acid observation. Time restraints unfortunately meant this experiment could not be performed.

*2.2.5 Effect of Protonation of **1** on Anion Binding*

Analysis of the phosphoric acid and tetrabutylammonium dihydrogen phosphate titrations highlighted the difficulties present concerning the protonation of **1**. As the

utilised acids (excluding phosphoric) are exceptionally strong, (Table 2) anion protonation will not occur. Therefore the rearrangement of the helicate and change in absorbance as observed for phosphoric acid addition will not occur for these acids.

Acid	pK_a
Phosphoric	2.1, 7.2, 11.9
Nitric	-1.64
Sulfuric	-3, 2.0
Hydrochloric	-7
Perchloric	-8
Hydrobromic	-9
Hydroiodic	-11

A pK_a value for HBF_4 has not been determined. HBF_4 is classified as a superacid[62] so that it will be completely dissociated during the titrations.

Table 2. Aqueous pKa values of the acids used in this study.[60]

The helicate amines are separated by a minimum of six atoms. At these distances the protonation of the amines can be considered as independent events.[63] The macrocycle [20]aneN_4 which possesses four methylene groups between its nitrogen atoms provides support for this. The pK_a values for this macrocycle are 11.8, 11.4,10.6 and 8.9 in water so that it is in its tetraprotonated form at neutral pH.[64] The autodissociation (K_s) constant for 10-70% aqueous IPA solutions has been determined using potentiometry by Kiliç and Aslan.[65] They found a strong correlation between the concentration of IPA and the solution pK_s. Assuming this relationship continues to pure IPA solution, extrapolation to 100% IPA produces a pK_s of 15.21 ± 0.07. From this value the pH of a pure IPA solution is 7.61 ± 0.07. The larger amine-amine distance in **1** compared with [20]aneN_4 suggests a greater independence of amine protonation than observed for [20]aneN_4. The pK_a of the forth amine protonation will therefore be higher than 8.9 found for [20]aneN_4. Additionally, the pK_a values will be higher in the IPA medium as it is a weaker Lewis base and possesses a lower relative permittivity[61] than water. Using the value of 8.9 as a lower limit for the pK_{a4} of **1** results in 95% of the helicate being in its tetraprotonated form upon dissolving in IPA. The helicate can therefore be assumed to be tetraprotonated upon titration with the acids used.

As the helicate is present in the tetraprotonated form, the stability constant calculated will be that for the encapsulation of anions within the tetraprotonated complex. A potentiometric study was proposed to determine the pK_a values of the amines within **1**. Due to the poor solubility of **1** in basic solutions and the resulting precipitation at a higher pH, this was not possible despite many attempts in a variety of solutions.

The tetraprotonation of **1** upon dissolving in IPA solution may also explain the change in the UV-visible spectrum. If the amines are protonated, the change in absorption may result from hydrogen bonding interactions with the phenolate moieties and may not be due to solvent interactions with the metal centres.

*2.2.6 Colourimetric Sensor Ability of **1** Upon Anion Binding*

Many examples of colourimetric anion receptor systems have been reported in the literature.[66-68] Many of these result from the deprotonation of an organic host by highly basic anions such as acetate or fluoride and are officially acid-base indicators.[69] Colourimetric sensors designed for binding anions produce a colour change in solution observable to the naked eye. Therefore these systems allow the detection of anions in solution without the need of spectrophotometric equipment. Solutions of **1** at a concentration of 360 μmol L^{-1} in the presence of 100 equivalents of acid are shown in Figure 23. The largest colour change occurs for the addition of hydrochloric acid. This comes as no surprise due to the breakdown of the helicate in the presence of hydrochloric acid. Addition of sulfuric, perchloric and tetrafluoroboric acid also results in a substantial colour change. Interestingly, despite the strong binding of phosphoric acid, the colour is very similar to the freebase solution. This is a consequence of the peculiar absorption peak forming close to the original freebase absorption band at higher equivalents of acid.

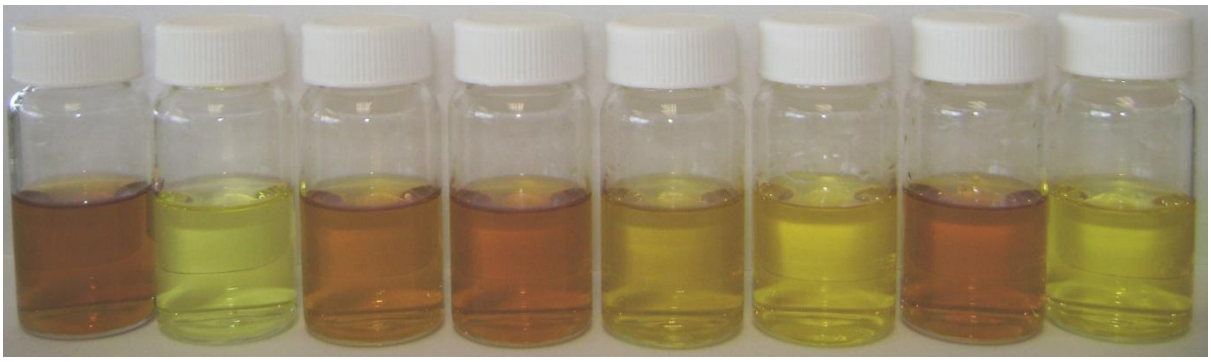

Figure 23. IPA solutions of **1** in the presence of the acids studied in this chapter. From left to right the solutions are; **1** only, **1**+HCl, **1**+HBr, **1**+HNO_3, **1**+HBF_4, **1**+$HClO_4$, **1**+H_3PO_4 and **1**+SO_4. Concentration of **1** is 360 μmol L^{-1} and acids are present at 100 equivalents.

*2.2.7 Conductivity of **1**.SO_4, **1**.ClO_4 and **1**.BF_4 in Nitromethane.*

The conductivity of **1**.SO_4 ($\left[SO_4 \subset Cu_2\mathbf{L}^1_2\right]SO_4$), **1**.$ClO_4$ ($\left[ClO_4 \subset Cu_2\mathbf{L}^1_2\right](ClO_4)_4$), and **1**.$BF_4$ ($\left[BF_4 \subset Cu_2\mathbf{L}^1_2\right](BF_4)_4$) over concentrations of 40 μmol L^{-1} to 1 mmol L^{-1} in nitromethane were investigated. The synthesis of these complexes is covered in Chapter 6. Aside from single conductivity measurements, the vast majority of studied electrolytes have been the symmetrical 1:1 electrolytes. Much less work has been performed on 2:1 electrolytes and even less has been performed on 3:1 and 4:1 systems. Additionally, the work performed on higher ratio electrolyte systems has only been performed on strong electrolytes. The **1**.BF_4, **1**.ClO_4, and **1**.SO_4 helicates studied are thus unique in that one ion is bound substantially stronger than the remaining ions so that they are both weak and strong electrolytes.

The most commonly reported method for the use of conductivity in the primary literature is the determination of a single conductivity measurement typically at one millimolar. This value is then converted to a molar conductivity and compared to other values reported for the solvent used for known electrolyte stoichiometries.[48] This methodology can be unambiguously applied to ideal systems but not for complicated systems involving weak or non-ideal electrolytes. The molar conductivity values recorded for the above complexes supports these assertions. The molar conductivities at one millimolar for **1**.BF_4, **1**.ClO_4, and **1**.SO_4 were 241, 205 and 101 S cm^2 mol^{-1} respectively. These values correspond to 3:1 electrolytes for **1**.BF_4 and **1**.ClO_4 and a 1:1 electrolyte for **1**.SO_4.[48] This of course contrasts with the known 4:1 and 2:1 counteranion:cation structure of these species. The results support the encapsulation of

anions within the cavity of the helicate in nitromethane and provides no evidence for the exterior binding of the anions to the metals.

If the encapsulated tetrafluoroborate and perchlorate anions remain bound for all concentrations then the helicates containing these anions should obey the Onsager equation for a 3:1 electrolyte. The Onsager equation is applied at dilute concentrations so that the electrolyte solution behaves as an ideal solution (ion columbic interactions are negligible).[46] The equivalent conductivity of **1**.BF_4 as a function of the helicate concentration (Figure 24) shows a sharp increase in conductivity at very low concentrations typical of weak electrolytes.[46] The encapsulated anion is forced out by the applied potential difference at low concentrations. Variations of the Onsager equation have been applied to 1:1 weak electrolytes and before the rise of potentiometry in the 1930s was the dominant method of stability constant determination for these electrolytes.[50] This cannot be applied to the helicate system under study due to the strong electrolyte ability of the non-coordinating counterions. If the equivalent conductivity is plotted as a function of the square root of concentration for the helicates, a linear section is observed at higher concentrations before deviation at lower concentrations. If the linear sections are fitted as 3:1 electrolytes to the Onsager equation, slopes of 1199 ± 85 and 855 ± 87 S cm^2 eq^{-1} $M^{-1/2}$ are obtained for **1**.BF_4 and **1**.ClO_4 respectively. A value of 1020 S cm^2 eq^{-1} $M^{-1/2}$ has been reported for the $[Co(bipy)_3](ClO_4)_3$ 3:1 electrolyte by Feltham and Hayter.[47] This value lies between the two values obtained. The average value obtained for 2:1 electrolytes in nitromethane by Hayter,[70] Feltham and Hayter[47] and Feltham and Nyholm[71] was 469 S cm^2 eq^{-1} $M^{-1/2}$. The **1**.BF_4 and **1**.ClO_4 helicates therefore fit a 3:1 electrolyte model for concentrations in the range of 3 x 10^{-4} to 1 x 10^{-3} M. This result implies that even in a non-equilibrium environment (applied potential difference) the anion remains encapsulated within the complex. A small proportion of encapsulated tetrafluoroborate being released would explain the increased value of $\frac{\Lambda_0-\Lambda_e}{\sqrt{c}}$ observed over the nitromethane solution of **1**.ClO_4 for which a higher binding constant was obtained from the UV-visible study. Interestingly, a measurable difference in the solution binding properties is observed for the perchlorate and tetrafluoroborate anions despite the identical X-ray crystal structures obtained for the two anions.

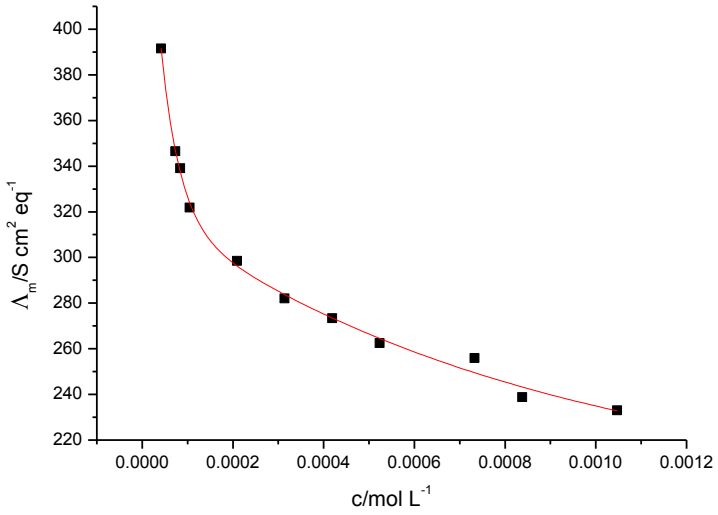

Figure 24. Molar conductivity plotted against concentration revealed a sharp increase in molar conductivity at low concentrations of complex. This behaviour is typical of weak electrolytes.

As **1**.BF_4 and **1**.ClO_4 were determined to correspond to 3:1 electrolytes at concentrations above 20 μmol L^{-1} it was expected that the strongly binding sulfate would also remain encapsulated over this concentration. The linear section of the equivalent conductivity as a function of $\sqrt{c}$ for the sulfate helicate produced a value for $\frac{\Lambda_0-\Lambda_e}{\sqrt{c}}$ of 2190 ± 351 S cm^2 eq^{-1} M$^{-1/2}$ if modelled as a 1:1 electrolyte. This value is far too high to represent a 1:1 electrolyte system. There have been no reports of 2:2 electrolytes studied under the utilised methodology. It is therefore unknown whether such a high slope is a characteristic of the 2:2 electrolyte type.

*2.2.8 X-Ray Crystal Structure of [I⊂**1**H_4]BF_4I_2*

Crystals of [I⊂**1**H_4]BF_4I_2 were grown by the slow diffusion of diethyl ether into an acetonitrile solution of **1** containing one equivalent of TBAI. Due to the poor quality of the crystal data (R_1=12.4 % for 8939 F_o>4σ and 31.5 % for all 26723 data), detailed analysis of the complex molecule was not possible. In particular, the tetrafluoroborate counter ions exterior to the helicate were poorly refined. The [I⊂**1**H_4]$^{3+}$ tricationic helicate is shown in Figure 25.

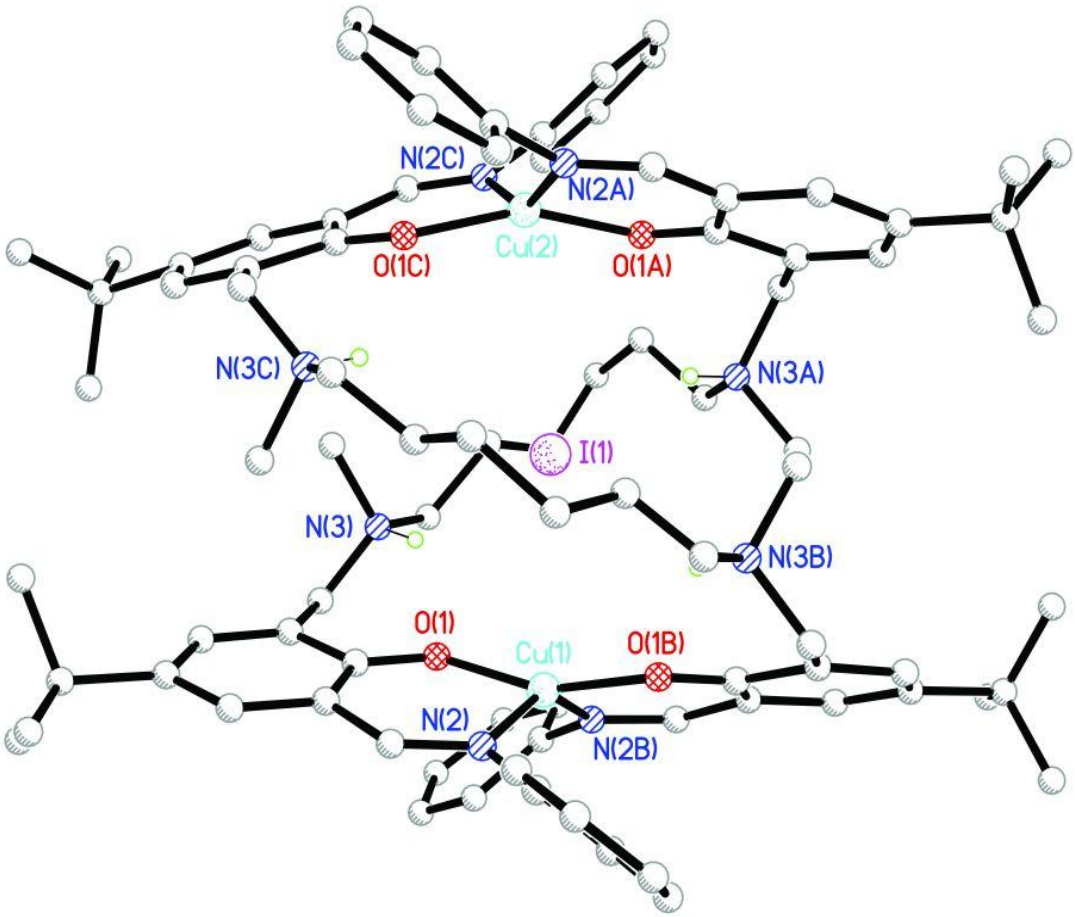

Figure 25. Solid state structure of [I⊂**1**H_4.]BF_4I_2.

The data presents a good representation of the helicate including the metal co-ordination sites and the encapsulated iodide anion. The average copper-iodide bond length is 3.50 Å. This large distance suggests that there is little interaction of copper and anion in the solid state. The stability constant for the encapsulation of iodide within **1** in IPA was unfortunately not obtained. Based purely on experimental observation, iodide possessed higher binding than that of tetrafluoroborate as iodide was able to displace this anion. The copper atoms are four coordinate with two phenolate and two imine donors comprising the coordination sphere (Figure 25). The copper centres possess a distorted tetrahedral geometry typical for anion encapsulated structures of **1**.[32, 45] An interesting observation for the iodide encapsulated structure was that the protonated amines of the alkyl strap were directed more toward the phenolate oxygen atoms than the iodide anion. The N...O distances of 2.81-2.97 Å are indicative of weak hydrogen bonding and are more significant than the N...I distances of 3.73-4.92 Å. The

amine-phenolate hydrogen binding results in the helicate acquiring a greater twist and consequently a closer Cu...Cu distance in comparison to the similar sized tetrafluoroborate anion encapsulated in **1** (Table 3). The volume of the helical cavity is calculated by assuming a cylinder with a height equal to the Cu...Cu distance and a diameter of the amine N...N distances. Despite the decreased distance between copper centres for $[I \subset \mathbf{1}H_4]^{3+}$ compared to $[BF_4 \subset \mathbf{1}H_4]^{3+}$ the cavity volume is equal to that of the $\mathbf{1}.BF_4$ crystal structure resulting from the wider radius of the alkyl arms.

	$[I \subset \mathbf{1}H_4]^{3+}$	$[BF_4 \subset \mathbf{1}H_4]^{3+}$
Cu...Cu distance/Å	6.970(4)	7.298(2)
Average Helical Twist[ǂ]	131.8(5)	134.3(4)
Cavity Volume/Å^3	400	400

ǂ The twist is calculated by measurement of the O-Cu-Cu-O torsion angle.

Table 3. Selected bond lengths, angles and the cavity volumes from the structures of receptor **1** containing the encapsulated iodide and tetrafluoroborate anions.

2.2.9 Summary

Within experimental error the binding of anions increases with the increasing size of the anion (Figure 19). This indicates that compatibility between the anion size and the cavity within **1** is an important factor in determining the strength of binding. The strength of binding increases substantially for the strongly co-ordinating phosphate and sulfate anions. The crystal structure of **1** encapsulating nitrate shows no interaction with the copper centres.[53] It is held in the cavity by a combination of hydrogen bonding and electrostatic forces. The log K value of nitrate was calculated as 2.95 which is the weakest binding of the anions studied. The larger tetrafluoroborate anion showed a weak interaction with the copper centres but only a marginally greater stability constant than nitrate encapsulation, further suggesting a weak interaction with the metal centres. The perchlorate anion exhibited a much weaker stability constant than either phosphate or sulfate supporting the weak interaction with the copper centres demonstrated in the solid state.[53] The phosphate anion exhibited very strong binding as might be expected by its structural similarity to sulfate for which the greatest stability constant was obtained. Additionally, the protonation state of the phosphate anion affected the absorbance spectra of the complex due to amine phenolate hydrogen bonding. Despite

the change in absorbance, the stability constants obtained for the $TBAH_2PO_4$ and H_3PO_4 titrations were well within error limits of each other. This supports the assumption that the binding of the anions is affected to a much greater extent by the presence of copper-anion interaction than the hydrogen bonding and electrostatic interactions of additional protonation of **1** for the more strongly co-ordinating anion. The high stability constant generated for the sulfuric acid titration of **1** agrees with the solid state data for sulfate encapsulated within **1**. The high binding of sulfate would enable the selective uptake of sulfate even in the presence of the other anions studied.

2.3 Experimental

2.3.1 Materials and Reagents

Spectrophotometric measurements in the UV-visible region were recorded at 294 K using a Shimadzu UV-3101PC spectrometer and one cm path length matched quartz cuvettes. The data was analysed and stability constants calculated using the software program SPECFIT/32™.[72-75] The conductivities were recorded using a Philips PW9509 Digital Conductivity Meter and a Philips PW9510/60 conductivity electrode. X-ray crystallographic data were collected on a Brunker SMART four circle diffractometer at the University of Canterbury. Chemicals and solvents were of AR grade unless otherwise stated and used as received. The synthesis of **1** is reported in chapter six. Free base **1** was dried under vacuum for one hour prior to preparation of the titration solutions and the titrations were prepared immediately.

2.3.2 Spectrophotometric Titrations

Solutions of **1** in isopropyl alcohol (2 mL, 2.69×10^{-5} – 2.82×10^{-5} mol L^{-1}) were titrated with IPA solutions of the acid of interest ~5×10^{-3} mol L^{-1} until no further spectrum changes were observed. Spectra were recorded following the addition of each aliquot over the wavelength range of 900 to 250 nm. Acid solutions were titrated at 0.5 molar equivalence increments for tetrabutylammonium dihydrogen phosphate ($TBAH_2PO_4$), H_3PO_4, H_2SO_4, $HClO_4$, HBF_4, HBr, and HI and 2.5 molar equivalence increments for HNO_3 using a 0.5 – 10.0 μL autopipette. This was at 4, 4, 5, 10, 10, 10, 6 and 40 equivalents for $TBAH_2PO_4$, H_3PO_4, H_2SO_4, $HClO_4$, HBF_4, HBr, HI and HNO_3 respectively. A 1:1 anion to **1** binding model was used for all spectrophotometric

titrations as determined by the method of continuous variation and supported by SPECFIT/32™ which was used to calculate stability constants for the binding of **1** to the corresponding anions of the acids used. In order to ensure reliable results, titrations were repeated until three concordant results were obtained. Stability constant errors are the standard deviations of the three concordant results.

2.3.3 Method of Continuous Variation

Solutions were prepared by mixing aliquots of two equimolar solutions (2.69 x 10^{-5} – 2.82 x 10^{-5} mol L^{-1}) of **1** and the acid of interest. These solutions were prepared so that the total analytical concentration of **1** and the acid remained constant while varying the mole fraction of acid from 0 through to 1 in 0.1 intervals. The corrected absorbance was then plotted as a function of the mole fraction of acid.

2.3.4 Solution Preparation

All solutions were prepared using IPA as the solvent. Phosphoric acid crystals were accurately weighed out under argon and made up with IPA to give a solution of concentration (5.09 ± 0.06) mmol L^{-1}. A standard nitric acid solution was produced by making up a standardised ampoule of nitric acid in H_2O to 500 mL (1 mol L^{-1}) and then diluting to give a final concentration of (6.8 ± 0.1) mmol L^{-1} with water content less than 0.1% based on residual water from standard solutions. A standard ampoule of sulfuric acid in H_2O was made up to 500 mL with IPA to give a 0.1 mol L^{-1} solution. This solution was then diluted giving a final concentration of (7.20 ± 0.03) mmol L^{-1} with less than 0.5% water content. A standard ampoule of perchloric acid in H_2O was made up to 500 mL with IPA to give a 0.2 mol L^{-1} solution. This solution was then diluted to produce a solution with a concentration of (8.00 ± 0.08) mmol L^{-1} containing less than 0.4% of water. A one molar solution of $TBAH_2PO_4$ in water was diluted to produce a solution with a concentration (5.0 ± 0.1) mmol L^{-1} with less than 0.5% water content. Concentrated aqueous hydrochloric (37%), hydrobromic (47.5%) and hydroiodic acid (55%) and 54% tetrafluoroboric acid in ether were diluted to concentrations of 4.6, 3.4, 2.9 and 2.9 mmol L^{-1} respectively. Perchloric acid solutions for titrations (4.7 mmol L^{-1}) were prepared from aqueous perchloric acid (70%). Solutions of **1** possessed a concentration of (26.9 ± 0.3 to 28.2 ± 0.3) μmol L^{-1}.

2.3.5 Reliability of Standard Solutions

The acid solutions of hydrochloric, hydrobromic, hydroiodic and tetrafluoroboric acid were prepared from dilution of concentrated aqueous acid solutions. In order to estimate the reliability of these solutions a perchlorate solution (**a**) derived from aqueous perchloric acid was compared with a perchloric acid solution (**b**) prepared from a standard solution. The titrations of **1** using **b** produced spectra which were indistinguishable from those from the titrations of **1** with **a**. When analysed with multivariable analysis using the SPECFIT/32^{TM} programme the stability constants were within error of each other. This suggested that the acid solutions made from concentrated acid solutions were of a quality approximate to that of the acids solutions from standard acid solutions.

2.3.6 Conductivity Measurements

Measurements of conductivity of solutions of each complex were recorded over the range of 10^{-5} to 10^{-3} mol L^{-1} using extra pure grade nitromethane. The molar conductivities were plotted as a function of concentration to determine the electrolyte strength. The equivalent conductivity (Λ_e) was plotted as a function of the square root of the equivalent concentration and extrapolated to infinite dilution to give Λ_0. The gradient of Λ_0-Λ_e as a function of $\sqrt{c}$ was then compared with that of reported electrolytes.

*2.3.7 Synthesis of [I⊂**1**H_4]BF_4I_2*

Solid TBAI (6 mg, 16 μmol) and **1**$(HBF_4)_4$(24 mg, 13 μmol) were dissolved in acetonitrile (1 mL) and filtered. Dark green rectangular crystals were obtained by diffusion of diethyl ether into the solution at 4^{o}C (Yield 17.6mg, 87 %). As these crystals appeared to be multi-jointed they were further dissolved in acetonitrile (0.6 mL) and filtered before recrystalising under the above conditions. These crystals were then analysed by X-ray crystallography. Found C, 54.77; H, 6.55; N, 6.65, $C_{88}H_{116}N_8O_4BF_4Cu_2I_3.2CH_3CN.Et_2O$ requires C, 54.89; H, 6.33; N, 6.67. *m/z* (ESI) 802.07 $(ICu_2\mathbf{L}^1(\mathbf{L}^1\text{-}H))^{2+}$.

Chapter 3

Titrations of $[Cu_2(L^2\text{-}2H)_2]$

3.1 Introduction

Salicylaldoxime ligands are known to form 14-membered pseudomacrocyclic structures shown in Figure 26. The resulting copper(II) complexes formed with these ligands possess a very high stability.[76] The intermolecular hydrogen bonds between the oxime hydroxyl groups and the phenolate oxygen atoms results in a high hydrolytic stability even in highly acidic medium.[77]

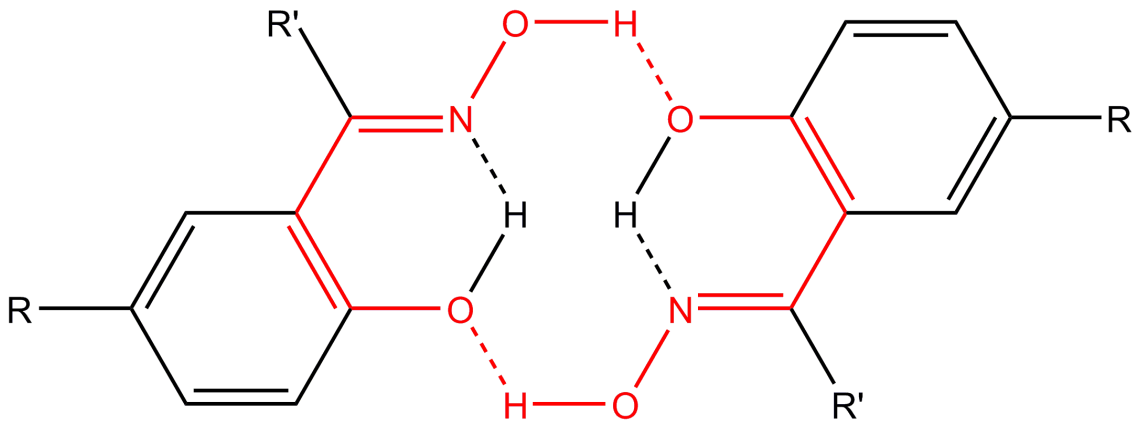

Figure 26. The 14-membered pseudo-macrocyclic structure formed by salicylaldoxime ligands.[76]

By replacing the iminophenyl groups of $\mathbf{L^1}$ with iminooxime moieties $\mathbf{L^2}$ was produced (Figure 27). Reaction of $\mathbf{L^2}$ with copper salts produces a helicate (**2**) analogous to **1**. The presence of the free base monopositive peak in the ESI-MS supports the increased stability of **2** over **1** in solution for which no free base helicate was observed. The comparison of the binding constants of anion encapsulation for **1**

and **2** will allow the effect of introducing the oxime functionality into the structure to be analysed. In particular, whether the rigid pseudo-macrocyclic structure will result in reduced flexibility of the complex. In order to investigate the anion binding properties of **2**, L^2 was reacted with copper(II) acetate in the same way observed for L^1 to produce the free base helicate **2**≡[Cu_2(L^1-2H)$_2$] shown in Figure 28 (synthesis contained in Chapter 6).

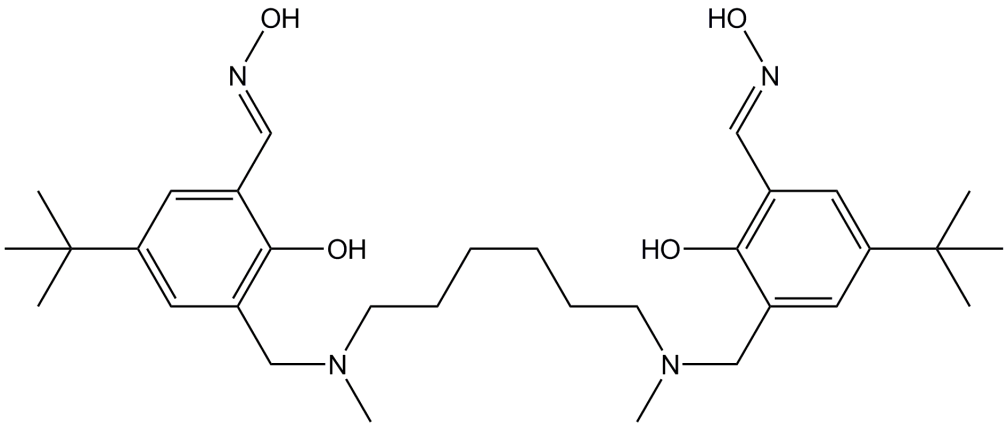

Figure 27. The ligand L^2 used to produce the free base complex **2**.

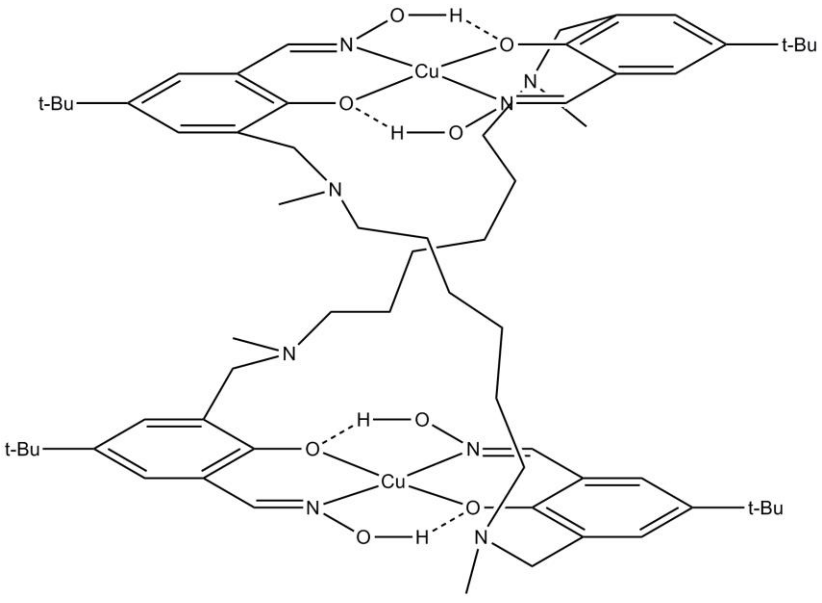

Figure 28. The helicate (**2**) formed between L^2 and copper(II) acetate and used in the UV-visible titrations.

3.2 Results and Discussion

*3.2.1 Absorption Spectra of **2***

In comparison to the titrations performed on the L^1 free base system, the oxime system was also investigated for its ability to incorporate protons and anions to form the zwitterionic complex. Unfortunately, the poor solubility of **2** meant the original IPA solvent system used for the titrations of **1** could not be used. As **2** was freely soluble in 1,2-dichloroethane, various proportions of a DCE-IPA solvent were trialled for acid titrations of **2**. A 50% (v/v) DCE-IPA mixture was found to be the most satisfactory solvent for the titrations.

The DCE-IPA solutions of **2** showed a slow reproducible change in UV-visible absorption until a fixed point in a similar manner observed with **1** in IPA (Chapter 2). This could be restored after drying and reproducing the solution. ESI-MS evidence of solvent co-ordination to the oxime helicate suggested that encapsulated IPA could be causing this spectral change. To minimise this potential solvent co-ordination the complex was dried under vacuum for one hour prior to preparation of the titration solutions and the titrations were performed immediately after as for the titrations of **1** in Chapter 2. Chapter 2 mentioned the immediate protonation of **1** upon dissolving in IPA which was described in Section 2.2.5 and the resulting hydrogen bonding toward the phenolate moieties. The low relative permittivity of DCE[78] along with its aprotic behaviour will be expected to lower the proton concentration in solution. Due to the high pK_a values of the complex, protonation should still take place to a large degree and the hydrogen bonding to the phenolate oxygen atoms may again be the basis of the absorbance change and not solvent coordination.

The complex exhibited very high absorbance (absorptivity greater than **2**) at the concentrations used below 250 nm, so the spectrum was recorded from 900 to 250 nm (Figure 29). A broad UV-visible spectral band with maximum at 338 nm was assigned as the phenolate related π to π_1^* electron transfer which was responsible for the yellow colour of the ligand solutions. Additionally, the shoulder of what was assigned as the π to π_2^* electronic transition appeared at 279 nm.[55] These peaks exhibited very high molar absorptivities of 4.7×10^4 and 2.0×10^4 M^{-1} cm^{-1} respectively for the 279 and 338 nm bands.

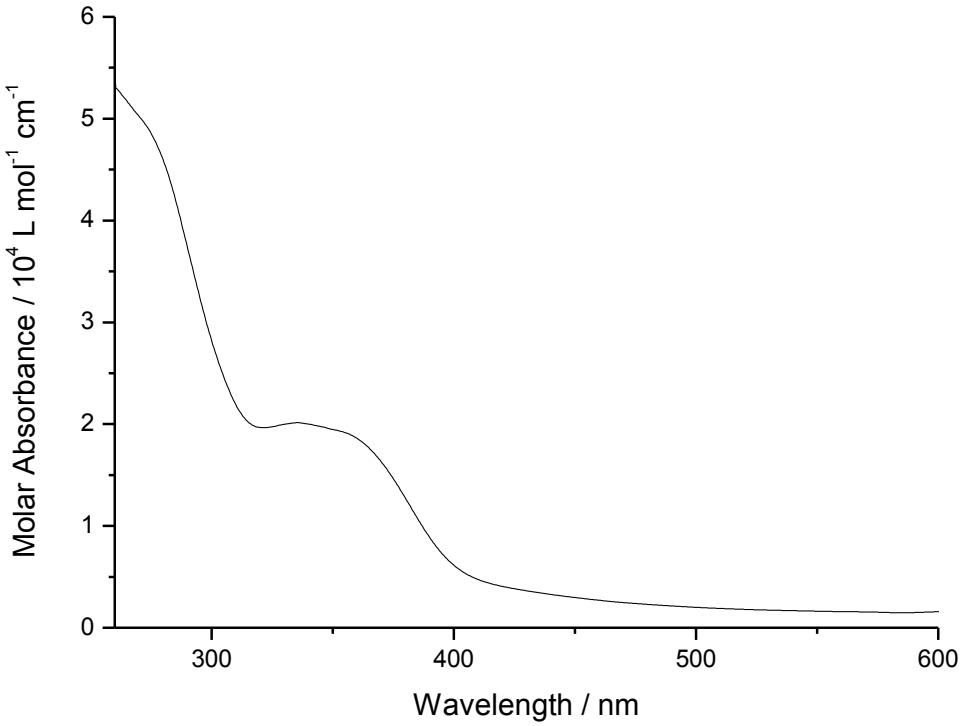

Figure 29. UV-Visible absorbance spectra of **2** in 50% DCE-IPA. The broad band at 343 nm is characteristic of the phenolate moiety.

As stated above, the complex was expected to be approaching its tetraprotonated form. Full protonation of the complex would occur immediately upon acid addition. The UV-visible spectra were recorded between titrations as for the titrations of **1** (Chapter 2). The anions were added as their conjugate acids. The titration solutions of **2** possessed a small amount of water in combination with acid. The free base **2** was expected to be more stable in these conditions than **1** due to the hydrogen bonding stabilisation of the oxime-phenolate moiety (Figure 30). It has been shown that copper co-ordinated salicylaldoximes compounds can be stable even in the presence of sulfuric acid at pH 1.[77] As for the titrations of **1** in Chapter 2, there are two important underlying assumptions for the titrations performed. These assumptions are that the titrated anion is capable of entering the cavity of **2** in solution and that the spectral change is the result of interactions of the anion within the cavity. The acids titrated were; sulfuric, phosphoric, perchloric, tetrafluoroboric, hydroiodic, hydrobromic,

hydrochloric and nitric acid. The tetrabutylammonium dihydrogen phosphate salt was also titrated.

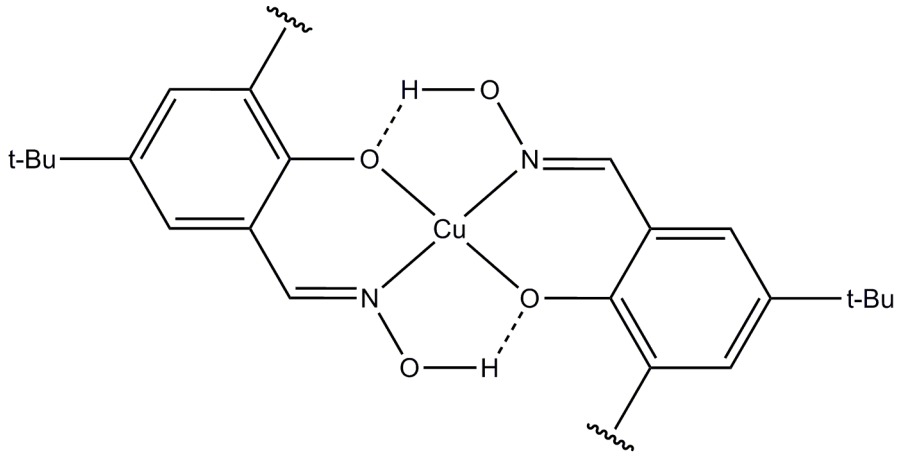

Figure 30. Copper co-ordination environment of **2**.

*3.2.2 Sulfuric Acid Titration of **2***

Sulfuric acid was expected to produce the highest stability constants based on results from the titrations of **1**. Upon titrating **2** with sulfuric acid a complicated series of spectra were observed. Upon the addition of two equivalents of H_2SO_4 the broad 338 nm band decreased in absorbance and shifted bathochromically to 352 nm, however no isosbestic points were observed (Figure 31). Once two equivalents of acid had been obtained the absorption of the new peak decreased and was further shifted to 357 nm. Most notable however was the sudden increase in absorbance to form a new peak at 309 nm with the emergence of three isosbestic points at 297, 326 and 329 nm (Figure 32). Titrations of **2** with the other acids studied resulted in the appearance of two peaks and the emergence of isosbestic points. This is in contrast to the results obtained for sulfuric acid addition. This suggested that sulfuric acid was interacting differently with **2** than the other acids. The sudden absorbance drop with no isosbestic points could be a result of a major rearrangement of the free base. This could be due to the direct effect of the sulfate binding to the copper centres, or the indirect effect of sulfate binding causing the ligand to strain and affecting absorbance. The job plot of the **2** sulfuric acid system suggested a more complicated binding than a simple 1:1 helicate:acid interaction. Modelling a 1:1 fit using SPECFIT/32™ resulted in a poor correlation between the predicted and observed spectra.

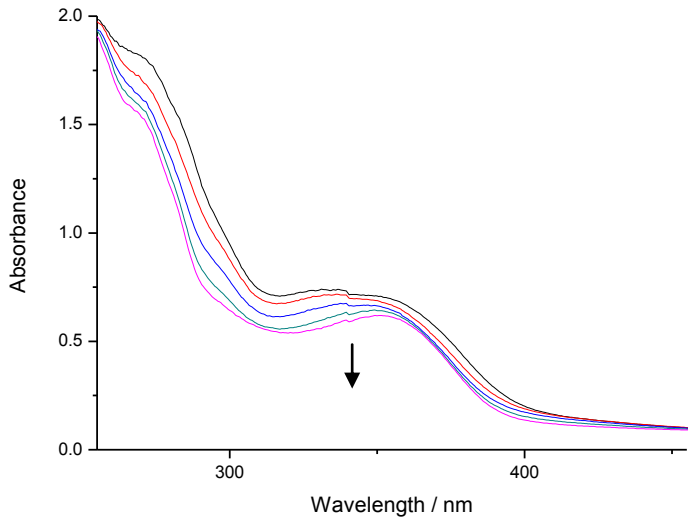

Figure 31. Recorded UV-visible titration spectra of **2** with up to two equivalents of H_2SO_4. Each spectrum corresponds to addition of 0.25 equivalences. The arrow indicates the intensity change.

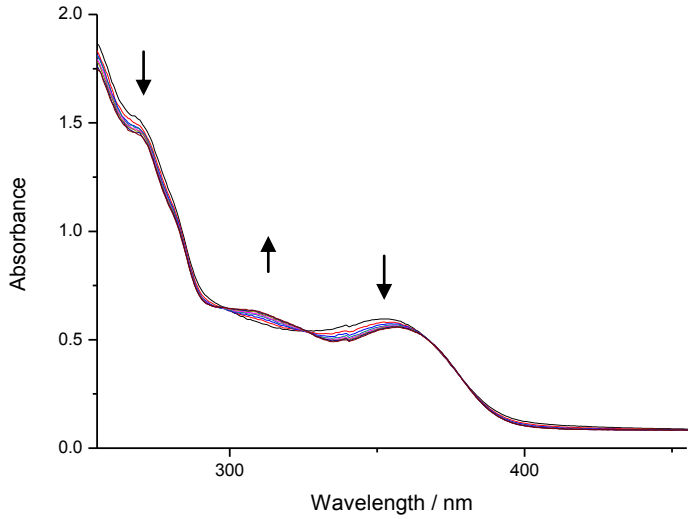

Figure 32. Recorded spectra of the sulfuric acid titration of **2** to six equivalents of added acid. Each spectrum corresponds to addition of 0.25 equivalences. Arrows indicate relative intensity changes.

*3.2.3 Base Titrations of **2**.SO_4*

As direct synthesis of the **2**-sulfate complex was possible and because the observed changes in the above spectra were puzzling, a back titration from **2**.SO_4 using

sodium acetate was proposed in order to produce the free base absorption spectra. As sodium acetate was found to be insoluble in the solvent system used, sodium hydroxide was utilised instead. The **2**.SO_4 absorbance spectra resembled the spectra produced after two equivalents of sulfuric acid had been added to **2**. The spectra produced above two equivalents of added acid differed from the **2**.SO_4 spectrum suggesting a product other than the encapsulated sulfate complex. Initial addition of sodium hydroxide to **2**.SO_4 resulted in the increase in absorbance of the 345 nm peak. After the addition of six equivalents of hydroxide a band began to emerge with two peaks at 307 and 319 nm and isosbestic points began forming at 291, 331 and 437 nm (Figure 33). The ESI-MS of the titration exhibited a very large peak representative of the $[SO_4\subset\mathbf{2}H_4]^{2+}$ species suggesting that the sulfate had not been removed from the cavity of **2** and therefore the back titration with sodium hydroxide had not been successful.

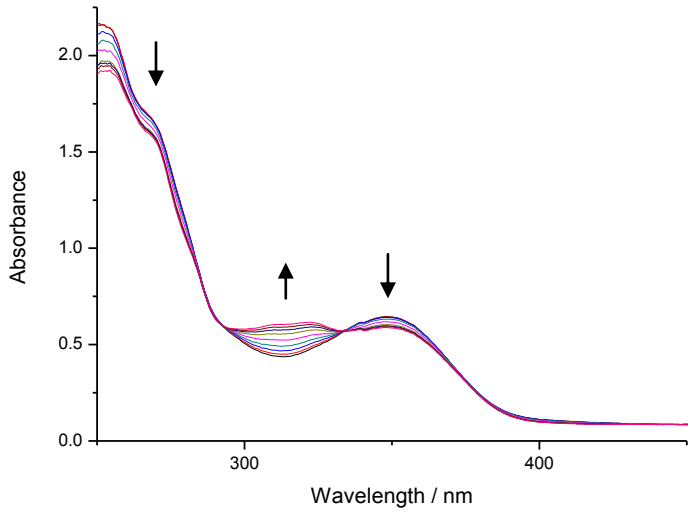

Figure 33. Recorded spectra of six equivalents of hydroxide to a solution of **2.**SO_4. Arrows indicate relative intensity changes.

In order to avoid hydroxide reacting unfavourably with **2**.SO_4, 1,8-diazabicyclo[5.4.0]undec-7-ene (DBU), (Figure 34); an organic non-co-ordinating base was titrated into a solution of **2**.SO_4. The spectra that evolved in this titration matched that of the free base species. The mass spectrum of the titration exhibited a very large peak due to the DBU-H^+ species, but showed no signs of any $[SO_4\subset\mathbf{2}H_{2+x}]^{x+}$ species. The free base helicate was detected suggesting that deprotonation of the sulfate complex had been achieved in combination with the removal of the sulfate anion. The **2**.SO_4-

DBU titration was modelled as a 1:1 binding system using SPECFIT/32^{TM}. This was based on the assumptions used for the acid titrations. Namely that the change in absorbance is attributable to the removal of sulfate from the cavity of **2**.SO_4. As DBU is colourless over the concentrations and wavelengths used, only two coloured species exist in solution and this assumption is valid. This was used as an approximation to sulfuric acid inclusion and produced a log K value of 4.43 (Table 4).

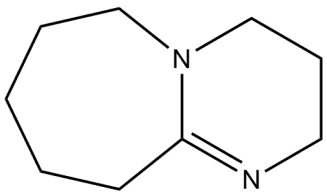

Figure 34. Structure of 1,8-diazabicyclo[5.4.0]undec-7-ene or DBU used to deprotonate the **2.**SO_4 complex.

*3.2.4 Acid Titrations of **2***

Acid titrations of phosphoric, nitric, perchloric, tetrafluoroboric, hydroiodic, hydrobromic and hydrochloric acid were performed for the oxime free base system (see Appendix B for spectra). The method of continuous variation for titrations of **2** with the said acids are shown in Figure 35. These consisted of a single peak situated at 0.5 mole ratio of acid as was observed for the **1**-anion systems. This was taken to support the presence of one dominant species consisting of a 1:1 stoichiometry of acid and free base complex **2**.

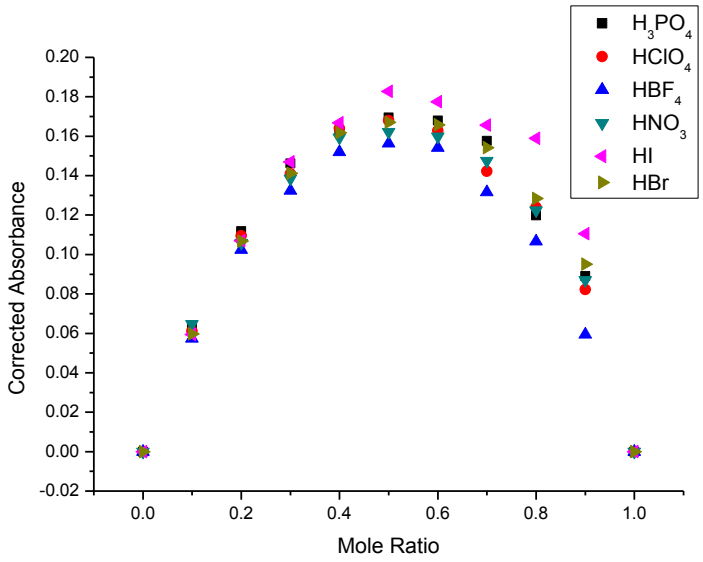

Figure 35. Method of continuous variation of acids titrated against **2** recorded at the phenolate absorption peak.

The 1:1 model was used with SPECFIT/32™ and produced good agreement between the predicted and recorded spectra. The values calculated for these acids are recorded in Table 4. Phosphoric acid and sulfuric acid exhibited expected strong bonding due to their co-ordinating ability and values for each were within the error limits of one another. The method of calculating the log K value for H_2SO_4 demonstrates the high strength of binding of the **2**-sulfate adduct, but it should be remembered that the method to calculate this differed from the other anions. The stability constants for perchloric and tetrafluoroboric acid were higher than might be expected from their known weakly coordinating properties, possibly resulting from forced interactions with the copper centres due to their size.[59] Hydroiodic acid produced a stability constant equivalent to that of tetrafluoroboric acid due to the similar volumes of these two anions.[59] A decrease in binding with decreasing anion size when going from perchlorate to tetrafluoroborate, is mirrored on moving from hydroiodic to hydrobromic acid. The magnitude of the decrease in binding is substantially larger which can be attributed to the much smaller size of the bromide anion. Nitrate exhibited a very strong binding constant for encapsulation within **1**. This was not expected from experience with [$NO_3\subset$**1**H_4] in solution (see Chapter 2) and the solid state.[53]

Acid	Log K	Stoichiometry	ESI-MS Peaks
H_3PO_4	4.53 ± 0.03	1:1	$[PO_4\subset\mathbf{1}H_4]^+$
H_2SO_4	4.43 ± 0.15	1:1	$[SO_4\subset\mathbf{1}H_4]^{2+}$
HNO_3	4.38 ± 0.06	1:1	$[NO_3\subset\mathbf{1}H_3]^{2+}$
$HClO_4$	4.25 ± 0.07	1:1	$[ClO_4\subset\mathbf{1}H_3]^{2+}$
HBF_4	4.02 ± 0.13	1:1	$[BF_4\subset\mathbf{1}H_3]^{2+}$
HI	4.01 ± 0.05	1:1	$[LCuI]^+$
HBr	3.54 ± 0.08	1:1	ǂ

*; not determined, ǂ; no evidence of encapsulation/binding

Table 4. Guest binding constants for **2** in 50% DCE-IPA at 294 K.

3.2.5 Large Scale Titration of the Tetrafluoroborate Encapsulated Complex

In order to support that the anion encapsulated species were being formed upon addition of acid, a titration was performed on a large enough scale to isolate the solid product. This product was then characterised by IR, ESI-MS, UV-visible and elemental analysis and compared to the species produced using the starting ligand and the copper salt from Chapter 6. The free base **2** with addition of methanoic tetrafluoroboric acid was chosen as the model 'titration' reaction. The model titration produced the same product as the reaction of copper(II) tetrafluoroborate salt with $\mathbf{L}^2$ offering further evidence that the encapsulated anion species was forming in the titration solutions.

*3.2.6 Reaction of Hydrochloric Acid with **2***

As mentioned above, the Job plot of **2** upon titration of HCl was ambiguous. It was mentioned in Chapter 2 that $\mathbf{L}^3$ when reacted with copper(II) chloride produced a complex of type LCu_2Cl_4 with chloride binding directly to the metal centres. When the possibility of this occurring upon addition of HCl to **1** was investigated no conclusive results were obtained. When HCl is titrated into the DCE-IPA solutions of **2**, a band at around 510 nm (Figure 36) emerged which was not observed in the other acid titrations of **2** (Figure 37). This band is of an appropriate wavelength to be a copper(II) chloride absorption band.[79] ESI-MS of the titration mixture showed peaks representative of LCu_2Cl_y species (y=2-4).

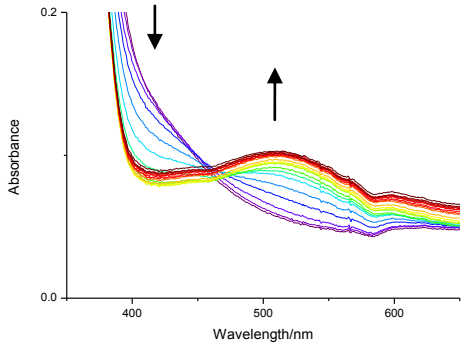

Figure 36. Expanded view of the assigned copper(II) chloride visible absorbance band. Taken from the UV-visible titration spectra of **2** with up to ten equivalents of HCl. Each spectrum corresponds to addition of 0.25 equivalences. The arrows indicate the relative intensity change.

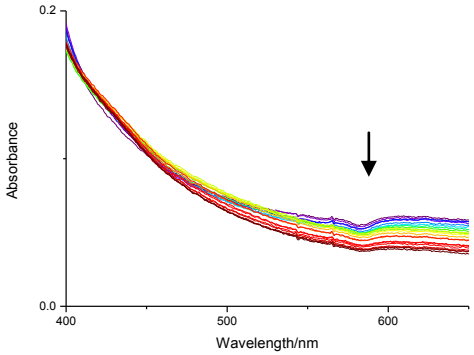

Figure 37. Expanded view of the same wavelength range from the UV-visible titration spectra of **2** with up to ten equivalents of HBF_4. Each spectrum corresponds to addition of 0.25 equivalences. The arrow indicates the relative intensity change.

Using a 1:1 model in SPECFIT/32™ for HCl addition gave unsatisfactory results. If a 1:4 model was chosen instead, an excellent fit was obtained. If the chloride anions are replacing one of the ligands of the original helicate then the absorbance of the helicate should roughly half since the absorbance of **2** is primarily from the ligand. Due to the free ligand that was replaced remaining in solution, the magnitude of the absorbance will remain roughly the same. As the free ligand remains in solution and contributes to absorbance, it is assumed for the sake of simplicity of the model used, that the chloride anions binding to the copper centres causes the only absorbance change and that the total absorbance of the host is given by that of the two ligands and two copper centres throughout the titration. This assumption should be valid, since the absorbance change of chloride binding directly to copper should be significantly different from the change due to the ligand no longer binding to copper. The stability constants for the successive binding of chloride are summarised in Table 5. The first two ligand replacements with chloride were very favourable. The second exhibited co-operative binding suggesting initial chloride binding weakens the strength of the helicate. The co-operative binding of the initial two binding interactions and the subsequent decrease in binding of further chloride may indicate the second chloride anion binds to the second copper centre. The binding of the first chloride ion to one copper centre weakens binding of the ligand to the second copper centre encouraging

binding to the second copper by another chloride anion. The binding of chloride to a copper-chloride centre would then be less favourable than to the copper centre free of chloride. The predicted formation of chlorinated products is shown in Figure 38. From this model, the $[LCu_2Cl_3]^-$ complex will be the dominant species in solution after three equivalents of added hydrochloric acid. By approximately four equivalents of added hydrochloric acid the amount of remaining helicate will be approximately zero percent. The trichloride species will make up 60% and the tetra- and dichloride complexes make up 20% each of the original helicate content. Complete chlorination to form LCu_2Cl_4 will not occur until very high concentrations of HCl have been added.

	Stability Constant
Log K_1	5.30 ± 0.39
Log K_2	5.61 ± 0.24
Log K_3	4.89 ± 0.30
Log K_4	3.81 ± 0.26

Table 5. Stability constants for the successive binding of chloride to **2** in 50% DCE-IPA at 294 K. The subscript of K represents the chloride ion bound.

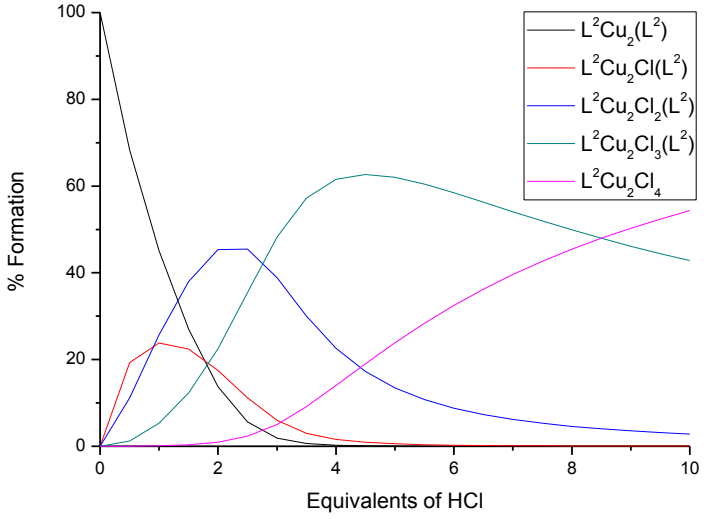

Figure 38. Predicted formation of $\mathbf{L^2}Cu_2Cl_4$ species as a function of hydrochloric acid equivalents. Formation based of the model fit with SPECFIT/32™ using the data obtained from the titration of **2** with hydrochloric acid in 50% DCE-IPA.

*3.2.7 Colourimetric Sensor Ability of **2** Upon Anion Binding*

The concept of colourimetric sensing of anions was discussed in Chapter 2. It was found that a substantial colour change was observed upon addition of hydrochloric, sulfuric, perchloric and tetrafluoroboric acid to solutions of **1**. Hydrochloric acid addition resulted in the largest colour change for the acid addition to **2** in DCE-IPA. From the calculated formation constants of the oxime-copper chloride system, no helicate will be present in this solution. The addition of acids to **2** results in the colour intensity of the original solutions decreasing. The darkening of the **2**-HI solution is attributable to the presence of the coloured hydroiodic acid.

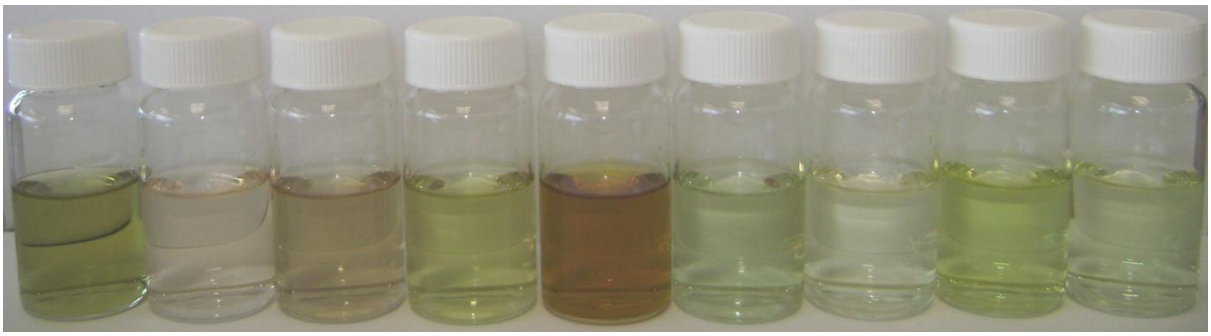

Figure 39. DCE-IPA solutions of **2** in the presence of the acids studied in this chapter. From left to right the solutions are; **2** only, **2**+HCl, **2**+HBr, **2**+HNO_3, **2**+HI, **2**+HBF_4, **2**+$HClO_4$, **2**+H_3PO_4 and **2**+H_2SO_4. The concentration of **2** is 349 μmol L^{-1} and acids are present at 100 equivalents.

3.2.8 Summary

It was observed for the acid titrations of **1** in Chapter 2 that there was an increase in binding with increasing size of the anion encapsulated. Figure 40 shows the stability constants calculated as a function of anion size. With the exception of nitrate, there is a trend of increasing binding strength with increasing anion size. Due to the method of which the sulfate binding was calculated detailed analysis of the binding value should be avoided. It can be noted that sulfate binding is likely to be greater than that of perchlorate and may be similar to phosphate binding. Iodide returned very similar values to that of tetrafluoroborate and this is likely a result of their similar volumes. The increase in binding between the spherical bromide and iodide anions is attributed to the increase in size. Similarly, the increase in binding between the tetrahedral tetrafluoroborate and perchlorate anions is again attributed to the increase in size potentially allowing greater metal anion interaction and hydrogen bond formation with

the protonated amines. The sulfate and phosphate anions are likely to possess increased binding due to high co-ordination ability in addition to their larger size. Nitrate binding is an abnormality in the trend of anion size. Nitrate binds exceedingly well despite its small size. It is bound selectively over bromide, iodide, tetrafluoroborate and the perchlorate anion. Attempts to grow crystals of the **2**-nitrate adduct were unsuccessful so it remains unknown why nitrate exhibits such high binding. The addition of hydrochloric acid to produce the linear $\mathbf{L^2}Cu_2Cl_4$ species was an interesting discovery. This mechanism was thought to be occurring at least to some extent for the freebase **1** system, but was the dominant process for **2**. Attempts at producing X-ray quality crystals of the $\mathbf{L^2}Cu_2Cl_4$ species were unsuccessful. The discussions on the protonation of **1** in Chapter 2 also applies to the protonation of **2**. The titrations of **2** in the DCE-IPA solvent system differed from those of **1** in IPA. Both systems exhibited a general trend of increasing stability constants with increasing size. The values calculated for **2** were generally stronger than for **1** but lacked any strong specificity like that obtained for sulfate encapsulation by **1**. It cannot be ignored that these differences could have been the result of the change in solvent system used for the titrations and not a result of the altered helicate structure. The comparison of the two systems and the affect of the altered solvent system are discussed further in Chapter 4.

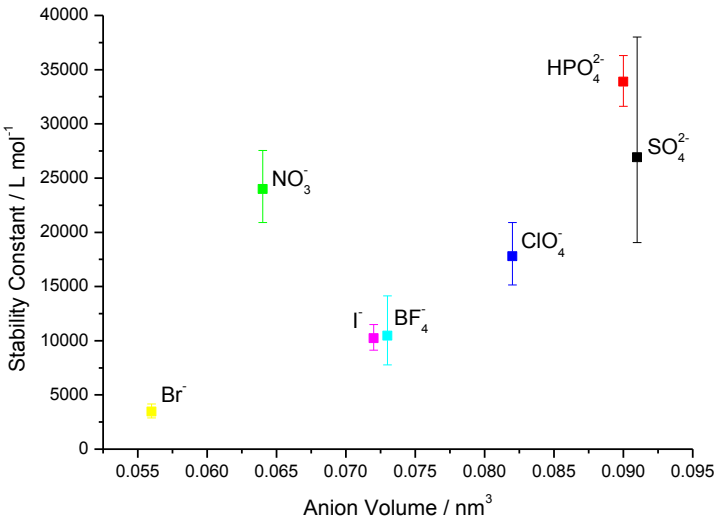

Figure 40. The calculated stability constants for anions binding within the cavity of **2** as a function of anion size. Error bars represent one standard deviation of the values obtained. Anion volumes are taken from the paper by Jenkins *et al.*[59]

3.3 Experimental

3.3.1 Materials and Reagents

The titration apparatus was used as for the titrations of **1** in Chapter 2. Stability constants were calculated using the software program SPECFIT/32™.[72-75] All reagents were of AR grade and used as received. Free base **2** and **2**.SO_4 were prepared as for the procedures in Chapter 6 and dried under vacuum for one hour prior to preparation of the titration solutions. Titrations were performed immediately after making up the complex solutions.

3.3.2 Spectrophotometric Titrations

Solutions of **2** in a 50% (v/v) DCE-IPA solution (2 mL, 3.25×10^{-5} – 4.06×10^{-5} mol L^{-1}) were titrated with 50% (v/v) DCE-IPA solutions of the acid of interest 2.3×10^{-3} – 8.16×10^{-3} mol dm^{-3} until no further spectrum changes were observed. Spectra were recorded following the addition of each aliquot over the wavelength range of 900 to 250 nm. Acid solutions were titrated in at 0.5 molar equivalence increments for the acids used. DBU was also titrated at 0.5 equivalents. The acid and DBU solutions were added using a 0.5 – 10.0 μL autopipette. The acids; $TBAH_2PO_4$, H_3PO_4, H_2SO_4, $HClO_4$, HBF_4 and HNO_3 were titrated until 10 equivalents. A 1:4 binding model was used for the HCl titration of **2** as suggested by experimental evidence. A 1:1 binding model was used for the remaining acid titrations of **2**. A 1:1 binding model was also used for the DBU titration of **2**.$(H_2SO_4)_2$. The data were analysed using the software program SPECFIT/32™. The titrations were repeated in order to obtain three stability constants within the error limits given by the programme. Stability constant errors are the standard deviations of the three obtained results.

3.3.3 Method of Continuous Variation

The method of continuous variation was applied to solutions of **2** and the various acids used as described in Chapter 2 for **1**. The concentrations of the equimolar solutions of **2** and the acid of interest were 3.25×10^{-5} – 4.06×10^{-5} mol L^{-1}.

3.3.4 Solution Preparation

The solutions used for the acid titration of **2** were prepared as for titrations of **1** in Chapter 2 with the following exceptions. All solutions were prepared using a 50% (v/v) DCE-IPA solvent mixture. Solutions of **2** possessed a concentration of (32.5 ± 0.8 to 40.6 ± 0.8) μmol L^{-1}.The final concentrations of the acid solutions are shown in Table 6.

Acid	Concentration/mmol L^{-1}
Phosphoric	8.16 ± 0.04
Nitric	3.0 ± 0.6
Sulfuric	3.600 ± 0.007
Perchloric	2.321 ± 0.009
Hydrochloric	4.6
Hydrobromic	3.5
Hydroiodic	2.9
Tetrafluoroboric	2.9

Table 6. Acid concentrations used for the titrations of **2** in DCE-IPA.

3.3.5 $[BF_4 \subset Cu_2 \boldsymbol{L_2^2}](BF_4)_3$ *(**2**.BF_4) Synthesis via the Free Base*

The oxime free base **2** (52.7 mg, 0.0428 mmol) was dissolved in warm methanol (20 mL) with stirring. A tetrafluoroboric acid solution in methanol was produced by diluting an ether solution of tetrafluoroboric acid (7.30 mol L^{-1}) by tenfold with methanol. The methanol acid solution (280 μL, 0.204 mmol, 4.78 equivalents) was then added to the solution of **2** and stirred overnight. The solution was then concentrated by evaporation and the product precipitated by diethyl ether diffusion and washed with diethyl ether to give a dark green powder (49 mg, 63%). In order to increase purity, the product was recrystalised two additional times by diethyl ether diffusion into acetonitrile (25 mg, 32%). Found: C 46.85; H 6.29; N 7.07%, $C_{64}H_{100}Cu_2N_8O_8B_4F_{16}.3H_2O$ requires: C 46.93; H 6.52; N 6.84%. *m/z* (ESI) 661.91 $[\mathbf{1}H_3 \supset BF_4]^{2+}$. ν_{max} (KBr)/ cm^{-1} 3630m (O-H), 1617s (C=N).

Chapter 4

Assessment of Anion Binding

4.1 Results and Discussion

*4.1.1 Trends in Binding Between the Helicates **1** and **2***

The anion stability constants of **1** in IPA and **2** in DCE-IPA are shown below (Figure 41). There is a general trend of increasing stability constants with the increasing size of the encapsulated anion. The larger size of the anions allows for more efficient hydrogen bond formation between the protonated amines. The closer proximity to the amine centres enabled by the larger sized anions also allows for greater electrostatic interactions. The high stability of sulfate and phosphate encapsulation within **1** and **2** is a direct consequence of co-ordination to the copper centres in solution. Excluding the nitrate anion, Log_{10} K of anion binding to **2** exhibits a high linear correlation with the size of the anions (R^2=98%). Anion binding to **1** is very strong for the co-ordinating phosphate and sulfate anions but much weaker for the non-coordinating anions.

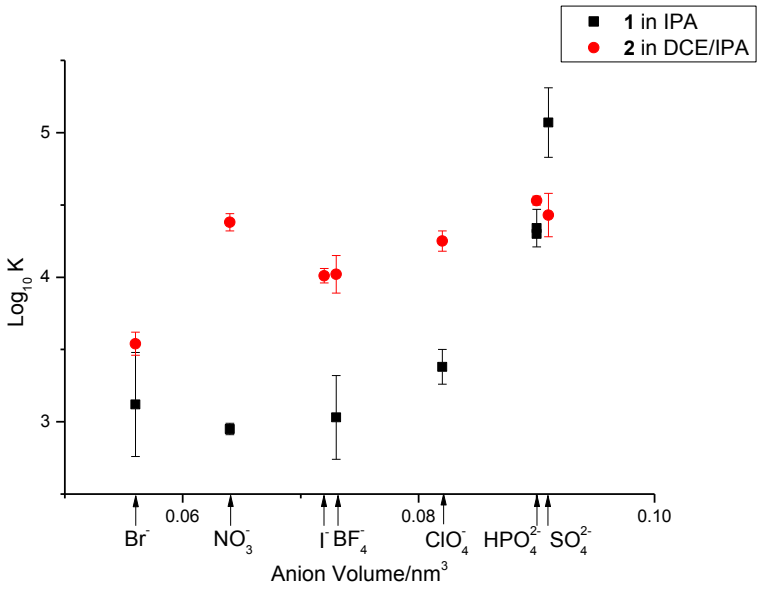

Figure 41. The determined anion stability constants of **1** in IPA and **2** in 50% DCE-IPA as a function of the anion volumes. The anion volumes used are taken from the paper by Jenkins *et al.*[59]

It is also obvious from Figure 41 that the binding of anions to **2** was substantially higher than for the binding to **1**. Sulfate is an exception to this trend and cannot be compared fairly due to the alternative method used to determine the binding constant of this anion with **1**. The greater binding of anions to **2** in contrast to **1** may have occurred as a result of the new solvent system rather than the stronger binding of anions by the oxime moiety. It has been previously shown that the introduction of even a small amount of protic solvent to an aprotic phase can substantially decrease the binding of anions by anion receptors via competition of hydrogen bonding and by the stronger solvation of anions.[80] In order to determine whether this was possible, some binding constants of **1** were obtained in the DCE-IPE solvent medium. The titration procedures and assumptions are as described in Chapter 2. Time restrictions did not allow for the full analysis of **1** in this system but a number of values were obtained and are overlaid on the values of **1** in IPA and **2** in DCE-IPA in Figure 42. The data shows that the solvent had little effect on the encapsulation of bromide and tetrafluoroborate and had a small increase for perchlorate and phosphate encapsulation. Judging from this data, phosphate must bind to both **1** and **2** equally well and the slight difference initially observed was a result of the differing solvent properties. This is not surprising as metal coordination will be the dominant binding mechanism for phosphate encapsulation.

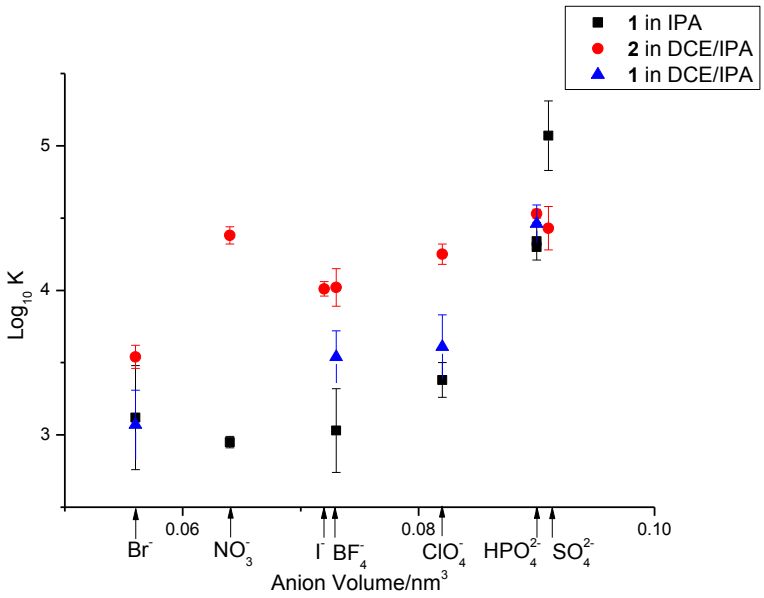

Figure 42. The determined anion stability constants of **1** in IPA, **2** in 50% DCE-IPA and **1** in 50% DCE-IPA as a function of the anion volumes. Anion volumes are taken from the paper by Jenkins *et al.*[59]

The values obtained for the encapsulation of anions within **1** in the DCE-IPA solvent system support that the increase in binding from **1** to **2** is an intrinsic property of the two host complexes.

*4.1.2 Interpretation of the Differences in Binding Between the Helicates **1** and **2***

The obvious structural difference between the oxime and the iminophenyl helicate is the environment of the copper centres. The presence of the oxime moiety results in the formation of a hydrogen bond to the phenolate oxygen on the opposing salicylaldimine moiety. This causes a favourable approximate square planar environment for the copper centre (Figure 43). The copper atom can then interact with an encapsulated anion to form a square pyramidal coordination environment. The hydrogen-bonds formed result in the stabilisation of the helicate compared to **1**. This is observed by the appearance of a singly positive peak representative of the free base oxime helicate which appears in the ESI-MS. The ESI spectrum of **1** shows only fragments of the helicate without the stabilising presence of a strongly bound anion such as sulfate. This added stabilisation appears to come at the expense of solubility hence the less polar/protic solvent system required for **2**.

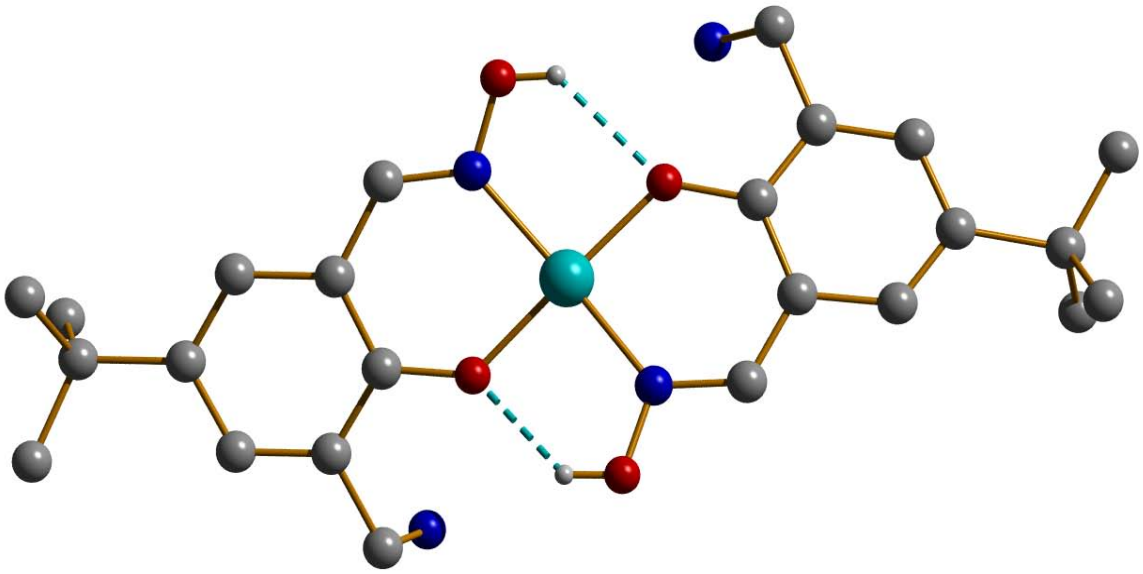

Figure 43. Copper square planar environment of $[BF_4 \subset \mathbf{2}H_4](BF_4)_3$. The oxime groups stabilise the copper centre by hydrogen bonding to the phenolate oxygen atoms.

In contrast to the planar salicylaldimine-Cu- salicylaldimine unit of **2**, the imine phenyl groups of **1** extend away from the centre of the helicate. This causes a distorted tetrahedral environment for the copper ions (Figure 44). Anions interacting with the copper centre from within the helicate cavity bind directly below the copper atom. Figure 41 and Figure 42 are ideal for rationalising the differences in stability constants between the two molecules. Table 7 summarises the key characteristics of the two structures. It is immediately apparent that despite binding the same sized anion, the copper centres of **2**.BF_4 are much closer together and the copper anion distances much smaller in comparison to the structure of **1**.BF_4. The anion free oxime helicate is not restricted to this compactness as the crystal structure of freebase **2** exhibits full extension of the alkyl straps and a copper-copper distance of 10.191(3) Å (Figure 45).[81] In the solid state the oxime helicate appears more conducive to the twisting of the arms in order to maximise binding of the encapsulated anions. The planar geometry of the hydrogen bonded oxime groups allow the alkyl chains to approach quite closely and results in a large twist angle, closer intramolecular copper-copper distance for the molecule and subsequently more effective binding of the tetrafluoroborate group. In the crystal structure of **1**.BF_4 the aromatic π electrons face C-H bonds from the alkyl chain. In solution however the phenyl groups would be rotating freely. The bulky phenyl groups would therefore restrict the twisting of the helicate due to steric repulsion

between them and the alkyl arms. The absence of this interaction in **2** explains the tighter cage obtained in the presence of tetrafluoroborate compared to **1**.BF_4.

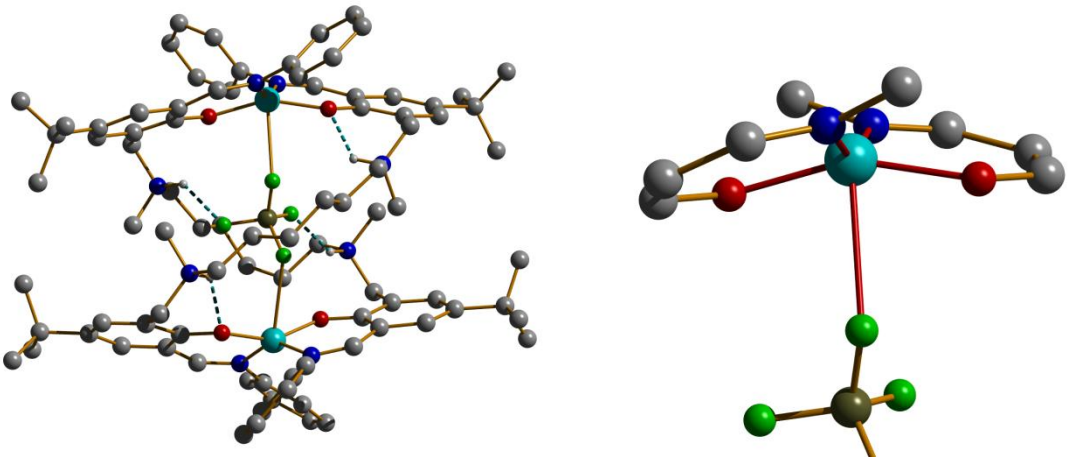

a. **b.**

Figure 44. a. Solid state structure of $[BF_4\subset\mathbf{1}H_4]^{3+}$. **b.** Enlargement of the distorted trigonal bipyramidal environment formed upon weak interaction with the copper centre of the BF_4^- anion.

	$[BF_4\subset\mathbf{1}H_4]^{3+}$	$[BF_4\subset\mathbf{2}H_4]^{3+}$
Cu-Cu distance/ Å	7.298(2)	6.938(2)
Cu-anion distance/ Å	2.676(5) and 2.729(5)	2.483(12) and 2.519(13)
Helical Twist/°‡	136.6(2) and 135.9(2)	119.3(4) and 120.6(3)

‡ The helical twist was calculated by measuring the torsional $O_{phenolate}$-Cu-Cu-$O_{phenolate}$ angle at each end of the ligand strand.

Table 7. Notable characteristics of $[BF_4\subset\mathbf{1}H_4]^{3+}$ and $[BF_4\subset\mathbf{2}H_4]^{3+}$.

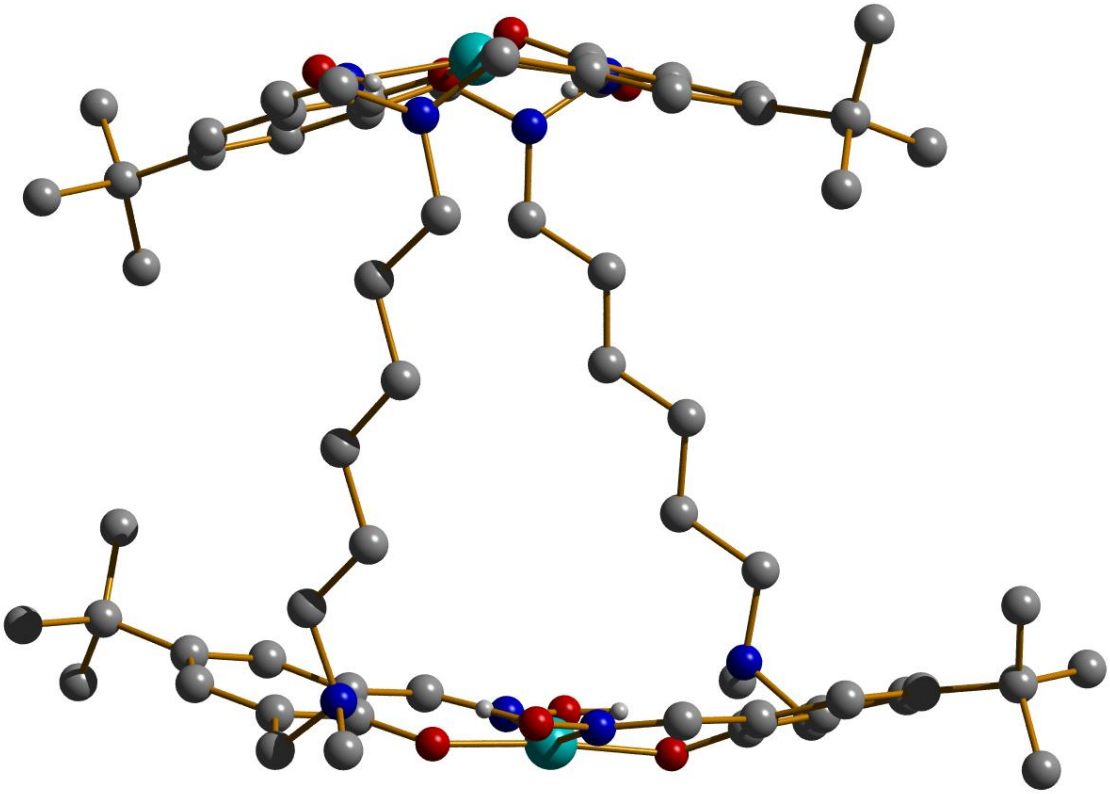

Figure 45. Solid state structure of the freebase helicate $[Cu_2(\mathbf{L}^2\text{-}2H)_2]$. Full extension of the alkyl straps results in a Cu···Cu distance of 10.191(3) Å.

The crystal structures of **1**.SO_4, **1**.I and **1**.NO_3 (Table 8) exhibit contraction of the iminophenyl helicate framework to more than what was expressed by the binding of tetrafluoroborate. The short Cu···Cu distance of the **1**.SO_4 crystal structure can be explained by the strong co-ordinating ability of sulfate, however the same cannot be said of the iodide and nitrate encapsulated structures. The structure of **1**.I has been described in detail in Chapter 2. The four strong hydrogen bonds are present between the protonated amines and the helicate phenolate oxygen atoms resulting in a favourable contraction of the helicate. The nitrate encapsulated structure of **1** possesses two hydrogen bonds to nitrate oxygen atoms which help to tighten the complex by contracting the alkyl arms toward this small molecule. Additionally, **1**.NO_3 possesses two intrahelical hydrogen bonds from the protonated amines towards the phenolate oxygen atoms of the salicylaldimine moiety as is shown in Figure 46.

	Cu...Cu distance/Å	Average Helical Twist‡
$[SO_4\subset\mathbf{1}H_4]^{2+}$	6.394(2)	120.6(2)
$[I\subset\mathbf{1}H_4]^{3+}$	6.970(4)	131.8(5)
$[NO_3\subset\mathbf{1}H_4]^{3+}$	7.0203(9)	130.8(1)
$[ClO_4\subset\mathbf{1}H_4]^{3+}$	7.2775(5)	133.50(8)
$[BF_4\subset\mathbf{1}H_4]^{3+}$	7.298(2)	134.3(2)

‡ The helical twist was calculated by measuring the torsional $O_{phenolate}$-Cu-Cu-$O_{phenolate}$ angle at each end of the ligand strand.

Table 8. Intramolecular copper distances for the solid state structures of **1** with differing encapsulated anions.

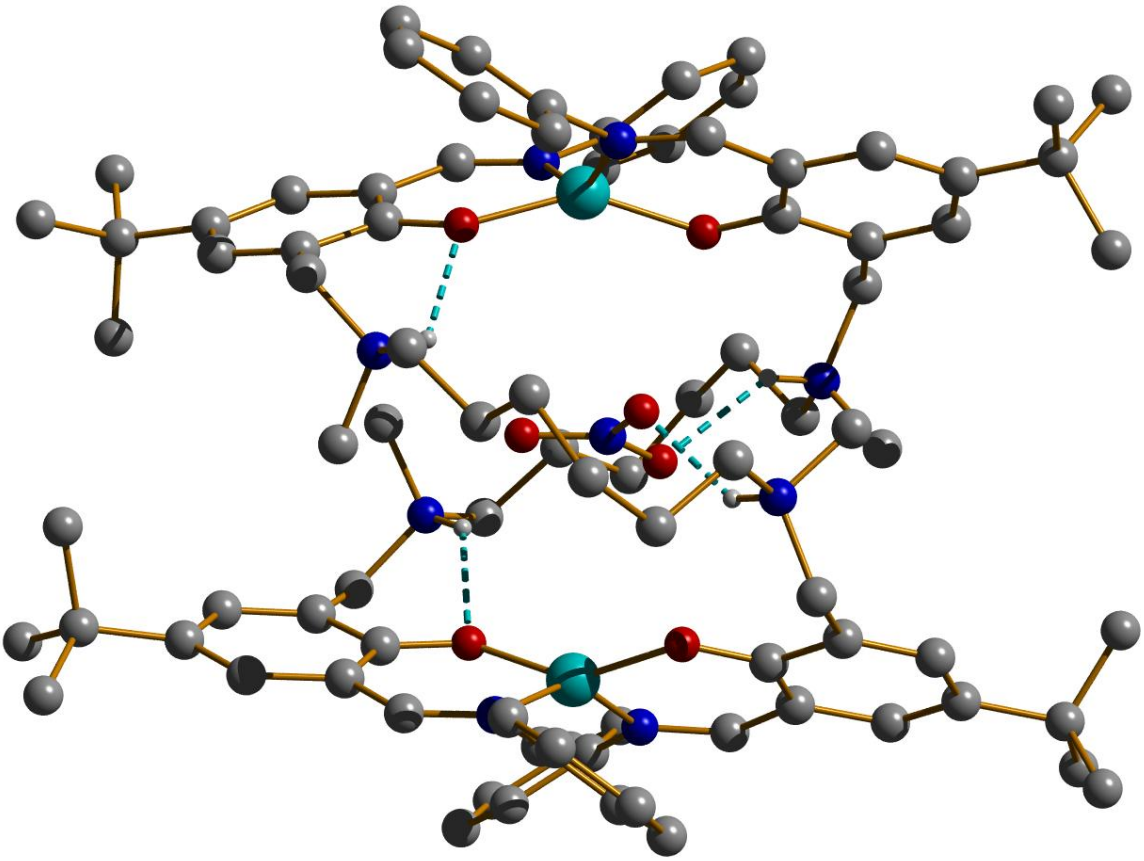

Figure 46. Solid state structure of $[NO_3\subset\mathbf{1}H_4]^{3+}$.[53] The two amine-phenolate hydrogen bonds and the two amine-nitrate hydrogen bonds are shown (dashed, turquoise).

*4.1.3 Summary of the anion binding between **1** and **2***

The high binding of **1** towards sulfate makes it ideally suited to the selective uptake over the remaining anions studied in IPA. For greater extraction of the remaining ions, the oxime helicate would be more effective, however this receptor suffers from a lack of selectivity for specific anions with the exception of perhaps nitrate. The high binding of the nitrate anion by **2** is intriguing. The 2.14 Å bite length of nitrate is far too small for strong Cu···O-NO-O···Cu binding. The structure of **1**.NO_3 showed two hydrogen bonds toward the nitrate anion and two toward phenolate oxygen atoms which were pointing into the complex as a result of the phenyls extending out of the helicate. The planar arrangement of the salicylaldimines around the copper centre means that the phenolate oxygen atoms are not approaching into the helicate and the formation of hydrogen bonds to the phenolate oxygen atoms from the amines may be inhibited. This may result in strong hydrogen bonding of the encapsulated nitrate anion and account for the increased UV-visible stability constant obtained. The increase in binding in the DCE-IPA solvent system suggests itself to a two phase extraction mechanism in which an aqueous acid phase is mixed with an organic host phase. The amount of anions transferred could then be calculated to determine efficiency.

4.2 Experimental

4.2.1 Materials and Reagents

All reagents were of AR grade and used as received. Free base **1** was prepared as in the procedure in Chapter 6 and dried under vacuum for one hour prior to the preparation of the titration solutions. Titrations were performed immediately after making the complex solutions. The titration apparatus used was the same as that used for the titrations of **1** (Chapter 2). Stability constants were calculated using the software program SPECFIT/32™.[72-75]

4.2.2 Spectrophotometric Titrations

Solutions of **1** in a 50 % DCE-IPA solution (2 mL, 3.06×10^{-5} – 3.73×10^{-5} mol L^{-1}) were titrated with 50 % DCE-IPA solutions of the acid of interest 3 – 5 x 10^{-3} mol dm^{-3} until no further spectrum changes were observed. Spectra were recorded following the addition of each aliquot over the wavelength range of 900 to 250 nm. Acid

solutions were titrated at 0.5 molar equivalence increments for H_3PO_4, $HClO_4$, HBF_4 and HBr using a 0.5 – 10.0 μL autopipette. This was at 5, 7, 10 and 8 equivalents for H_3PO_4, $HClO_4$, HBF_4 and HBr respectively. The data were analysed using the software program SPECFIT/32^{TM}. The titrations were repeated in order to obtain three stability constants within the error limits given by the programme. Stability constants errors are the standard deviations of the three obtained results.

4.2.3 Solution Preparation

All solutions were prepared using a 50% v/v DCE-IPA solvent mixture. Solutions of **1** possessed a concentration of (30.6 ± 0.7 to 37.3 ± 0.7) μmol L^{-1}. The concentrations of the acids used are shown in Table 9.

Acid	**Concentration/mmol L^{-1}**
Phosphoric	8.16 ± 0.04
Perchloric	2.321 ± 0.009
Tetrafluoroboric	2.9
Hydrobromic	3.5

Table 9. Acid concentrations used for the titrations of **1** in DCE-IPA.

Chapter 5

Conclusions and Future Work

5.1 Conclusions

A solution study of the dicopper helicates formed with salicylaldimine ligands has been completed. To the authors knowledge this is the most extensive study of anion encapsulation within a helicate cavity. The stability constants for encapsulation of seven anions were determined for **1** in IPA and for **2** in a DCE-IPA medium. The destructive binding of chloride to **2** was also determined. Anions encapsulated within receptors **1** and **2** included tetrafluoroborate and several oxyanions, the trigonal nitrate anion and the spherical iodide and bromide ions. The binding of four anions to **1** in DCE-IPA was also determined for the spherical chloride anion. Extensive experience was obtained in the area of solution binding and the determination of stability constants. Binding studies were supported by electrospray ionisation mass spectrometry and conductivity studies. The solid state structure of iodide encapsulated within protonated **1** was obtained by X-ray crystallography. The results within this thesis have greatly enhanced the knowledge of **1** and **2** and their interactions with anions in solution.

The iminophenyl copper helicate was investigated initially for its ability to bind the anions studied. Many spectra were recorded to study the evolution of properties upon addition of various acids. Due to the similarity of the UV-visible absorbances of the host and anion encapsulated species, monochromatic analysis of data obtained did not provide reliable binding constant values. For this reason, multivariate analysis of the recorded data across the entire spectrum was performed using the software program SPECTFIT/32^{TM}. The stability constants obtained were spread across two orders of magnitude from the weakly bound nitrate anion ($10^{2.95}$ M^{-1}, encapsulation into **1**) to the

impressive binding of the sulfate anion ($10^{5.07}$ M^{-1}, encapsulation into **1**). The remaining anions were bound between these extremes. The recorded conductivity data supported the encapsulation of sulfate, perchlorate and tetrafluoroborate in nitromethane in a non-equilibrium situation. This data can be used as a reference for future conductivity studies concerning similar macromolecules. ESI mass spectrometry data fully supported the binding of anions. The fragmentation of **1** in the mass spectrometer in the absence of a stabilising anion is support for the encapsulation of the bound anions.

Armed with the experience of the IP system, the solution properties of the oxime system were investigated. As a result of decreased solubility DCE was introduced into the solvent medium. With no available data on the effect of anion binding upon addition of chloroalkanes or similar solvents to an alcoholic solution, the solvent effect was purely speculative. In order to gain an understanding of this effect additional titrations of **1** in DCE-IPA with acids were performed. In addition to the understanding it added to this study it will provide an example of the effects of changing the solvent system on encapsulation for the literature. On switching to the oxime system it was observed that an increase in anion binding strength was evident over the iminophenyl in a pure IPA system, however there was less discrimination in binding strength between the anions studied in the freebase **2** system. The reaction of **2** with chloride led to an interesting discovery. Despite the high stability of the oxime centre, chloride is able to break the copper imine and copper phenolate bonds. Decomposition of approximately 100% of the helicate concentration can occur by the introduction of four equivalents of chloride in solution.

Only tetrafluoroborate has been observed encapsulated in the internal cavity of **1** and **2** in the solid state. The study of the structural differences between tetrafluoroborate encapsulated in **1** and **2** provides clues as to why binding is different in solution for anions with the two helicates. The increased binding is a result of the ability of the oxime helicate to contract more efficiently than the sterically hindered iminophenyl helicate. The UV-visible titrations of tetrafluoroborate into **1** and **2** revealed greater binding to **2**. Increased binding to **2** was additionally observed for bromide, nitrate, perchlorate, and phosphate. Stability constants of anion binding in DCE-IPA revealed that the solvent medium was only responsible for a portion of the increase.

During the course of this thesis the crystal structure of iodide encapsulated within **1** was obtained. The structure possessed the typical distorted tetrahedral copper environment and encapsulated anion for copper salts of $\mathbf{L^1}$. It differed from the previous structures of **1** (or **2**) in that there was no hydrogen bonding present to the central anion. Instead, four hydrogen bonds were formed with the phenolate oxygen atoms bound to the copper centres. This resulted in the contraction of the helicate to a much greater extent than expected for a non-coordinating anion substrate. The similar volume tetrafluoroborate anion for example possessed a Cu···Cu distance 0.32 Å greater than that of iodide encapsulated within **1**.

5.2 Applications

Many of the anions studied are of environmental importance. Prevention of leeching of phosphate and nitrate into the environment is important in the prevention of eutrophication of lakes and waterways.[6] Perchlorate has been used as a model for binding of pertechnate which can leech into the environment from radioactive waste disposal.[9] Radioactive $^{131}I^-$ can also be located in radioactive waste.[9] Sulfuric acid is the most produced inorganic chemical in the United States as of 2007[82] and its recovery is important in applications such as mining.[76] The efficient binding by receptors for these anions and research on the mechanisms involved are a necessary contribution to this field of study. It was mentioned briefly in Chapter 4 that a two phase extraction mechanism could be utilised for the copper helicates studied. This would involve mixing an organic phase possessing the helicate. This organic phase could be mixed with a pH adjusted aqueous phase in order to remove anions or could be mixed with excess aqueous acid in order to recover the acid. This method, if found to be effective, could be extremely beneficial in industry processes by preventing the release of environmentally damaging anions and acids. Additionally, the anions could be recovered and reused.

5.3 Future Endeavours

The helicates studied exhibited efficient binding of a number of anions. For the oxime helicate in particular little selectivity was demonstrated. Increasing the selectivity of these helicates by modification of the aliphatic straps to provide additional hydrogen bonding is currently in progress. This may lead to the creation of receptors

with very high selectivity toward certain anions of interest. Exploration of phase extraction studies will provide an indication of how effective the helicates will be in the removal of acids or anions under industrial conditions.

Chapter 6

Synthesis of Ligands and Complexes

6.1 General Procedures

All reagents were purchased from standard chemical suppliers and were used without further purification unless stated. Copper(II) tetrafluoroborate hydrate was dried before use. All syntheses were carried out with analytical grade solvents.

Mass spectra were recorded using a Micromass ZMD 400 electrospray mass spectrometer. Microanalyses were completed by Campbell Microanalytical Laboratory at the University of Otago. IR spectra were run on a Perkin-Elmer FT-IR Paragon 1000 spectrometer using KBr discs. UV-visible spectra were recorded on a Shimadzu UV-3101PC UV-Vis-NIR Scanning Spectrophotometer. NMR spectra were recorded on a Bruker Avance 400 spectrometer.

6.2 Ligand Synthesis

3,3-[1,6-hexanediylbis[(methylimino)methylene]]bis[2-hydroxy-5-*tert*butyl-benzaldehyde] (**L^0**)

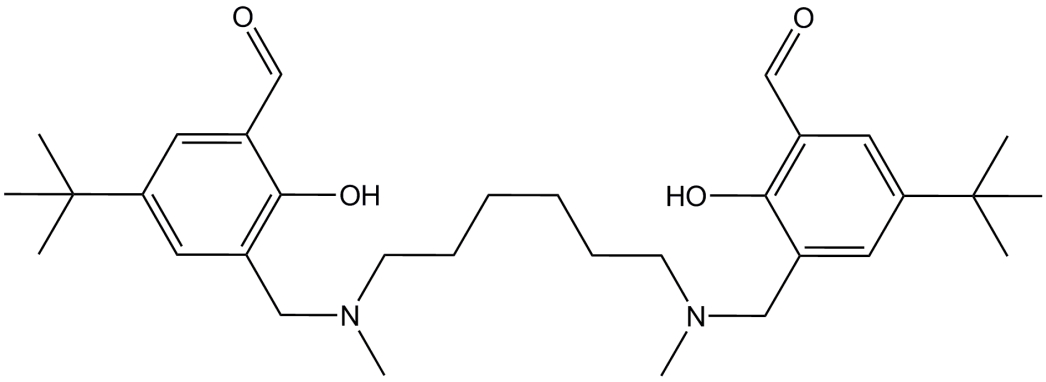

Figure 47. The precursor for ligand **L^1** and **L^2**

The precursor for ligands **L^1** and **L^2** was synthesised according to the literature procedure.[83] The ^{1}H NMR and IR data agreed with the reported data. δ_H (400 MHz; solvent $CDCl_3$, reference TMS): 10.36 (1H, s, C*H*=O), 7.63 (1H, s, Ar-*H*), 7.27 (1H, s, Ar-*H*), 3.73 (2H, s, Ar-C*H$_2$*-N), 2.50 (2H, t, N-C*H$_2$*-CH$_2$), 2.30 (3H, s, N-C*H$_3$*), 1.60 (2H, m, N-CH$_2$-C*H$_2$*), 1.36 (2H, m, N-CH$_2$-CH$_2$-C*H$_2$*) 1.29 (9H, s, C(*CH$_3$*)$_3$), 1.27 (2H, m, C*H$_2$*). *m/z* (ESI) 525.52 (**1a**)$^+$. ν_{max} (KBr)/cm^{-1} 3335br (O-H), 1676s (C=O), 1049s (C-N), 887s, 825s, 813s, 794s, 743s, 733s (Ar-R).

2,2-[1,6-hexanediylbis[(methylimino)methylene]]bis[4-*tert*butyl-6-(phenylazomethinyl)phenol] (**L**^{1})

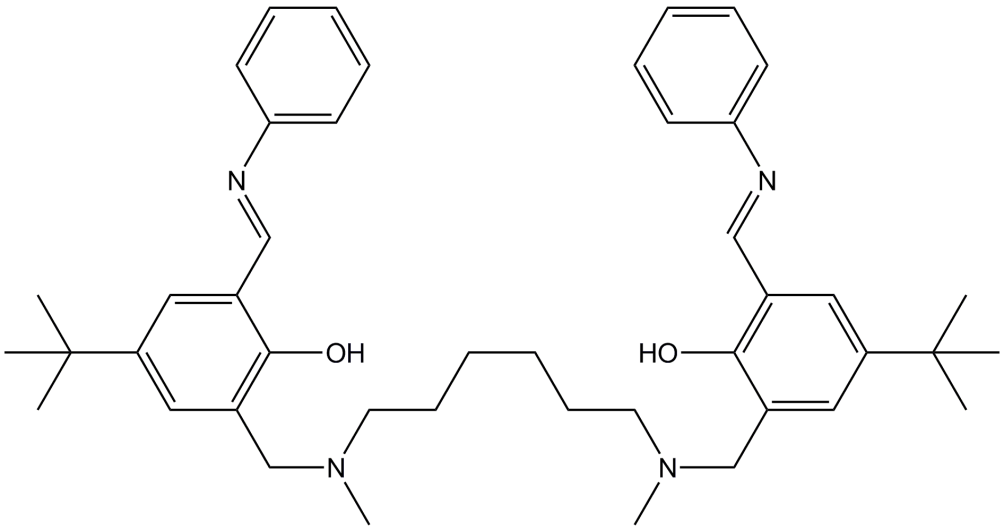

Figure 48. L^{1}.

Aniline (71 µL, 0.762 mmol) was added to a stirred solution of Ligand **L**^{0} (200 mg, 0.381 mmol) in acetonitrile (20 mL) and stirred for four hours. Ligand **L**^{1} was complexed by the addition of copper salts directly to the stirring solution.

3,3-[1,6-hexanediylbis[(methylimino)methylene]]bis[2-hydroxy-5-*tert*butyl-benzaldehyde oxime] **(L^{2})**

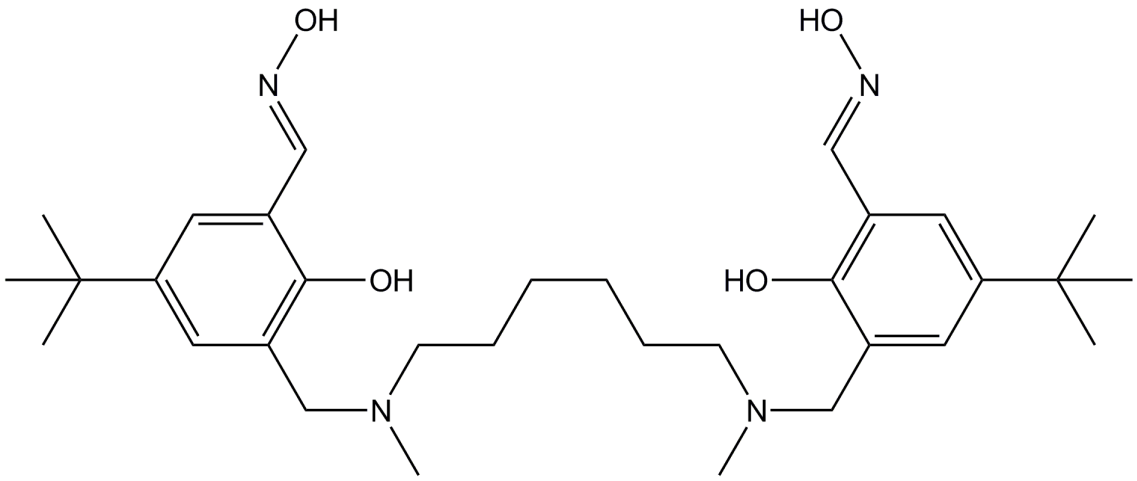

Figure 49. L^{2}.

$\mathbf{L^2}$ was synthesised from $\mathbf{L^0}$ according to the procedure used by Forgan.[84] A heated ethanolic solution (15 mL) of potassium hydroxide (41.2 mg, 0.734 mmol) was added to a heated ethanolic solution (15 mL) of hydroxylamine hydrochloride (59.2 mg, 0.852 mmol). The solution was cooled to room temperature and the white KCl precipitate was removed by filtration. Powdered $\mathbf{L^0}$ (189.6 mg, 0.3614 mmol) was added to the filtrate and the solution was refluxed for 24 hours. The solution was cooled to room temperature and the white precipitate was collected by filtration (171 mg, 84). *m/z* (ESI) 555.93 $(\mathbf{L^2})^+$. ν_{max} (KBr)/cm^{-1} 3431br (O-H), 1630s (C=N).

6.3 Complex Synthesis

*6.3.1 $Cu_2(\mathbf{L^1}\text{-}2H)_2$ (**1**) Synthesis*

Aniline (71 µL, 0.762 mmol) was added to a stirred solution of Ligand $\mathbf{L^0}$ (200 mg, 0.381 mmol) in acetonitrile (20 mL). Solid copper(II) acetate monohydrate (76 mg, 0.381 mmol) was added directly to the solution and the reaction was stirred for 24 hours. An immediate colour change from pale yellow to an intense brown was observed on addition of the copper salt. The solvent was removed under reduced pressure and dried under vacuum. The complex was dissolved in diisopropyl ether (20 mL), filtered, and the solvent removed and dried under vacuum to give a brown powder. The product was dissolved in 20 mL of chloroform and washed with 0.1 mol L^{-1} sodium hydroxide (3 x 10 mL) followed by water (3 x 10 mL). (239 mg, 85%). Found: C, 69.21; H, 7.58; N, 7.14%. $C_{88}H_{112}N_8O_4Cu_2.3H_2O$ requires C, 69.22; H, 7.79; N, 7.34%. *m/z* (ESI) 736.97 $[(\mathbf{L^1}\text{-H})Cu]^+$, 369.37 $[\mathbf{L^1}Cu]^{2+}$, ν_{max} (KBr)/cm^{-1} 3423br (O-H), 1618s (C=N).

*6.3.2 $[BF_4 \subset Cu_2\mathbf{L_2^1}](BF_4)_3$ (**1**.BF_4) Synthesis*

Aniline (69 µL, 0.742 mmol) was added to a stirred solution of Ligand $\mathbf{L^0}$ (200 mg, 0.381 mmol) in acetonitrile (20 mL) and stirred for four hours. Aqueous copper(II) tetrafluoroborate hexahydrate (1.60 mL, 252 mmol L^{-1}, 0.403 mmol) was then added to the reaction mixture resulting in a colour change from pale yellow to brown. This solution was stirred for a further 24 hours. The product was then precipitated by diethyl ether diffusion, collected and washed with diethyl ether to obtain a brown powder. The product was purified twice by recrystalisation with diethyl diffusion from acetonitrile. (363 mg, 52%). Found: C, 55.02; H, 6.32; N, 5.87%. $C_{88}H_{116}N_8O_4B_4F_{16}Cu_2 \cdot 5H_2O$

requires C, 55.21; H, 6.63; N, 5.85%. *m/z* (ESI) 782.11 ($[BF_4Cu_2\mathbf{L_2^1}]$-H)$^{2+}$, 521.89 $[BF_4Cu_2\mathbf{L_2^1}]^{3+}$. ν_{max} (KBr)/cm^{-1} 3425m (O-H), 1621s (C=N).

6.3.3 $[SO_4 \subset Cu_2\boldsymbol{L_2^1}]SO_4$ *(**1**.SO_4) Synthesis*

Aniline (75 µL, 0.821 mmol) was added to a stirred solution of Ligand $\mathbf{L^0}$ (212 mg, 0.404 mmol) in acetonitrile (20 mL) and stirred for four hours. Copper(II) sulfate pentahydrate (109 mg, 0.437 mmol) was then added to the reaction mixture resulting in a colour change from pale yellow to dark green. This solution was stirred for a further 24 hours. The product was then precipitated by diethyl ether diffusion, collected and washed with diethyl ether to obtain a green powder. The product was purified twice by recrystalisation with diethyl diffusion from acetonitrile. (226 mg, 67%). Found: C, 63.24; H, 7.14; N, 8.17%. $C_{88}H_{116}N_8O_{12}S_2Cu_2 \cdot 2CH_3CN$ requires C, 63.10; H, 7.02; N, 8.00%. *m/z* (ESI) 787.06 $[SO_4Cu_2\mathbf{L_2^1}]^{2+}$. ν_{max} (KBr)/cm^{-1} 3409m (O-H), 1619s (C=N).

6.3.4 $\left[ClO_4 \subset Cu_2\boldsymbol{L_2^1}\right](ClO_4)_3$ *(**1**.ClO_4) Synthesis*

Aniline (35 µL, 0.0.381 mmol) was added to a stirred solution of Ligand $\mathbf{L^0}$ (100 mg, 0.191 mmol) in methanol (20 mL) and stirred for four hours. Copper(II) perchlorate hexahydrate (102 mg, 0.202 mmol) dissolved in methanol (20 mL) was then added to the reaction mixture resulting in a colour change from pale yellow to brown. This solution was stirred for a further 24 hours. The product was then precipitated by diethyl ether diffusion, collected and washed with diethyl ether to obtain a brown powder. (96 mg, 47%). Found: C, 55.24; H, 6.37; N, 5.70%. $C_{88}H_{116}N_8O_{20}Cl_4Cu_2 \cdot 2H_2O \cdot MeOH$ requires C, 55.02; H, 6.43; N, 5.77%. *m/z* (ESI) 788.01 ($\left[ClO_4Cu_2\mathbf{L_2^1}\right]$-H)$^{2+}$. ν_{max} (KBr)/cm^{-1} 3426m (O-H), 1619s (C=N).

6.3.5 $Cu_2(\boldsymbol{L^2}$*-2H)$_2$ (**2**) Synthesis*

$\mathbf{L^2}$ (190 mg, 0.342 mmol) was stirred in hot ethanol (50 mL) to form a cloudy white suspension. Copper(II) acetate dihydrate (72 mg, 0.361 mmol) was added directly to the ligand solution causing a colour change to dark green. The mixture was refluxed for 24 hours over which time the solution darkened to a dark green colour and clarified. The solution was then concentrated by evaporation and the product precipitated by diethyl ether diffusion and washed with diethyl ether to give a green-

brown powder. The powder was dissolved in chloroform (25 mL) and washed with dilute ammonia (2 x 10 mL) followed by water (2 x 10 mL). The complex solution was then evaporated to dryness and dried under vacuum to constant weight. Yield (136 mg, 65 %). Found: C, 50.96; H, 5.97; N, 7.46%. $C_{64}H_{96}N_8O_8Cu_2 \cdot 3CH\ Cl_3$ requires C, 50.59; H, 6.27; N, 7.04%. *m/z* (ESI) 1233.99 $[Cu_2(\mathbf{L^2}\text{-}2H)_2]^+$. ν_{max} (KBr)/ cm^{-1} 3422m (O-H), 1629s (C=N).

6.3.6 $[BF_4 \subset Cu_2\boldsymbol{L_2^2}](BF_4)_3$ *(**2**.BF_4) Synthesis*

$\mathbf{L^2}$ (102 mg, 184 mmol) was stirred in hot ethanol (20 mL) to form a cloudy white suspension. Copper(II) tetrafluoroborate hexahydrate (71 mg, 0.207 mmol) was added to the ligand solution causing a colour change to a very dark green. The mixture was refluxed for 24 hours over which time the solution darkened further. The solution was then concentrated by evaporation and the product precipitated by diethyl ether diffusion and washed with diethyl ether to give a green powder. The product was recrystalised twice by diethyl ether diffusion into acetonitrile. Yield (95 mg, 65 %). Found: C, 46.93; H, 6.52; N, 6.84%. $C_{64}H_{100}N_8O_8B_4F_{16}Cu_2 \cdot 3H_2O$ requires C, 46.85; H, 6.29; N, 7.07% *m/z* (ESI) 661.93 $([BF_4Cu_2\mathbf{L_2^2}]\text{-}H)^{2+}$. ν_{max} (KBr)/cm^{-1} 3632m (O-H), 1620s (C=N).

6.3.7 $[SO_4 \subset Cu_2\boldsymbol{L_2^2}]SO_4$ *(**2**.SO_4) Synthesis*

$\mathbf{L^2}$ (100 mg, 0.180 mmol) was stirred in hot ethanol (20 mL) to form a cloudy white suspension. Copper(II) sulfate pentahydrate (47 mg, 0.188 mmol) was then added to the reaction mixture resulting in a colour change to dark green. This solution was then refluxed for a further 24 hours. The product was then precipitated by diethyl ether diffusion, collected and washed with diethyl ether to obtain a green powder. The product was recrystalised twice by diethyl ether diffusion into acetonitrile. Yield (96 mg, 75%). Found: C, 53.54; H, 7.22; N, 7.74%. $C_{64}H_{100}N_8O_8S_4O_{16}Cu_2$ requires C, 53.80; H, 7.05; N, 7.84% *m/z* (ESI) 666.92 $[SO_4Cu_2\mathbf{L_2^2}]^{2+}$. ν_{max} (KBr)/cm^{-1} 3417m (O-H), 1633s (C=N).

Appendix A

Beginners Guide to SPECFIT/32

SPECFIT/32™ is a multivariate data analysis program for modelling and fitting chemical kinetics and equilibrium titration data. The spectral information is imported as three dimensional data sets obtained from multi-wavelength spectrophotometric measurements. These 3D data sets usually contain measurements of absorbance vs. wavelength as a function of an independent variable such as time, pH, or titrant concentration.

There are two types of files that need to be created for use in SPECFIT/32^{TM}. The raw data can be imported using either *.txt*, or *.csv* file formats and is converted to program specific files. The *.dat* file which is created by SPECFIT/32^{TM} contains all of the titration information; volumes and concentrations of solutions used, wavelengths and absorbances of the recorded titrations and the temperature recorded over. The *.fix* file contains the said data for a single spectrum only. If the titrant absorbs over the wavelengths studied then two *.fix* files will need to be created; one for the analyte, and one for the titrant, otherwise only an analyte *.fix* file is needed. In order for SPECFIT/32™ to create the files needed they must be imported in *.txt* or *.csv* format. The simplest way to do this is to edit the spectrometric data using Microsoft Office Excel and save it as a *.txt* file. The first column should contain the wavelength in nm while subsequent columns should contain the measurement taken; absorbance, intensity etc. in titration order. The data should only contain numerical cells and not headings. The precursor to the *.dat* file will contain all of the titration measurements. Precursors to *.fix* files contain only two columns; the wavelength and the recorded measurement values.

To import the *.fix* files, under the *Import Menu* in SPECFIT/32^{TM}, select *Single Scan Spectra*. The *Single Scan File Import Control* window will open (Figure A-1).

Under the heading *Import Converter ASCII-XY .TXT Single Scan Spectra* should be selected, and the search pattern should be set to **.TXT*. Locate the file required, and ensure the *Experiment Type* is set to *Known Spectrum (.FIX) File Import*. Select *Import Files* and input the values for $[Sample]_o(M)$ and *Temperature* before selecting *OK*. Agree to the default file location and exit the import window. The molar absorbance as a function of wavelength of the spectra you just imported should now be displayed.

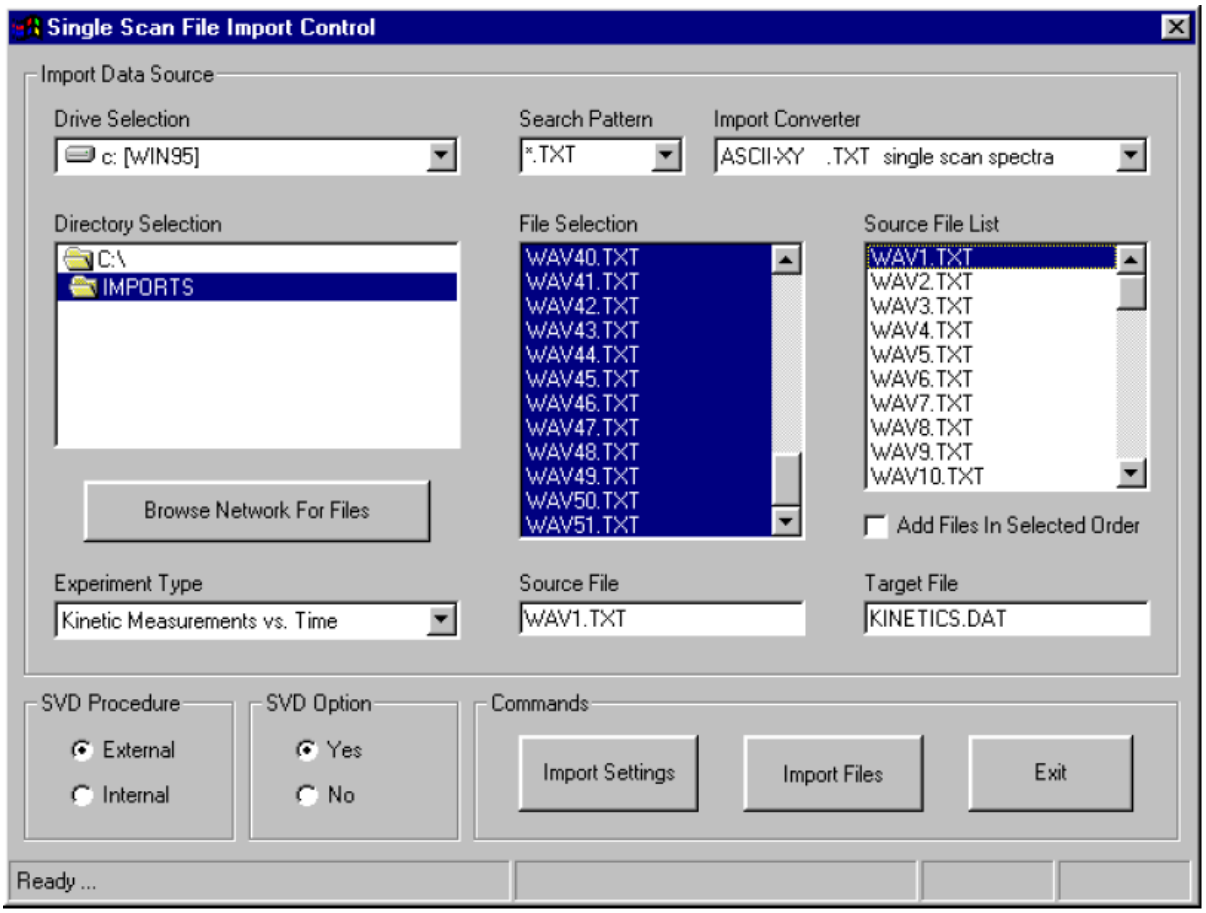

Figure A-1

In order to import the titration *.txt* file created, open the *Import Menu* and this time select *Multiscan File Import*. Select *ASCII-XYY.ASC block XYY & Z* worksheet from the *Import Converter* drop down menu and select **TXT* under search pattern. Select the *Import Files* option and choose the experiment type from the *Data Type* window and select *OK*. For the addition of a single titrant component into a solution of a reacting species, the *Complexation vs. [Ligand]* or the *Complexation vs. [Metal]* models are ideal. The *Complexation / pH Titration File Information* window will open (Figure A-2). Ensure that the correct *Titration Type* is selected and that the *Volumetric*

Method is set to *Dilution with Aliquots* and the *Volumetric Dilution* is set to *Dilute Sample and Titrant*. The *Component Style* menu defines the component labels (for example to a host guest titration) but does not affect the calculations utilised. The concentration and volumes of the solution used and the temperature must be entered. Before selecting *OK* it is advised to confirm the correct values have been entered by selecting the *Auto-Fill Concentrations* option below the *Volumetric Data* options and comparing with the manually calculated values. If the *.fix* file window previously imported was closed then the titration spectra will be displayed onscreen in red. If not, use the *Open* command and locate the *.dat* file in the *Data* folder within the *Specfit* folder.

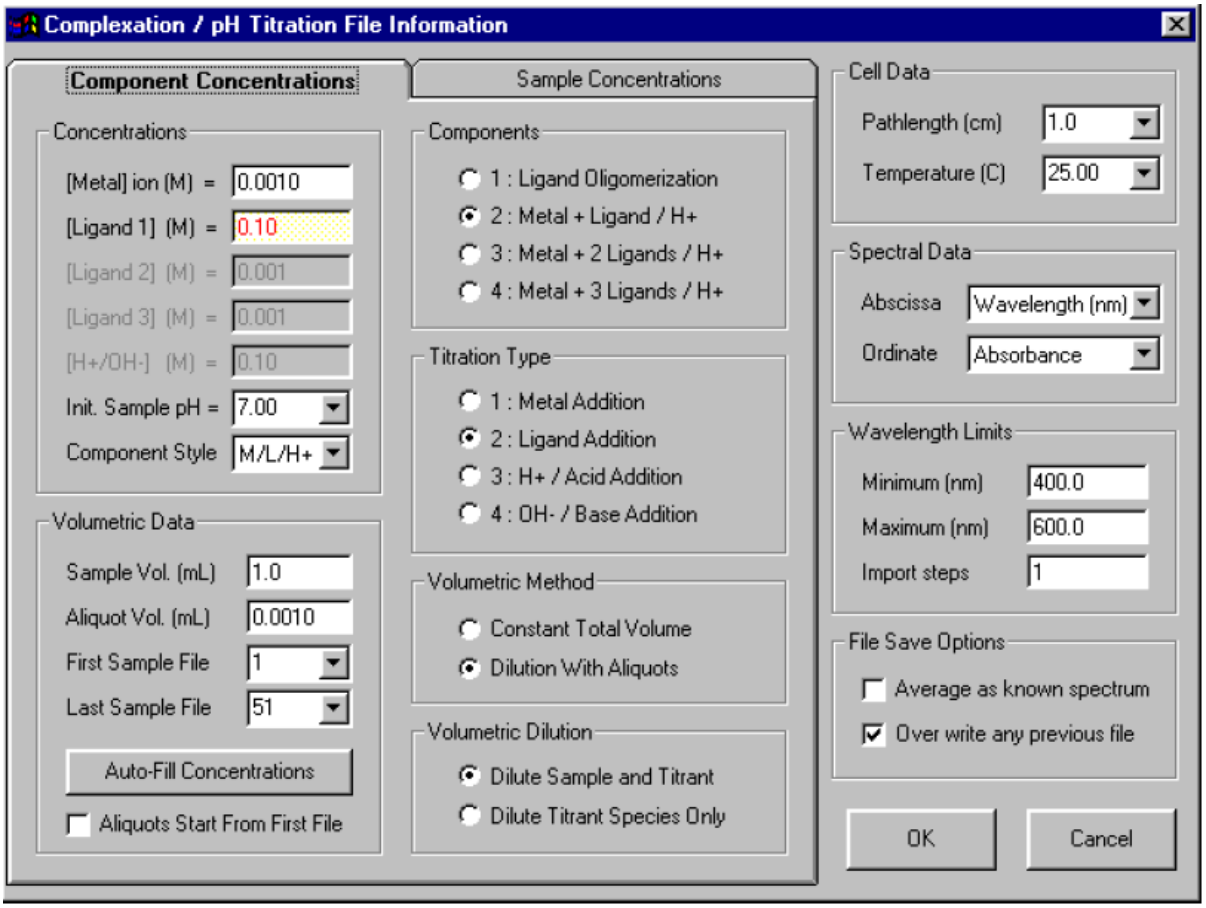

Figure A-2.

In order to fit a formation constant, the *Fitting Toolbar* on the left side of the screen can be used. It also provides options for viewing the results. Additional display modes can be located from the *Plot Menu*. To calculate the formation constant, select the *Model* command from the *Fitting Toolbar*. The *Speciation Model* window will now

open. Each solution species is represented by a series of numbers. The numbers for the *Complexation vs. [Ligand] Titration Data Type* with a single ligand addition are as follows. The first number is the number of metal/host moieties present in the species. The second is the number of bound ligands/guest. The stoichiometry needed can be determined by the method of continuous variation. The concentration eigenvector analysis (*U* option on the *Fitting Toolbar*) also effectively indicates how many coloured species are present in solution. Coloured components of the titration must be selected and the *.fix* files for these components may be imported in the *Known Spectra* drop down menus. The titrant and analyte species must be set at zero formation constant and the *Fixed* box selected. If protonation of the complex is to be calculated, then the ligand protonation constants are required. Once the values are set select the *Save* command which closes the window. Selecting the *Fit* menu item in the *Fitting Toolbar* will solve the model using the selected model and parameters. Any convergence errors suggest problems with the data or model used. Usually data problems can be corrected by recording further titration data or adjusting the titration increments.

Selecting the *Info* button from the *Fitting Toolbar* will open the *Fit Results* window (Figure A-3). The *Convergence Statistics* are displayed to the left and the formation constants (*Log β*) are displayed with a calculated error value to the right. Selecting the *Residuals Analysis* tab allows the analysis of the errors, species concentration profiles and the calculated absorbance spectra. The latter two can be viewed via the *Fitting Toolbar menu*. Details will produce a *.txt* file of the input and modelled details which can be saved or printed. The initial check that an adequate model has been obtained is if the calculated absorbances match the titration spectra obtained experimentally. The percent error of the standard deviation errors should also be symmetrical. Close the window, highlight a peak on the displayed spectra with the cross-hair and select the *Extract* option on the *Fitting Tool* bar. This allows the fitted and calculated absorbances to be compared as a function of titrant addition. This should be confirmed at any major absorption peaks. Significant differences between the predicted and recorded absorbance profiles indicates an inappropriate model has been applied. The absorbance may deviate from that predicted in areas of very low absorbance without concern. The *Residuals* option from the *Fitting Toolbar* will illustrate if there is any remaining spectral information which has not been incorporated into the model produced.

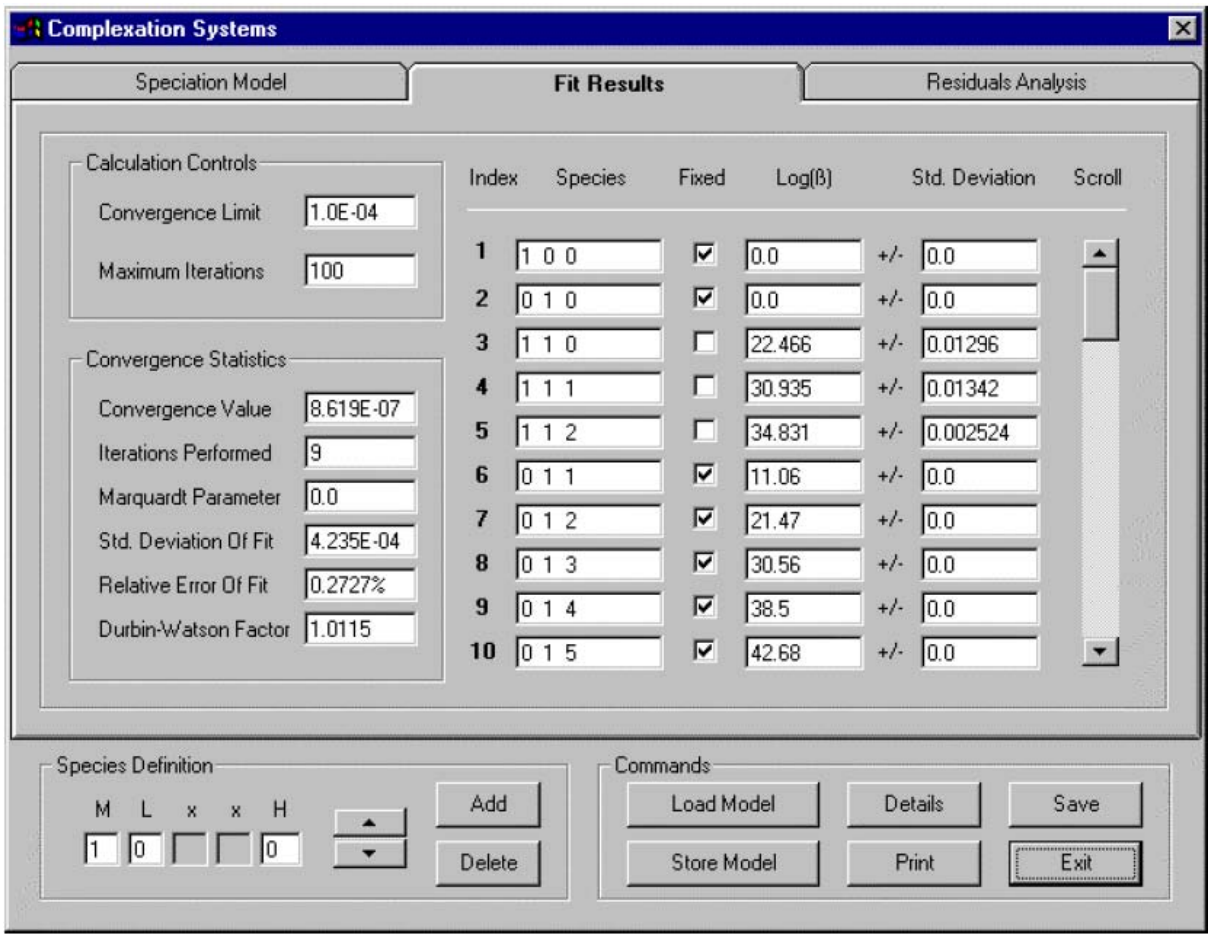

Figure A-3

Various plotting options are possible within SPECFIT/32™. The *Main Toolbar* above the spectra window contains graphing options including cross section and three dimensional plots. The abscissa and ordinate can be adjusted by selecting the *Plot Menu* and selecting *Plot Options*. The colour can be adjusted by selecting *Graph Colors* under the *Graphics Menu*. It is advised that the print setup be set to landscape for printing spectra. Selecting the *Export* command from the *File* menu allows the numerical values of the current spectral file to be extracted. This allows editing by software such as Microsoft Office Excel or ORIGIN®.

This guide only covers the very basics that are required to calculate formation constants from titration data. It is highly recommended that the user also examines the manual within the *Specfit* folder. It covers in great detail the mathematics used, the test statistics produced and the many other methods of its use.

Appendix B

Recorded UV-Visible Spectra for Acid Addition to $[Cu_2(L^1\text{-}2H)_2]$

Isopropanol Titration Medium

1+H_2SO_4

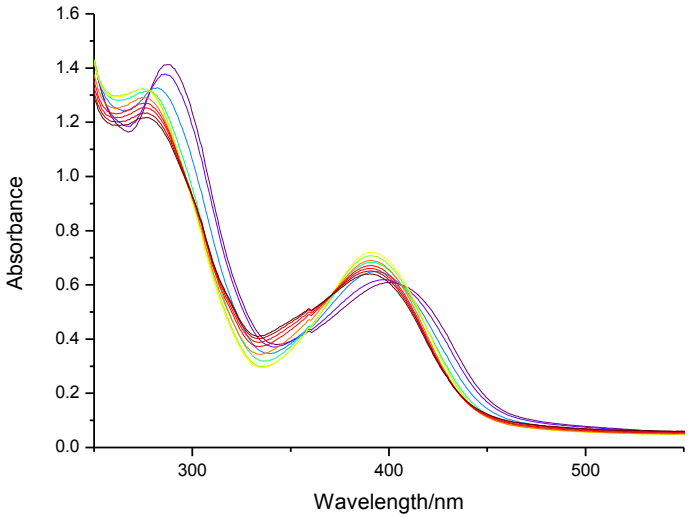

Figure B-1. Recorded UV-visible titration spectra of **1** upon titration of up to five equivalents of H_2SO_4. Each spectrum corresponds to addition of 0.5 equivalences. The colour transition from indigo to red indicates increasing concentration of acid.

1+H_3PO_4

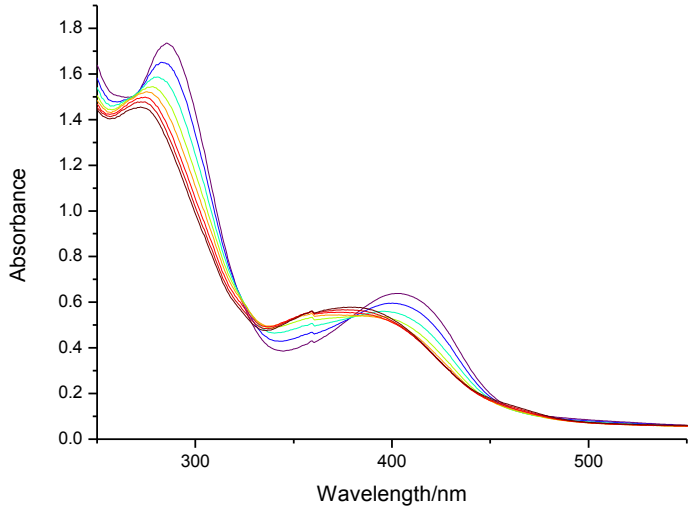

Figure B-2. Recorded UV-visible titration spectra of **1** upon titration of up to four equivalents of H_3PO_4. Each spectrum corresponds to addition of 0.5 equivalences. The colour transition from indigo to red indicates increasing concentration of acid.

1+$TBAH_2PO_4$

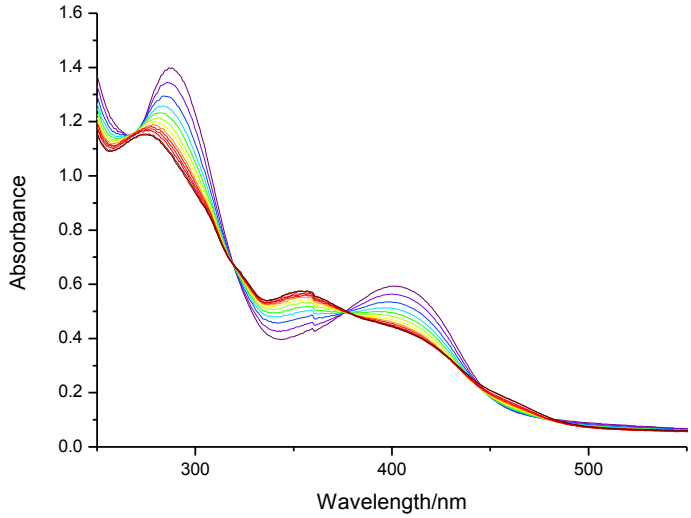

Figure B-3. Recorded UV-visible titration spectra of **1** upon titration of up to three equivalents of $TBAH_2PO_4$. Each spectrum corresponds to addition of 0.25 equivalences. The colour transition from indigo to red indicates increasing concentration of acid.

1+$HClO_4$

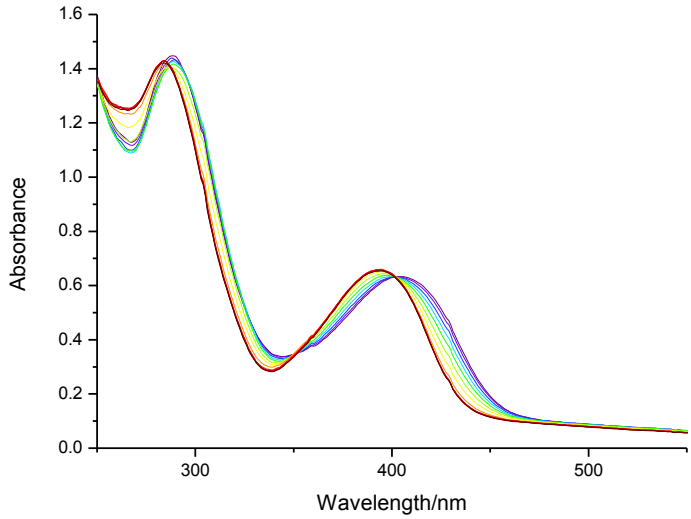

Figure B-4. Recorded UV-visible titration spectra of **1** upon titration of up to six equivalents of $HClO_4$. Each spectrum corresponds to addition of 0.5 equivalences. The colour transition from indigo to red indicates increasing concentration of acid.

1+HBF_4

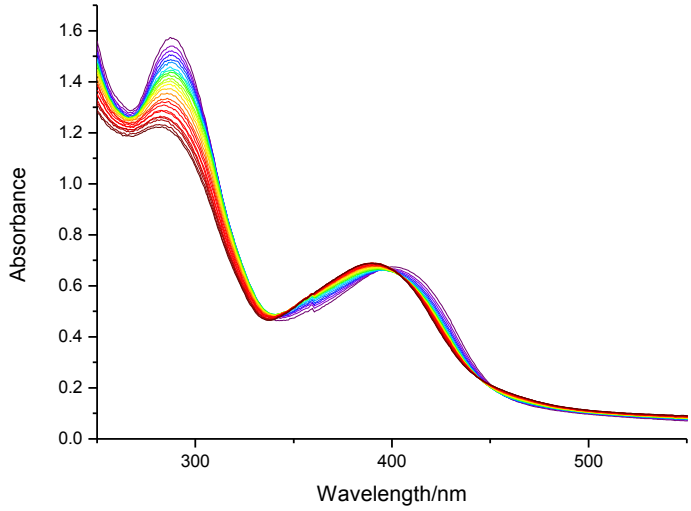

Figure B-5. Recorded UV-visible titration spectra of **1** upon titration of up to six equivalents of HBF_4. Each spectrum corresponds to addition of 0.25 equivalences. The colour transition from indigo to red indicates increasing concentration of acid.

1+HNO_3

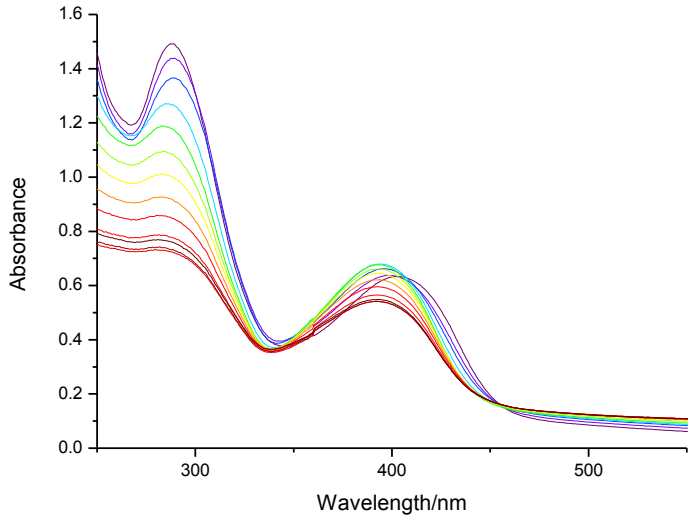

Figure B-6. Recorded UV-visible titration spectra of **1** upon titration of up to thirty equivalents of HNO_3. Each spectrum corresponds to addition of 2.5 equivalences. The colour transition from indigo to red indicates increasing concentration of acid.

1+HBr

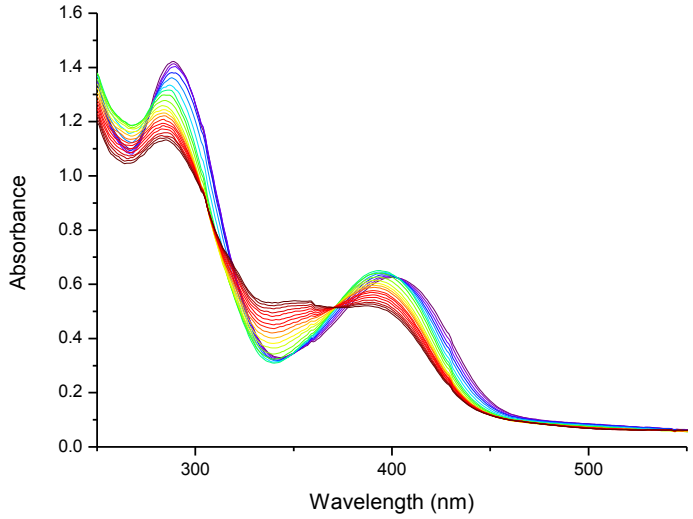

Figure B-7. Recorded UV-visible titration spectra of **1** upon titration of up to ten equivalents of HBr. Each spectrum corresponds to addition of 0.5 equivalences. The colour transition from indigo to red indicates increasing concentration of acid.

1+HCl

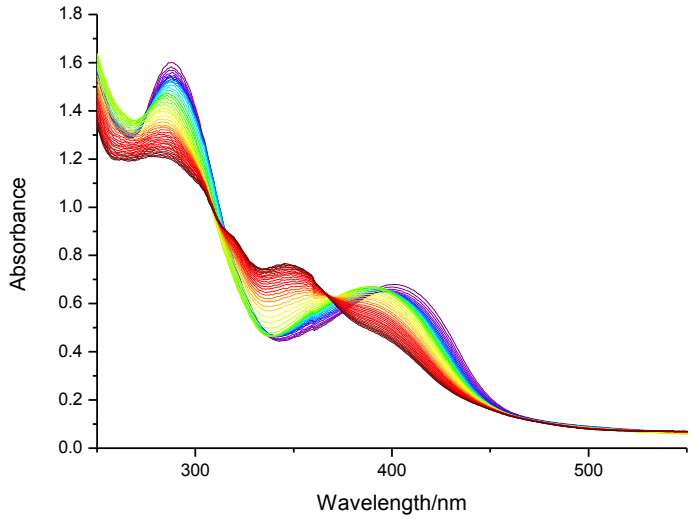

Figure B-8. Recorded UV-visible titration spectra of **1** upon titration of up to ten equivalents of HCl. Each spectrum corresponds to addition of 0.5 equivalences. The colour transition from indigo to red indicates increasing concentration of acid.

1+HI

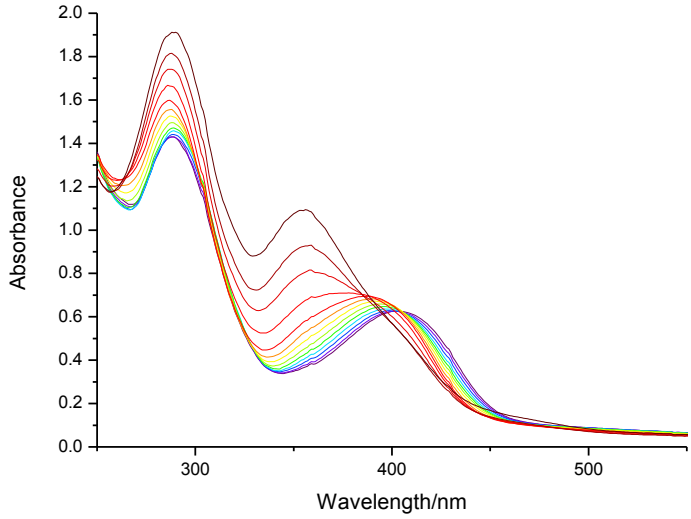

Figure B-9. Recorded UV-visible titration spectra of **1** upon titration of up to six equivalents of HI. Each spectrum corresponds to addition of 0.5 equivalences. The colour transition from indigo to red indicates increasing concentration of acid.

50%(v/v) 1,2-Dichloroethane/Isopropanol Titration Medium

1+H_3PO_4

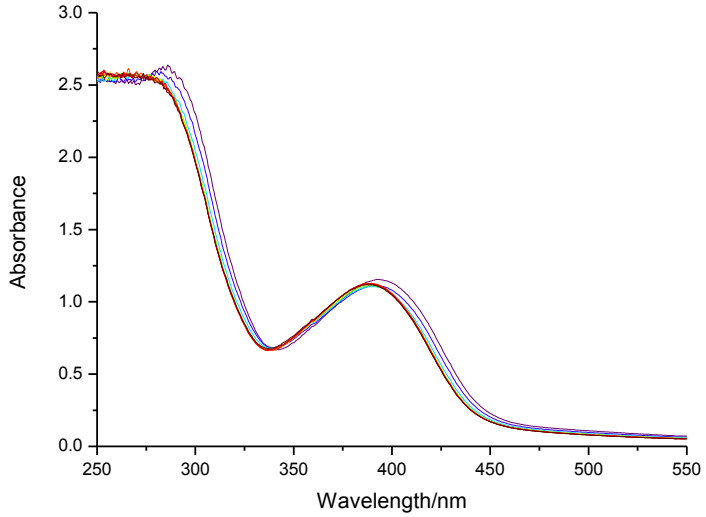

Figure B-10. Recorded UV-visible titration spectra of **1** upon titration of up to four equivalents of H_3PO_4. Each spectrum corresponds to addition of 0.5 equivalences. The colour transition from indigo to red indicates increasing concentration of acid.

1+$HClO_4$

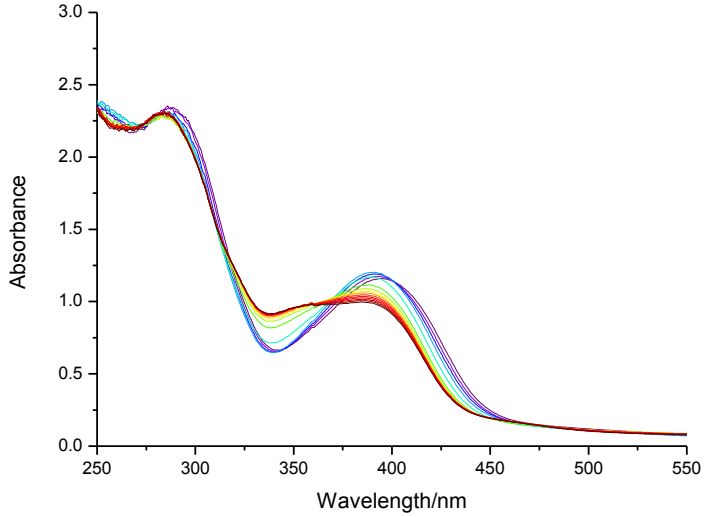

Figure B-11. Recorded UV-visible titration spectra of **1** upon titration of up to seven equivalents of $HClO_4$. Each spectrum corresponds to addition of 0.5 equivalences. The colour transition from indigo to red indicates increasing concentration of acid.

1+HBF_4

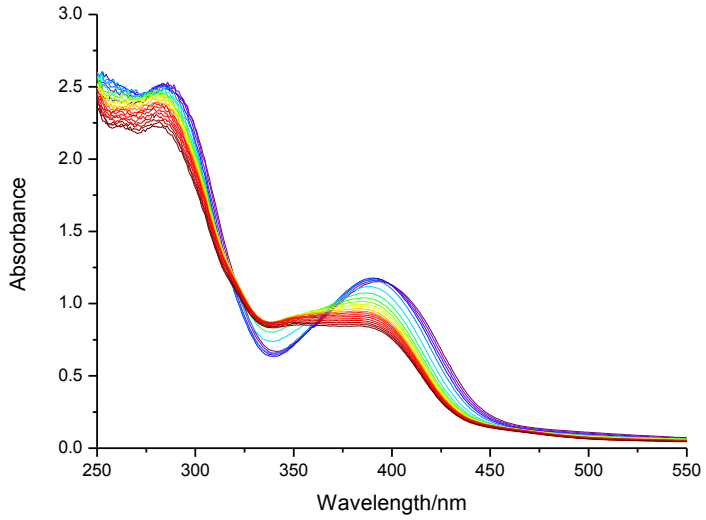

Figure B-12. Recorded UV-visible titration spectra of **1** upon titration of up to ten equivalents of HBF_4. Each spectrum corresponds to addition of 0.5 equivalences. The colour transition from indigo to red indicates increasing concentration of acid.

1+HBr

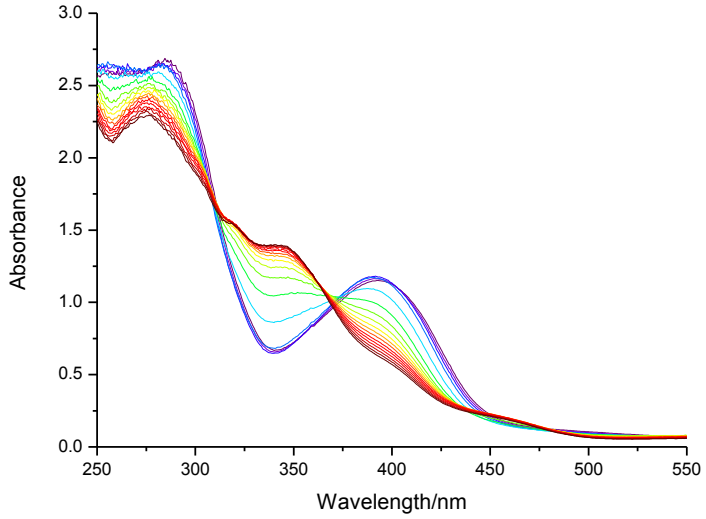

Figure B-13. Recorded UV-visible titration spectra of **1** upon titration of up to ten equivalents of HBr. Each spectrum corresponds to addition of 0.5 equivalences. The colour transition from indigo to red indicates increasing concentration of acid.

Recorded UV-Visible Spectra for Acid Addition to $[Cu_2(L^2\text{-}2H)_2]$

50%(v/v) 1,2-Dichloroethane/Isopropanol Titration Medium

2+H_3PO_4

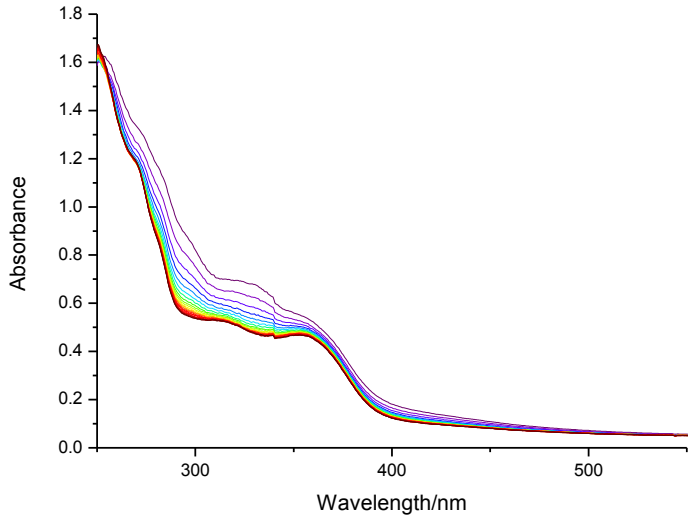

Figure B-14. Recorded UV-visible titration spectra of **2** upon titration of up to ten equivalents of H_3PO_4. Each spectrum corresponds to addition of 0.5 equivalences. The colour transition from indigo to red indicates increasing concentration of acid.

2+$HClO_4$

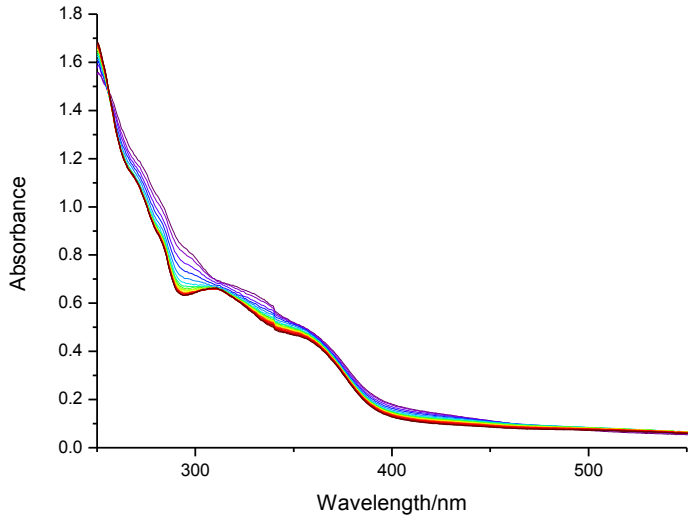

Figure B-15. Recorded UV-visible titration spectra of **2** upon titration of up to ten equivalents of $HClO_4$. Each spectrum corresponds to addition of 0.5 equivalences. The colour transition from indigo to red indicates increasing concentration of acid.

2+HBF_4

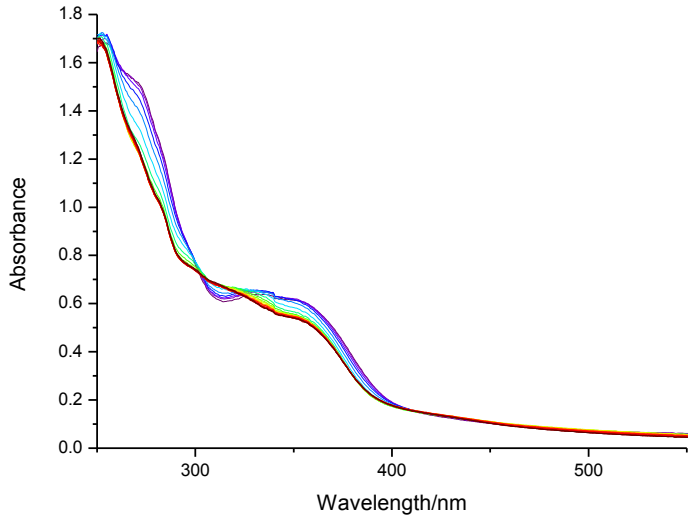

Figure B-16. Recorded UV-visible titration spectra of **2** upon titration of up to ten equivalents of HBF_4. Each spectrum corresponds to addition of 0.5 equivalences. The colour transition from indigo to red indicates increasing concentration of acid.

2+HNO_3

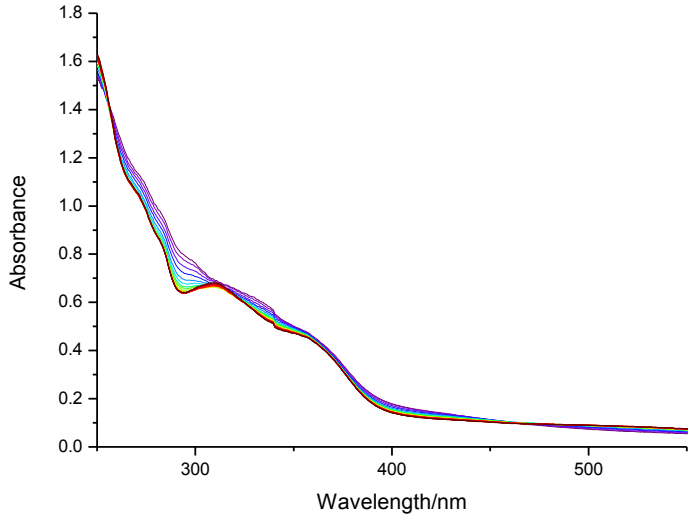

Figure B-17. Recorded UV-visible titration spectra of **2** upon titration of up to ten equivalents of HNO_3. Each spectrum corresponds to addition of 0.5 equivalences. The colour transition from indigo to red indicates increasing concentration of acid.

2+HI

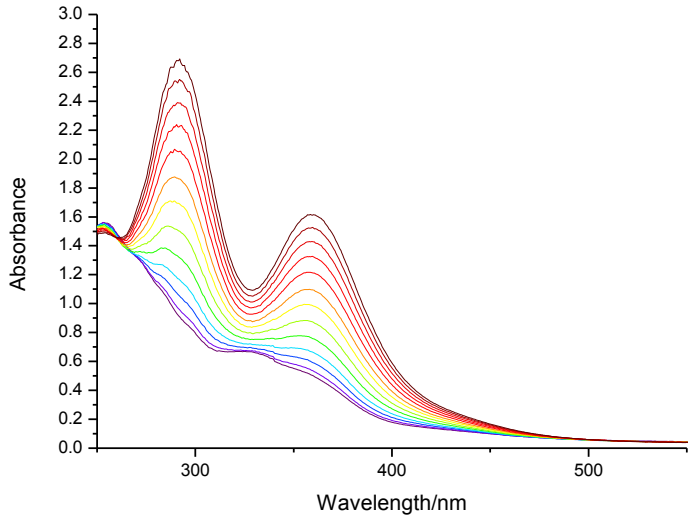

Figure B-18. Recorded UV-visible titration spectra of **2** upon titration of up to six equivalents of HI. Each spectrum corresponds to addition of 0.5 equivalences. The colour transition from indigo to red indicates increasing concentration of acid.

2+HBr

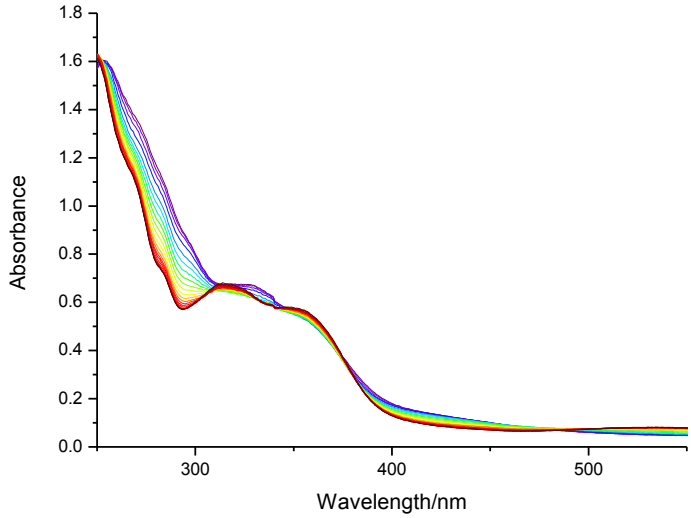

Figure B-19. Recorded UV-visible titration spectra of **2** upon titration of up to ten equivalents of HBr. Each spectrum corresponds to addition of 0.5 equivalences. The colour transition from indigo to red indicates increasing concentration of acid.

2+HCl

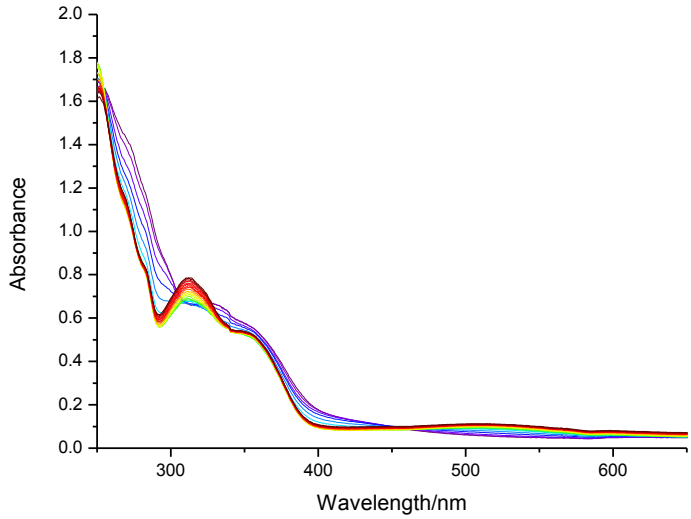

Figure B-20. Recorded UV-visible titration spectra of **2** upon titration of up to ten equivalents of HCl. Each spectrum corresponds to addition of 0.5 equivalences. The colour transition from indigo to red indicates increasing concentration of acid.

References

1. L. G. Lange, J. F. Riordan and B. L. Vallee, *Biochemistry*, 1974, **13**, 4361-4370.
2. R. Vilar, *Angew. Chem., Int. Ed.*, 2003, **42**, 1460-1477.
3. C. H. Henkels, J. C. Kurz, C. A. Fierke and T. G. Oas, *Biochemistry*, 2001, **40**, 2777-2789.
4. V. Gorteau, G. Bollot, J. Mareda, A. Perez-Velasco and S. Matile, *J. Am. Chem. Soc.*, 2006, **128**, 14788-14789.
5. T. Hardarson, J. O. Skarphedinsson and T. Sveinsson, *J. Appl. Physiol.*, 1998, **84**, 411-416.
6. A. K. De, *Environmental Chemistry*, New Age Intl. pub Co, New Delhi, 1990.
7. S. Mattsson, L. Johansson, H. Joensson and B. Nosslin, *Acta Oncol.*, 2006, **45**, 1031-1036.
8. X. Wang and B. List, *Angew. Chem., Int. Ed.*, 2008, **47**, 1119-1122.
9. C. R. Bryan and M. D. Siegel, *Environmental geochemistry of radioactive contamination* SAND2003-2063, 2003.
10. M. R. Rosenthal, *J. Chem. Educ.*, 1973, **50**, 331-335.
11. J. L. Sessler, P. A. Gale and W.-S. Cho, *Anion Receptor Chemistry*, Royal Society of Chemistry, Cambridge, 2006.
12. E. A. Archer, H. Gong and M. J. Krische, *Tetrahedron*, 2001, **57**, 1139-1159.
13. C. H. Park and H. E. Simmons, *J. Amer. Chem. Soc.*, 1968, **90**, 2431-2432.
14. C. H. Park and H. E. Simmons, *J. Amer. Chem. Soc.*, 1968, **90**, 2429-2431.
15. H. E. Simmons and C. H. Park, *J. Amer. Chem. Soc.*, 1968, **90**, 2428-2429.
16. E. Graf and J. M. Lehn, *J. Am. Chem. Soc.*, 1976, **98**, 6403-6405.
17. R. P. Rohrbach, L. J. Rodriguez, E. M. Eyring and J. F. Wojcik, *J. Phys. Chem.*, 1977, **81**, 944-948.
18. J. M. Lehn, E. Sonveaux and A. K. Willard, *J. Am. Chem. Soc.*, 1978, **100**, 4914-4916.

19. P. A. Gale, S. E. Garcia-Garrido and J. Garric, *Chem. Soc. Rev.*, 2008, **37**, 151-190.
20. P. A. Gale and R. Quesada, *Coord. Chem. Rev.*, 2006, **250**, 3219-3244.
21. P. A. Gale, *Coord. Chem. Rev.*, 2003, **240**, 191-221.
22. P. A. Gale, *Coord. Chem. Rev.*, 2001, **213**, 79-128.
23. P. D. Beer and P. A. Gale, *Angew. Chem., Int. Ed.*, 2001, **40**, 486-516.
24. P. A. Gale, *Coord. Chem. Rev.*, 2000, **199**, 181-233.
25. R. Vilar, *Eur. J. Inorg. Chem.*, 2008, 357-367.
26. B. L. Schottel, H. T. Chifotides and K. R. Dunbar, *Chem. Soc. Rev.*, 2008, **37**, 68-83.
27. P. A. Gale, J. L. Sessler, V. Kral and V. Lynch, *J. Am. Chem. Soc.*, 1996, **118**, 5140-5141.
28. S. L. Tobey, B. D. Jones and E. V. Anslyn, *J. Am. Chem. Soc.*, 2003, **125**, 4026-4027.
29. T. H. Kwon and K.-S. Jeong, *Tetrahedron Lett.*, 2006, **47**, 8539-8541.
30. M. Cametti, A. Dalla Cort, L. Mandolini, M. Nissinen and K. Rissanen, *New J. Chem.*, 2008, **32**, 1113-1116.
31. D. J. White, N. Laing, H. Miller, S. Parsons, P. A. Tasker and S. Coles, *Chem. Commun. (Cambridge)*, 1999, 2077-2078.
32. P. G. Plieger, S. Parsons, A. Parkin and P. A. Tasker, *J. Chem. Soc., Dalton Trans.*, 2002, 3928-3930.
33. C. Geraci, G. Chessari, M. Piattelli and P. Neri, *Chem. Commun. (Cambridge)*, 1997, 921-922.
34. R. M. Fairchild and K. T. Holman, *J. Am. Chem. Soc.*, 2005, **127**, 16364-16365.
35. K. Komatsu, M. Murata and Y. Murata, *Science (Washington, DC, U. S.)*, 2005, **307**, 238-240.
36. D. Fiedler, R. G. Bergman and K. N. Raymond, *Angewandte Chemie, International Edition*, 2006, **45**, 745-748.
37. H. Luecke and F. A. Quiocho, *Nature (London)*, 1990, **347**, 402-406.
38. C. Piguet, G. Bernardinelli and G. Hopfgartner, *Chem. Rev. (Washington, D. C.)*, 1997, **97**, 2005-2062.
39. D. S. Lawrence, T. Jiang and M. Levett, *Chem. Rev. (Washington, D. C.)*, 1995, **95**, 2229-2260.

40. B. Hasenknopf, J.-M. Lehn, B. O. Kneisel, G. Baum and D. Fenske, *Angew. Chem., Int. Ed. Engl.*, 1996, **35**, 1838-1840.
41. D. A. McMorran and P. J. Steel, *Angew. Chem., Int. Ed.*, 1998, **37**, 3295-3297.
42. S. Goetz and P. E. Kruger, *Dalton Trans.*, 2006, 1277-1284.
43. W. Henderson and J. S. McIndoe, *Mass Spectrometry of Inorganic and Organometallic Compounds*, John Wiley & Sons, Chester, 2005.
44. N. B. Cech and C. G. Enke, *Mass Spectrom Rev*, 2001, **20**, 362-387.
45. S. Bruere, *Structural Aspects of a Perchlorate Encapsulated Cu(II) Helicate*, PGDipSc, Massey University, 2006.
46. M. R. Wright, *The Nature of Electrolyte Solutions*, Macmillan Education Ltd, Hampshire, 1988.
47. R. D. Feltham and R. G. Hayter, *J. Chem. Soc.*, 1964, 4587-4591.
48. W. J. Geary, *Coordination Chemistry Reviews*, 1971, **7**, 81-122.
49. K. A. Connors, *Binding Constants: The Measurements of Molecular Complex Stability*, Wiley, 1987.
50. F. J. Rossotti, *The Determination of Stability Constants, and Other Equilibrium Constants in Solution*, 1961.
51. B. J. Clark, *UV Spectroscopy: Techniques, Instrumentation, Data handling*, Chapman & Hall, London, 1993.
52. W. Massa and Editor, *Crystal Structure Determination*, 1996.
53. P. G. Plieger and S. Bruere, Unpublished Work, Institute of Fundamental Sciences, Massey University, Palmerston North, Editon edn., 2006.
54. P. Jungwirth, J. E. Curtis and D. J. Tobias, *Chem. Phys. Lett.*, 2002, **367**, 704-710.
55. M. R. Wagner and F. A. Walker, *Inorganic Chemistry*, 1983, **22**, 3021-3028.
56. P. Di Bernardo, P. L. Zanonato, S. Tamburini, P. Tomasin and P. A. Vigato, *Dalton Trans.*, 2006, 4711-4721.
57. C. R. Bondy, P. A. Gale and S. J. Loeb, *J. Am. Chem. Soc.*, 2004, **126**, 5030-5031.
58. P. G. Plieger and R. Forgan, Unpublished Work, Institute of Fundamental Sciences, Massey University, Palmerston North, Editon edn., 2008.
59. H. D. B. Jenkins, H. K. Roobottom, J. Passmore and L. Glasser, *Inorg. Chem.*, 1999, **38**, 3609-3620.

60. A. Albert and E. P. Serjeant, *Ionization Constants of Acids and Bases*, Methuen A Co Ltd, London, 1962.
61. *Pure Appl. Chem.*, 1986, **58**, 1411-1418.
62. A. Ghenciu, 1996.
63. B. Dietrich, *Pure Appl. Chem.*, 1993, **65**, 1457-1464.
64. E. Suet and H. Handel, *Tetrahedron Lett.*, 1984, **25**, 645-648.
65. E. Kilic and N. Aslan, *Microchim. Acta*, 2005, **151**, 89-92.
66. K. S. Moon, N. Singh, G. W. Lee and D. O. Jang, *Tetrahedron*, 2007, **63**, 9106-9111.
67. S. Basurto, O. Riant, D. Moreno, J. Rojo and T. Torroba, *J. Org. Chem.*, 2007, **72**, 4673-4688.
68. T. Gunnlaugsson, M. Glynn, G. M. Tocci, P. E. Kruger and F. M. Pfeffer, *Coordination Chemistry Reviews*, 2006, **250**, 3094-3117.
69. V. Amendola, D. Esteban-Gomez, L. Fabbrizzi and M. Licchelli, *Acc. Chem. Res.*, 2006, **39**, 343-353.
70. R. G. Hayter and F. S. Humiec, *Inorg. Chem. (Washington, DC, U. S.)*, 1963, **2**, 306-312.
71. R. D. Feltham and R. S. Nyholm, *Inorg. Chem. (Washington, DC, U. S.)*, 1965, **4**, 1334-1339.
72. H. Gampp, M. Maeder, C. J. Meyer and A. D. Zuberbuehler, *Talanta*, 1985, **32**, 95-101.
73. H. Gampp, M. Maeder, C. J. Meyer and A. D. Zuberbuehler, *Talanta*, 1985, **32**, 257-264.
74. H. Gampp, M. Maeder, C. J. Meyer and A. D. Zuberbuehler, *Talanta*, 1985, **32**, 1133-1139.
75. H. Gampp, M. Maeder, C. J. Meyer and A. D. Zuberbuehler, *Talanta*, 1986, **33**, 943-951.
76. S. G. Galbraith and P. A. Tasker, *Supramol. Chem.*, 2005, **17**, 191-207.
77. R. S. Forgan, J. E. Davidson, S. G. Galbraith, D. K. Henderson, S. Parsons, P. A. Tasker and F. J. White, *Chem. Commun. (Cambridge, U. K.)*, 2008, 4049-4051.
78. K. M. Kadish, J. E. Anderson and et al., *Pure Appl. Chem.*, 1987, **59**, 703-706.
79. M. Elleb, J. Meullemeestre, M. J. Schwing-Weill and F. Vierling, *Inorganic Chemistry*, 1980, **19**, 2699-2704.

80. C. Denekamp, K. Suwinska, H. Salman, Y. Abraham, Y. Eichen and J. Ben Ari, *Chem.--Eur. J.*, 2007, **13**, 657-665.

81. M. Wenzel, G. B. Jameson, L. A. Ferguson, Q. W. Knapp, R. S. Forgan, F. J. White, S. Parsons, P. A. Tasker and P. G. Plieger, *Chem. Commun. Submitted*, 2009.

82. *Facts & Figures Of The Chemical Industry*, http://pubs.acs.org/cen/coverstory/86/8627cover.html, Accessed 15th Feburary, 2009.

83. P. G. Plieger, P. A. Tasker and S. G. Galbraith, *Dalton Trans.*, 2004, 313-318.

84. R. Forgan, *Modification of Phenolic Oximes for Copper Extraction*, PhD, University of Edinburgh, 2008.